Photonic effects in microstructured conjugated polymer films and light emitting diodes

Benjamin James Matterson

Photonic Effects in Microstructured Conjugated Polymer Films and Light Emitting Diodes

By

Benjamin James Matterson

A thesis submitted to the faculty of science,
Durham University for the degree of
Doctor of Philosophy

Department of Physics
University of Durham
March 2002

ABSTRACT

This thesis reports an investigation into the photonic effects caused by wavelength scale microstructure patterned onto films of conjugated polymers. The efficiency of light emitting diodes (LEDs) made from conjugated polymers is limited in part by the trapping of light into waveguide modes caused by the high refractive index of these materials. Waveguide modes in films of poly(*p*-phenylene vinylene) (PPV) and poly(2-methoxy, 5-(2'ethylhexyloxy)-*p*-phenylene vinylene) (MEH-PPV) are analysed and the refractive index of these materials is calculated.

The photoluminescence of conjugated polymer films that have been spun onto textured substrates is analysed. It is found that the photoluminescence quantum yield of a film spun onto a substrate inscribed with a grating is increased. It is also found that the photoluminescence spectrum of the film is dramatically altered and varies substantially with viewing angle. The features in the spectrum caused by the grating are strongly polarized. These effects are analysed and are attributed to the scattering of waveguided light out of the film.

It is found that films spun onto metal gratings exhibit especially strong scattering. The effect of metal gratings with various grating depths is analysed. The possible contribution of band gaps to the photoluminescence spectrum from polymers on strong metal gratings is discussed.

LEDs that include grating structures are constructed and analysed. It is found that having grating structures on the metal layers that are used as electrodes in the LED does not adversely affect the electrical properties of the LED. It is demonstrated that the grating in the LED is able to substantially increase the light emission without using extra electrical power. The emission spectra from LEDs are observed to vary with angle, and exhibit considerable polarization.

DECLARATION

The material submitted in this thesis has not been submitted for examination for any other degree, or part thereof, at Durham University or any other institution. The material in this thesis is the work of the author except where formally acknowledged by reference.

ACKNOWLEDGEMENTS

Many thanks to Ifor Samuel, Andy Monkman, Graham Cross, David Bloor, Bill Barnes and John Rarity. Extra thanks to Norman Thompson, Dave Pattison, and Kevin McGee. Thanks also to Mounir, Pete, Phil, Steve, Eymard, John, Anna, Loquar, Lars, George, Phil, Graham, Justin, Nathan, Ricardo, John, James, Simon, Pat and several other people that I have temporarily and unreasonably forgotten to mention.

Contents

List of Figures

Chapter 1

Introduction

The study of photonic structures is an important and exciting area of research with applications in several fields, including light emitting diodes (LEDs), semiconductor lasers and optical fibres[1]. The effects that can occur when light interacts with periodic structures that have a similar scale to the wavelength of the radiation itself are also interesting from a fundamental scientific point of view[2,3]. Phenomena associated with periodic structure with an optical length scale can also be observed in nature. For example, there are species of butterfly and moth that have colourations in their wings that are not caused by coloured pigment, but rather by the grating structures formed on their scales.

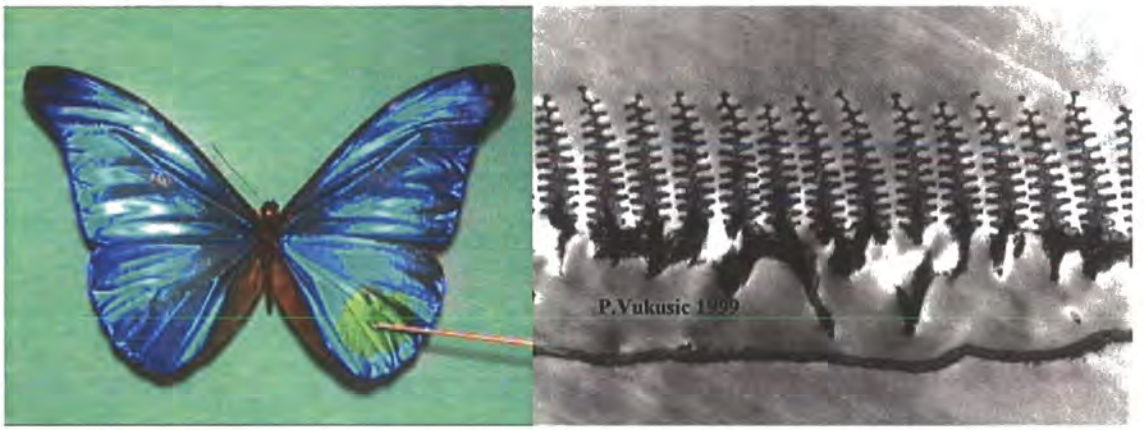

Figure 1.1 *Naturally occurring photonic microstructure. Light at specific wavelengths is reflected by the grating-like structures within the butterfly wings. The photograph on the left shows that placing a drop of solvent on the wing of a Morpho rhetenor butterfly changes its colour by altering the interference conditions. The photograph on the right shows a transmission electron microscope image of a wing scale. It is interesting to ask the question, 'what would happen to light that was generated within such a microstructured region, rather than being reflected from it?' The photographs were provided by Dr P.Vukusic at the University of Exeter* [4].

Photonic structures can be designed to extend into one, two or three dimensions. A simple example of the effects of one dimensional periodic structure is the use of alternating thin film layers of high and low refractive index materials to form a dielectric mirror, capable of achieving much higher reflectivity than a metal mirror. In a similar way, it is possible to construct a periodic structure that extends in three dimensions, creating a region of complete optical bandgap, where radiation within a certain range of wavelengths cannot propagate, or be emitted at all.

The importance of considering photonic effects in the design of light emitting diodes has attracted much attention recently, especially in the use of microcavities to control and modify light emission. Placing a luminescent material in between two highly reflective mirrors, forming an optical cavity, can be used to increase luminescence at certain wavelengths, while emission at other wavelengths is almost completely inhibited[5,6,7,8]. Most of the work that has been done investigating microcavity structures has focused on simple one dimensional planar designs, since depositing layers of thin films onto a flat surface is relatively simple. Despite the interesting effects that can be obtained using planar designs, there are limits to what can be achieved with such structures.

One of the problems of using planar structures for LEDs is that many light emitting materials that are used tend to have fairly high refractive indices, causing light to become trapped in the active layer by the effects of total internal reflection. The trapped light is channelled into discreet waveguide modes, and thus causes a very substantial loss in efficiency in commercial designs for light emitting diodes. Breaking the planar symmetry of an LED structure provides several mechanisms by which losses to waveguiding might be avoided.

Figure 1.2 illustrates two methods that could be used to avoid losses into waveguide modes in a light emitting diode. Light can be scattered into the normal emission direction by using a sinusoidal grating structure with a period identical to the effective wavelength of the trapped light. A grating with half of this wavelength will reflect incident light back on its own path[9] (a mechanism often used to generate feedback in solid state lasers). Emission within the corrugated region is suppressed at this wavelength, which is often referred to as a stop band (a band gap in less than three dimensions). Emission with wavelength at the edge of the stop band (band edge) can actually be enhanced.

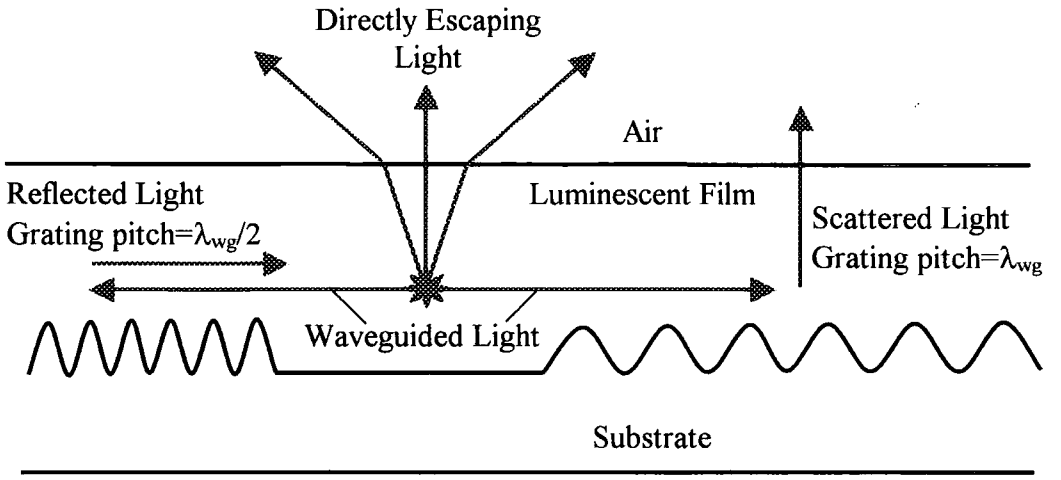

Figure 1.2 *Methods by which a grating might be used to block the propagation of waveguide modes in a high refractive index film. Light can be scattered out of the film, or light emission can actually be inhibited in certain directions by the corrugations.*

The work in this thesis is primarily concerned with investigating the potential use of photonic structures in LEDs using luminescent conjugated polymers as the light emitting materials. Conjugated polymers have attracted much attention recently since they combine the ease of processing associated with many organic materials with semi-conducting electrical properties and interesting optical properties. Several conjugated polymers are highly luminescent, with broad emission spectra. Since the discovery that some of these materials exhibit electroluminescence[10], they have become serious contenders for use in a variety of applications, including large area displays. Exotic applications such as television screens that could be made flexible are being taken seriously. Semiconducting polymers are especially suitable for investigating the effects of wavelength scale microstructure, since they are usually solution processable, or physically soft, allowing structures to be imprinted upon them.

Several semiconducting polymers have refractive indices in the region of 2 at visible wavelengths, making the issue of loss of light to waveguide modes important to consider[11]. Blocking waveguide modes using bandgaps would be difficult due to the breadth of the emission spectra of these materials. The work in this thesis demonstrates that scattering techniques can be used to recover waveguided light from

conjugated polymer light emitting diodes, and that the use of microstructure in general has the potential to modify the colour and polarisation of light emitted from such devices.

Chapter two provides a short introduction to conjugated polymers. The chapter gives the chemical structures of the conjugated polymers used in this work, and a brief discussion of the effects of conjugation and the resulting semi-conducting and luminescent properties of these materials.

Chapter three provides a review of some of the work previously carried out using photonic effects with organic materials. Most prior work has concentrated on investigating the effects that can be achieved with planar microcavity structures, including modifying the lifetime of excited states and altering the colour of emission from LEDs.

Chapter four explains the mathematical modelling methods that can be used to understand planar layered thin film structures. It is possible to understand some of the effects occurring in corrugated structures by treating them as slight deviations from the planar case. The computer program written to optimise and model the effects of arbitrary microcavity structures is explained in this chapter. Figure 1.3 shows a diagram created with this computer program that gives a visual impression of how much light is trapped in waveguide modes by a planar microcavity.

Chapter five explains methods that were used to measure the refractive index of various conjugated polymers, a surprisingly challenging task. Clearly an accurate knowledge of refractive index is vital if the modelling techniques are to have any practical value.

Chapter six discusses the effects that were observed from luminescent films spun onto corrugated grating structures etched into photoresist or glass. The gratings dramatically modified the emission spectra. It was also found the emission became substantially polarised, and varied dramatically with viewing angle. These effects were successfully modelled by considering the scattering effects of waveguide modes propagating near a grating.

Chapter seven records the increasingly complex effects that were obtained from strong gratings coated in metal. The modifications to emission spectra became increasingly dramatic, and more challenging to understand. Finally the practicality of incorporating a grating structure within a conjugated polymer LED is discussed. Surprisingly, it was found that using corrugated electrodes within an LED did not

cause disruption to the electrical properties of the LED, or noticeably decrease its working life expectancy. It was found that these methods could be used to dramatically increase the efficiency of a realistic LED.

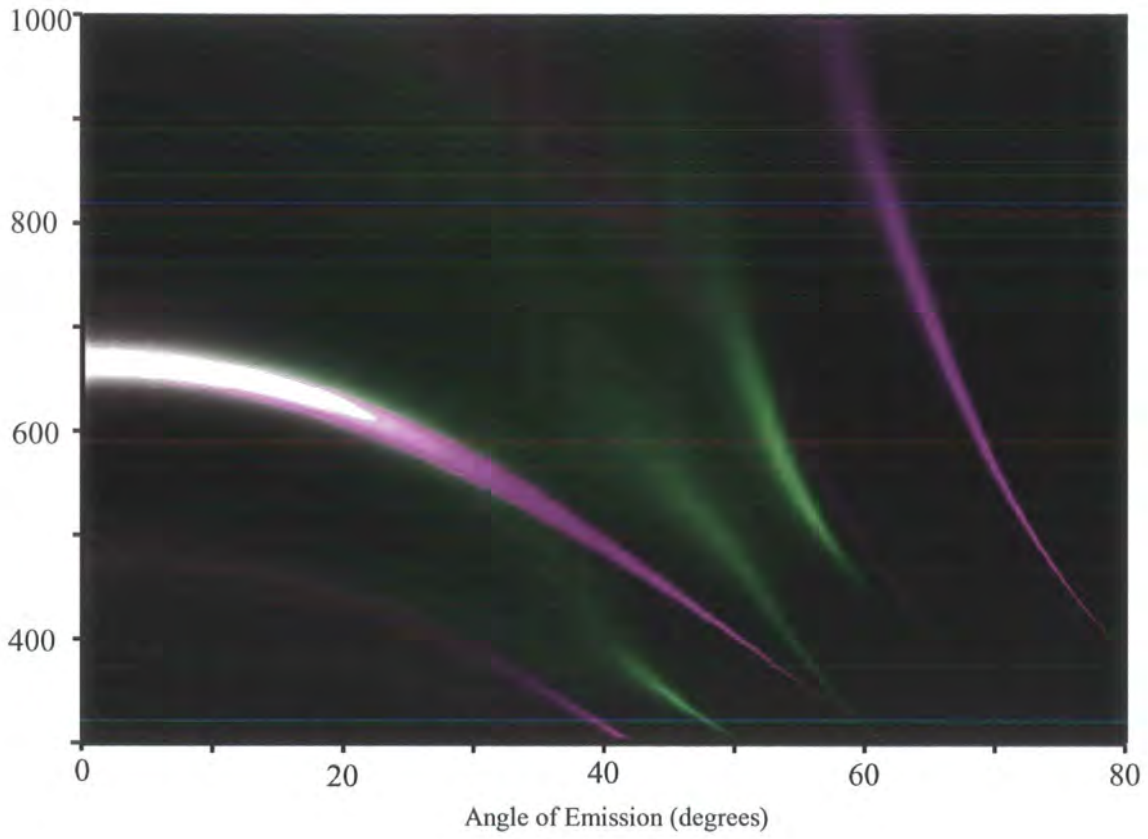

Figure 1.3 *An example of mathematical modelling of the kind of mode structure that can be obtained with a planar microcavity. The structure modelled here is a luminescent film with a refractive index of 2 (thickness 153 nm), confined between one metal mirror (aluminium 45 nm) and one dielectric mirror (5 layers, alternating indices of 2.2 and 1.44, quarter wave thickness). The cavity was optimised using the computer program discussed in chapter 4, to maximise emission at 675 nm for normal emission (shown by the bright white region). Strongly enhanced emission is plotted in brighter colours. TE modes (s-polarised emission) is plotted in magenta, TM modes (p-polarised emission) is plotted in green, unpolarised emission appears white. The angle of emission is the propagation direction of the light within the emitting layer (0 is normal emission) and is plotted on the x axis. The y axis shows the wavelength of the light in nanometers. This diagram gives a good visual impression of the amount of radiation that can be trapped and lost in waveguide modes. All the emission at greater than 45° (i.e. most of the right half of the diagram) represent trapped light.*

[1] Microcavities and Photonic Bandgaps: Physics and Applications, Edited by John Rarity and Claude Wiesbuch, Nato ASI Series E: Applied Science Vol 324, published by Kluwer Academic Publishers

[2] E. Yablonovitch, Phys. Rev. Lett. 58, 271 (2000)

[3] C. Weisbuch, H. Bensity, R. Houdré, J. Lumin 85, 271 (2000)

[4] P. Vukusic, J.R.Sambles and H. Ghiradella, Photonics Science News, 6, 61-66 (2000)

[5] A. Dodabalapur, L. J. Rothberg, R. H. Jordan, T. M. Miller, R. E. Slusher, J. M. Philips, J. Appl. Phys. 80, (12), 6954 (1996)

[6] J. Gruner, F. Cacialli, R. H. Friend, J. Appl. Phys 80, 207-215 (1996)

[7] D. G. Lidzey, M. A. Pate, D. M. Whittaker, D. D. C. Bradley, M. S. Weaver, T. A. Fisher, M. S. Skolnick, Chemical Physics Letters 263 655-660 (1996)

[8] V. Cimrova, D. Neher, Journal Of Applied Physics 79 3299-3306 (1996)

[9] S. Fan, P. R. Villeneuve, J. D. Joannopoulos, E. F. Schubert, Phys. Rev. Lett. 78, 3294 (1997)

[10] J. H. Burroughes, D. D. C. Bradley, A. R. Brown, R. N. Marks, K. Mackay, R. H. Friend, P. L. Burn, A. B. Holmes, Nature 374, 539-541, (1990)

[11] N. C. Greenham, R. H. Friend, D. D. C. Bradley, Adv. Mater. 6, 491 (1994)

Chapter 3

Review of Microcavity Applications in Organic Luminescence

3.1 Introduction

This chapter is intended to provide a review of attempts to utilise and understand photonic effects with luminescent organic materials. It is found that almost all the work that has been done investigating the modification of spontaneous emission from these materials has focused on using planar microcavity structures[1,2,3]. Non planar corrugated structures have been used in the design of lasers[4] but there has been limited investigation into their potential use in altering spontaneous emission, and no prior work at all investigating the effect of corrugating the active layer of an LED. Although this thesis is primarily concerned with investigating non planar structures, the motivation for this work can only be understood by first understanding the achievements and limitations of previous work done investigating planar structures.

The simplest photonic effect that can occur in planar structures is the confinement of light into waveguide modes. In the context of conjugated polymer LEDs, waveguiding generally causes a loss of useful light, and hence best avoided. Unfortunately, conjugated polymers have a high refractive index, which makes it inevitable that a considerable amount of light will be trapped. This is discussed further in the mathematical analysis of chapter four.

Microcavities are a more useful photonic tool for LED applications, providing a method of altering light emission rates in different directions or affecting the colour of emission.

3.2 Emission Near a Metal Layer

Most designs for organic LEDs tend to use at least one metal electrode for charge injection[5]. It has been found that when the region of emission in an organic layer is close to a layer of metal, dramatic losses in the efficiency of the luminescence have been observed. It is generally accepted that the primary reason for this is the interference with reflected light, although here are other possible effects that should

be considered including the availability of non radiative decay mechanisms for excitons near a metal interface[6,7].

Clearly when light from the luminescent material has to pass through the metal layer there will be a loss due to absorption. Most practical designs of LEDs use one metal electrode with sufficient thickness to reflect most of the light emitted in that direction and one electrode with low absorption such as ITO or a very thin layer of metal. All the light generated in the LED will either escape through the electrode with low absorption, or become channelled into waveguide modes, but little will be absorbed while escaping through the electrode. Using a design like this, it is found that interference between light reflected from the thick metal layer and direct light from the emissive region plays a major role in determining the potential efficiency of a device[8].

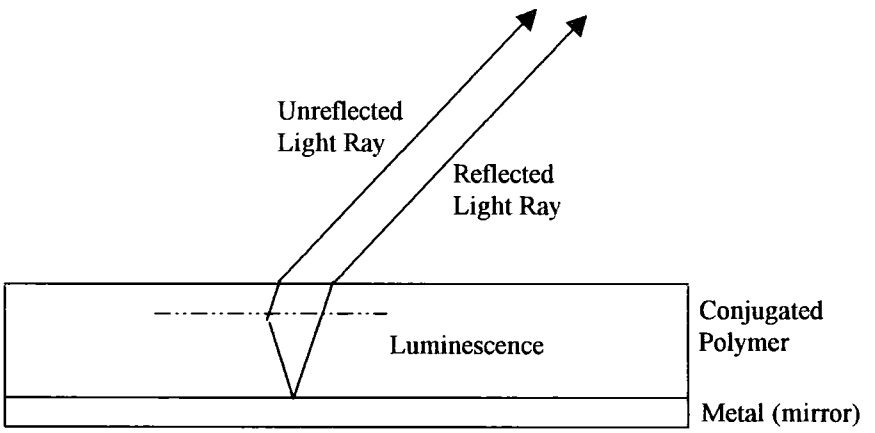

Figure 3.1 *Interference effects from a single metal layer.*

Studies have been done using the simple sample design above, using variable thicknesses of conjugated polymer in contact with a single metal layer of variable thickness[9]. Clearly the emission is expected to be strongest when the direct ray and reflected ray interfere constructively, as occurs when the path difference between the rays equals a whole number of wavelengths for the light emitted. Thus if luminescence is excited near the top of the film, then the strongest emission at normal angle will occur for light with a wavelength of twice the film thickness. It is also clear that when emission is very close to the metal layer, then the interference between the two rays will be destructive no matter what the wavelength of the emitted light, thus decreasing the efficiency of the luminescence. The importance of these interference

effects is most easily demonstrated by varying the thickness of the polymer layer, while ensuring that the emissive area of the film is at the top by exciting the film using ultraviolet light, absorbed within a thin region of the film. Interestingly, experiments using only thin layers of metal suggest that interference effects may not be the only process affecting the efficiency. Potential loss mechanisms to the metal include the generation of non radiative surface plasmon modes, most likely to occur when the excited region of the film is very close to the metal.

3.3 Microcavities

It is found that the effects of interference on the spontaneous emission from luminescent materials are much more dramatic when the materials are confined by reflective surfaces both above and below, forming a microcavity. The simplest microcavity effects using conjugated polymers can be observed by evaporating a metal layer onto a substrate, depositing the polymer layer (usually by spinning), and then evaporating another metal layer on top[10]. The metal layers need to be thick enough to provide high reflection, but with at least one thin enough to allow radiation to escape.

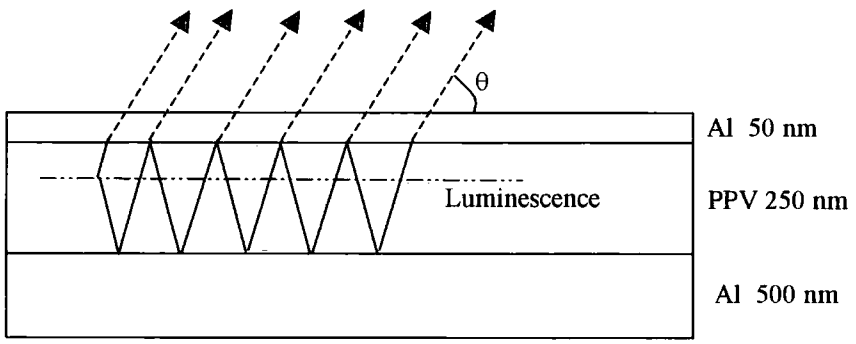

Figure 3.2 *Example of a simple microcavity structure.*

In the simple microcavity structure shown in figure 3.2, a layer of PPV could be excited optically or potentially also electrically (In practice, efficient electrical excitation requires optimisation of the layer thicknesses and metal contact materials used). The emitted light is able to make multiple reflections from the metal layers, with a portion of the light escaping through the thinner metal layer on each reflection.

For wavelengths emitted at an angle that allow the rays undergoing multiple reflection to interfere constructively emission will be enhanced in that direction. For other wavelengths the emission will be suppressed. Thus using this structure, it is possible to take a material like PPV with a broad emission spectrum, and use a microcavity structure to enhance that emission at a single wavelength for a desired emission direction, ending up with a narrowed emission spectrum at a wavelength controlled by the cavity thickness. It is found that this structure causes angular dispersion, so that the emission wavelength enhanced by the cavity will vary as the viewing angle θ is altered. In some applications, a variation of colour with direction of emission is undesirable, for example a display screen that appeared to change colour when viewed from different angles is far form ideal. Problems associated with angular dispersion can be reduced by choosing different metals for the cavity mirrors[11,12], and using these techniques it is possible to design a conjugated polymer microcavity that enhances a colour but does not noticeably change colour across the range of emission angles that would be required for a VDU screen.

In general, optical cavities can be used to alter the decay rate of excited states into radiation modes. In any situation where an excitation can decay by both radiative and non radiative means, then by using a microcavity to increase the radiative decay rate, there is less time for the excitation to decay non radiatively and thus the cavity can, in theory at least, be used to improve the efficiency of such a device. In conjugated polymers, it is believed that a most of the excitons formed from electron and hole recombination decay non radiatively, so that a mechanism that speeds up the radiative decay rate is of considerable interest. In practice, using a planar (one dimensional) microcavity to improve the overall efficiency of a conjugated polymer LED would be difficult, and perhaps impossible. This is largely due to the fact that the high absorption associated with conjugated polymers means that multiple reflections between the mirrors across the polymer layer would cause high losses, and also the broad emission spectrum of the polymers means that the cavity could never be optimised for the entire spectrum. By contrast, improving the efficiency of an LED designed to emit one colour in one direction is most certainly feasible. Planar microcavities are of great interest for controlling the colour of the emission from conjugated polymers.

An important consideration in the design of an LED using a microcavity is the positioning of the emissive region relative to the nodes and antinodes of optical modes available in the cavity. When a cavity has highly reflective mirrors (high finesse), photons trapped in the cavity form a standing wave with nodes and anti nodes. This is similar to the behaviour of quantum particles trapped in a square potential well often discussed in quantum mechanics.

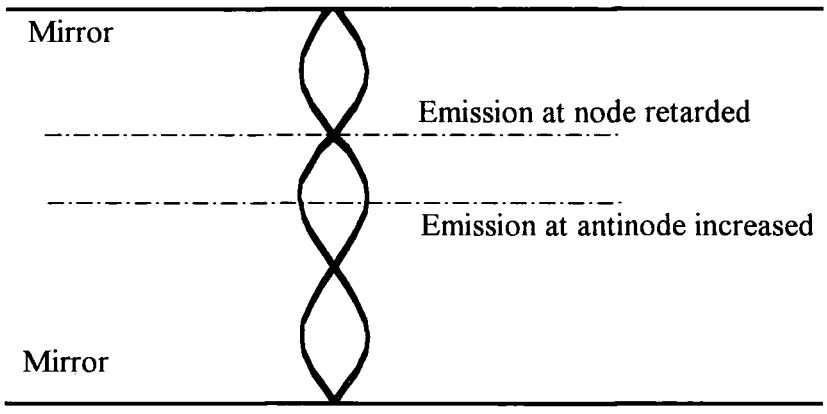

Figure 3.3 *Schematic diagram of optical modal structure of an ideal microcavity mode. Forward emission from a material positioned at an antinode is dramatically increased at this wavelength. This cavity is optimised so that it has a thickness of one and a half times the emission wavelength of a material positioned within it.*

In an ideal microcavity such as that shown in figure 3.3, the optical mode structure forms with clear nodes and antinodes. A material emitting light within the microcavity will have its emission enhanced most at wavelengths for which an antinode is able to form at a depth within the stack where the material is emitting[13]. Emission at a perfect node would be completely inhibited in the forward direction. In the context of LEDs, it is clear that the region in the layer where most electrons and holes meet to form excitons would ideally be positioned at an antinode of the cavity. Much work on LEDs has focussed on determining the mobility of charge within various conjugated polymers, allowing the prediction of the charge recombination region to be taken into account in the design of LEDs.

The diagram in figure 3.3 is idealised, having mirrors with perfect reflectivity. Clearly in practice, the mirrors will not be perfect. For all mirrors, whether metal or dielectric, there is a certain penetration of light into the mirror causing a phase change

that must be taken into account. Since one of the mirrors needs to be partially transmissive in order to allow radiation to escape, the nodes and antinodes that form in practice will be imperfect. Studies using a very thin emissive layer of organic material carefully positioned within a cavity structure have demonstrated that under photoexcitation, the emission intensity can be a factor of fifty greater for samples with the active layer at an antinode compared to samples with the active layer at a node[14].

The coupling of emitted light into cavity modes and the resulting effect on the lifetimes of excited states can be analysed quantum mechanically and classically[15]. Although very high finesse cavities can exhibit properties that require a quantum mechanical analysis, the effects on emission from the weak cavity structures that can be achieved with conjugated polymer LEDs can be predicted using purely classical analysis. By modelling an emitter as a classical oscillator, and summing the field from reflected light from all the interfaces within a structure, the damping force and hence lifetime of the excited state can be predicted.

3.4 LEDs Incorporating Microcavities

Simple metal microcavity structures using conjugated polymers have been investigated using both photoluminescence and electroluminescence. Clearly using metal mirrors allows the mirrors to act as electrodes. The choice of metals used requires that the energy of the Fermi level is appropriate. An effective LED design using a microcavity has been demonstrated using aluminium and gold electrodes, with MEH-PPV as the active layer[16]. Aluminium is reasonably effective at injecting electrons. Gold is found to be suitable for injecting holes, and since it has relatively low absorption in the mid region of the visual spectrum, it is a reasonable choice for the partially transmissive mirror.

Using metal mirrors for a microcavity structure has the obvious disadvantage that the emitted light must pass through one of the metal layers, thus incurring a considerable loss due to absorption. To make the cavity effective at narrowing the emission to the desired wavelength, the cavity needs to have a reasonably high finesse. This occurs when the reflectivity of both of the mirrors forming the cavity are high. Making metal mirrors highly reflective requires that the metal is reasonably thick, thus the absorption loss as the light passes through the metal is bound to be

fairly high. A method of avoiding this loss is to use a dielectric mirror rather than a metal one.

A dielectric mirror is formed by using alternating layers of dielectric material with high and low refractive index, each one a quarter of a wavelength thick, for the wavelength of light that the mirror is designed to reflect[17]. Increasing the reflectivity of the mirror can be achieved by increasing the difference in refractive index between the high and low index materials used, which also widens the range of wavelengths reflected, or by increasing the number of layers in the stack. The advantage of using a dielectric mirror is that high reflection can be obtained while absorption of light passing through the mirror is kept negligibly low. Since dielectric materials commonly used in dielectric mirrors are insulators, an LED using such a mirror would require an extra layer such as ITO to be deposited to provide an electrode.

The most efficient designs for organic LEDs using microcavities that have been demonstrated in practice have generally used a structure with one dielectric mirror with an anode (usually ITO or gold) deposited on top of it, and one metal mirror, usually aluminium of silver, that also serves as a cathode[18,19,20,21]. In theory the best way to optimise this design would be to make the dielectric mirror partially reflective to allow light to escape without absorption, and make the metal mirror thick enough to maximise its reflection. In practice, partially reflective dielectric mirrors are quite expensive, and thus most work has used cheap totally reflective dielectric mirrors, combined with partially reflective metal layers for the other mirror, to allow light to escape. The absorption incurred as the light passes through the metal layer makes it difficult to use such a device to increase the emission from a conjugated polymer LED. An LED using PPV in a cavity like this has been demonstrated, and it has been shown that if the absorption in the metal could be avoided then the total emission from PPV could be increased by a factor of two using a microcavity, integrating spectrally and spatially[22]. This is comparable to the increase in emission generated using grating structures that is demonstrated in this thesis in chapter seven, although using the gratings the increase is demonstrated without needing to adjust for losses in the metal layers. Using a microcavity to increase emission purely in the forward direction (normal emission) is considerably easier that trying to obtain an overall increase in light emission from an LED. Increases of at least a factor of four have been demonstrated, using one dielectric mirror and one gold mirror[23].

There are other interesting effects that can be achieved using dielectric mirrors. By using a chirped mirror, where different regions of the dielectric stack are optimised to different wavelengths, it is possible to design multiple mode microcavities combining different colours. This method has been demonstrated to create an LED emitting white light[24].

An impression of the potential increases in efficiency that could be a achieved with polymer LEDs can be gained by analysing some of the results obtained with other organic materials. Devices using AlQ_3 [25], have demonstrated the advantage of using a partially reflecting dielectric stack as one of the microcavity mirrors. A device using such a mirror combined with a thick aluminium mirror has demonstrated a spectrally and spatially integrated efficiency enhancement factor of 1.6, and a forward enhancement factor of 4, compared to a device without the microcavity[26]. Although it is clear that very considerable enhancements can be made to LED efficiency using planar microcavities, the work in this thesis suggests that further improvements could be made by using non planar LED designs[27].

3.5 Photonic Effects in Non Planar Structures

Most of the work previously done investigating photonic effects in organic materials has concentrated on planar structures. Although planar microcavities do have the potential to control and perhaps increase emission from polymer LEDs, there is always a factor that limits the effectiveness of such devices. Maintaining the planar structure while the emissive layer has a high refractive index makes it almost impossible to avoid a considerable amount of radiation being lost into waveguide modes.

There has been previous work done using non planar substrates with conjugated polymers. Substrates etched with gratings are often used to provide feedback in investigation of lasing applications[28]. In such an application it is intended that light is trapped in a waveguide mode. Rather than being absorbed, is actually amplified through stimulated emission, while the film is optically excited (it is currently widely agreed that electrically pumped polymer lasers would be extremely difficult and perhaps impossible to construct).

Non planar structures also hold potential interest in controlling spontaneous emission. As discussed in this chapter it is difficult to increase overall spontaneous

emission (summed over all directions) with a one dimensional planar cavity. However, a photonic structure that extends in two or three dimension would provide an opportunity for much greater control of light emission. Emission at undesired wavelengths could be blocked using an optical band gap (or stop band), or emission in waveguide modes could be blocked or scattered into useful directions.

Very little investigation has been done into the effects of corrugated structure on the spontaneous emission from conjugated polymers in either photoluminescence or electroluminescence, and this is the main focus of the work in this thesis.

---

[1] H. Becker, R. H. Friend, T. D. Wilkinson, Applied Physics Letters 72 (11): 1266-1268 (1998)

[2] M. Berggren, O. Inganas, T. Granlund, S. Guo, G. Gustafsson, M. R. Andersson Synthetic Metals 76 (1-3): 121-123 (1996)

[3] V. Bulović, V. B. Khalfin, G. Gu, P. E. Burrows, D. Z. Garbuzov, S. R. Forrest, Physical review B 58, 7, 3730 (1998)

[4] M. Berrgren, A. Dodabalapur, R.E. Slusher, A. Timko, O. Natamasu, Applied Physics Letters, 72, 410 (1998)

[5] H. Becker, Lux.A, Holmes.A.B, Friend.R.H, Synthetic metals 85 1289-1290 (1997)

[6] N. C. Greenham, S. C. Moratti, D. D. C. Bradley, R. H. Friend, A. B. Holmes, Nature 365, 628 (1993)

[7] J. Gruner, F. Cacialli, R. H. Friend, Journal Of Applied Physics 80 207-215 (1996)

[8] S. E. Burns, N. C. Greenham, R. H. Friend, Synthetic Metals 76 205-208 (1996)

[9] H. Becker, S. E. Burns, R. H. Friend, Physical Review B-Condensed Matter 56 1893-1905 (1997)

[10] J. Gruner, F.Cacialli, I.Samuel and R.Friend, 1995 Conference Procedings NATO-ARW on Quantum Optics in Wavelength Scale Structures, Cargese, corsica, Aug 26-Sept 2 1995

[11] N. Tessler, S. Burns, H. Becker, R. H. Friend, Applied Physics Letters 70 556-558 (1997)

[12] H. Becker, S. E. Burns, N. Tessler, R. H. Friend, Journal Of Applied Physics 81 2825-2829 (1997)

[13] S. E. Burns, N. Pfeffer, J. Gruner, M. Remmers, T. Javoreck, D. Neher, R. H. Friend, Advanced Materials 9 395 (1997)

[14] D. G. Lidzey, M. A. Pate, D. M. Whittaker, D. D. C. Bradley, M. S. Weaver, T. A. Fisher, M. S. Skolnick, Chemical Physics Letters 263 655-660 (1996)

[15] W. Lukosz, Phys. Rev. B 22, 6, 3030-3037 (1980)

[16] H. F. Wittmann, J. Gruner, R. H. Friend, G. W. C. Spencer, S. C. Moratti, A. B. Holmes, Advanced Materials 7 541-544 (1995)

[17] H. A. Macleod, Thin Film Optical Filters (2nd edn), Adam Hilger (1986)

[18] D. G. Lidzey, M. S. Weaver, T. A. Fisher, M. A. Pate, D. M. Whittaker, M. S. Skolnick, D. D. C. Bradley, Synthetic Metals 76 129-132 (1996)

[19] S. Tokito, K. Noda, Y. Taga, R. E. S. Toyota Cent Applied Physics Letters 68 2633-2635 (1996)

[20] T. Tsutsui, N. Takada, S. Saito, E. Ogino, Applied Physics Letters 65 1868-1870 (1994)

[21] J. Gruner, F. Cacialli, I. D. W. Samuel, R. H. Friend, Synthetic Metals 76 137-140 (1996)

[22] J. Gruner, F. Cacialli, R. H. Friend Journal Of Applied Physics 80 207-215 (1996)

[23] V. Cimrova, D. Neher, Journal Of Applied Physics 79 3299-3306 (1996)

[24] L. J. R. Dodabalapur.A, and T. M. Miller, Applied Physics Letters 65 2308 (1994)

[25] A. Dodabalapur, L. J. Rothberg, R. H. Jordan, T. M. Miller, R. E. Slusher, J. M. Phillips, Journal Of Applied Physics 80 6954-6964 (1996)

[26] R. H. Jordan, L. J. Rothberg, A. Dodabalapur, R. E. Slusher, Applied Physics Letters 69 1997-1999 (1996)

[27] B. J. Matterson, J. M. Lupton , A. F. Safonov, M. G. Salt, W. L. Barnes, I. D. W. Samuel, Advanced Materials, 13 (2): 123-127 (2001)

[28] M. Berrgren, A. Dodabalapur, R.E. Slusher, A. Timko, O. Natamasu, Applied Physics Letters, 72, 410 (1998)

Chapter 4

Basic Mathematics of Thin Film Optics

4.1 Introduction

Most of the work in this thesis is concerned with the effects of corrugated structures on the photoluminescence of conjugated polymers. A complete theoretical analysis of the photonic effects resulting from a light emitting substance being contained within a corrugated layered structure is non trivial and beyond the scope of this work. A mathematical analysis of the classical photonic effects created by a layered planar structure is considerably simpler. The reason it is discussed here is not only because it is important to understand the limitations imposed by planar structures, but also because the effects of weak grating structures can be understood by treating them as a slight perturbation from the planar case. For structures that deviate further from the planar ideal, it is at least possible to make qualitative observations on how the behaviour changes from the weak grating limit.

4.2 Dielectric Planar Waveguides

The photonic effects of layered thin film structure of the type used in polymer LEDs can be analysed mathematically by considering the boundary conditions of the electromagnetic fields at the interfaces between layers of different refractive index. There is always some reflected light at every interface between layers of different refractive index, so even in the simplest of structures, interference effects need to be taken into account. One of the most important effects related to the interference of light reflected from the film interfaces is the trapping of light in waveguide modes[1]. This effect will occur for any film of luminescent material that has a refractive index higher than the materials that bound it.

Analysis of photoluminescence from a layer of conjugated polymer spun onto a planar glass substrate show that a considerable amount of light is trapped in waveguide modes, and then reabsorbed by the polymer. Using very simple analysis, a first estimate of the amount of light lost to waveguide modes can be made. Figure 4.1 shows the possible modes available to the generated light. All the light that is emitted at an angle θ that is less than the critical angle between the polymer and the air will

not be channelled into a waveguide mode, and can be considered 'useful light'. Light emitted at an angle greater than this will be totally internally reflected at the top surface, and become trapped in a waveguide mode, either a substrate mode, or a mode in the polymer film if the emission angle is greater than the critical angle between the polymer and the glass substrate. In general, light in substrate waveguide modes is not absorbed, but escapes through the sides of the substrates. This is inconvenient, but there are methods that allow some of this light to be recovered, such as roughening the lower face of the substrate. Light waveguiding purely in the polymer is much more difficult to recover. It is absorbed before it is able to propagate very far along the film, a typical propagation distance being no more than 200 microns before at least eighty percent of the energy is absorbed. This was measured in the work described in chapter six of this thesis.

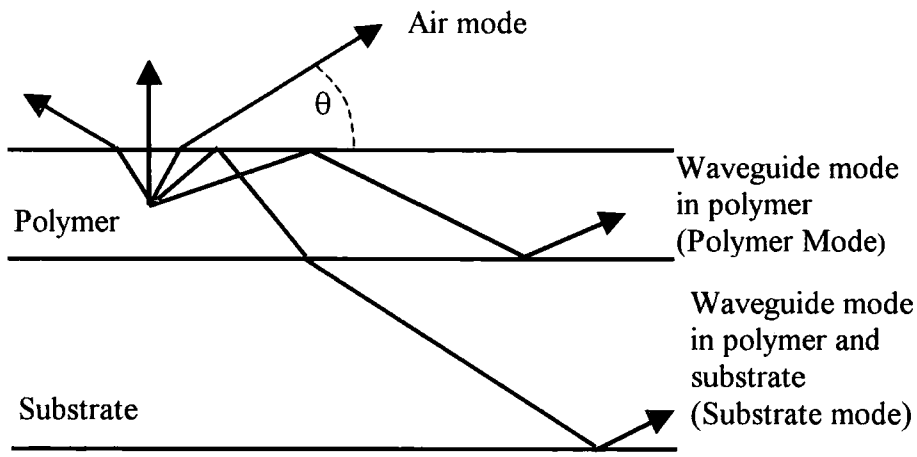

Figure 4.1 *Types of waveguide mode.*

Using the simple interpretation that all light beyond the critical angle is absorbed, it can be shown that for a film of high refractive index the fraction of light escaping the film tends to a fraction $1/2n^2$, where n is the refractive index of the film. This estimate makes the assumption that substrate modes cannot escape[2]. In the example shown in figure 4.1, half of the escaping light the light ($1/4n^2$) would be emitted upwards and half downwards. It is a simple matter to put a reflective layer underneath the polymer to ensure that all the escaping light passes through the top face, however this will not affect the amount of light trapped in waveguide modes. It

is clear that loss of efficiency through this mechanism becomes quite dramatic for high refractive index luminescent materials.

In reality, the situation is rather more complex than this[3]. Firstly, waveguiding can only occur at all if the guiding layer is above a minimum thickness, dependent on the refractive indices of the various layers. If waveguiding does occur (which is certainly the case for polymer films with dimensions commonly used in LEDs) then all the energy within the film is forced to propagate at discreet angles forming a modal structure. Even at emission angles below the critical angle, where total internal reflection does not occur, there is still a considerable amount of reflection at the interfaces. This gives rise to 'leaky' modes that propagate along the film in a similar way to full waveguide modes, but allowing light to gradually escape at each reflection. Leaky modes can still lose considerable energy due to absorption within the polymer film itself, and thus should be taken into account when determining the net loss to efficiency. Microcavity modes are essentially just leaky modes that are more strongly defined by making the film boundaries highly reflective using metal or dielectric mirrors. The more leaky a mode is, or the higher the absorption of guided mode light within the polymer film is, the less clearly defined the waveguiding angle of the mode becomes.

A further factor that complicates the analysis of waveguide modes in conjugated polymer is that the material is birefringent, when spun as a film. Since the film has different refractive indices for transverse electric (TE), and transverse magnetic (TM) waveguide modes, it is important to consider these separately. It is found that the effective refractive index for a TM mode actually changes depending on the internal angle that the light is waveguiding with. In general it is expected that more light will be emitted into TE modes due to the orientation of the polymer chains. These issues are discussed in greater depth in chapter five.

4.3 Waveguide Modes

Using a model that excludes any absorption effects, it can be shown that the minimum thickness of a polymer film on a glass substrate that will allow at least one waveguide mode for light with a wavelength λ is given by:

$$w_{min}(\lambda) = \frac{\lambda}{\left[2\cdot\pi\cdot\left(\sqrt{n_s^2 - n_g^2}\right)\right]}\left(\operatorname{atan}\left(\sqrt{\frac{n_g^2 - n_a^2}{n_s^2 - n_g^2}}\right)\right) \qquad (4-1)$$

where n_s is the refractive index of the polymer film and n_g and n_a are the indices of the glass substrate and the air (or whatever dielectric material is in contact with the top surface of the polymer film). Taking a typical value for the index of a conjugated polymer film (n_s) to be 1.9 and taking the glass substrate index (n_g) as 1.45 gives the minimum thickness (w_{min}) required to waveguide light with a wavelength (λ) of 550 nm can be found. The index of air n_a is taken as 1.

$$n_s = 1.9 \qquad n_g = 1.45 \qquad n_a = 1 \qquad \lambda = 550$$

$$w_{min}(\lambda) = 50.44$$

This model would therefore suggest that films of polymer with refractive indices in this region and thickness greater than 50 nm will have at least one full waveguide modes (films thinner than this could still have leaky modes).

For light that is emitted with angle θ (as defined in figure 4.1) greater than the critical angle for the interface it reflects from, there will be a phase change on reflection (the Goos-Haenchen shift). The phase change is different for s polarised light (in TE modes) and p polarised (in TM modes). For a TE mode reflecting from the polymer air interface is given by:

$$\Phi_{aTE}(\theta) = \operatorname{atan}\left[\frac{\sqrt{\left(n_s^2 \sin(\theta)^2 - n_a^2\right)}}{n_s \cos(\theta)}\right] \qquad (4-2)$$

and for a TM mode by:

$$\Phi_{aTM}(\theta) = \operatorname{atan}\left[\frac{\sqrt{\left(n_s^2 \sin(\theta)^2 - n_a^2\right)}}{n_s \cos(\theta)}\cdot\frac{n_s^2}{n_a^2}\right] \qquad (4-3)$$

If light is also totally internally reflected from the substrate and thus trapped in a waveguide mode, then there will be another phase change on reflection from the substrate interface defined similarly but dependant on the substrate index. Taking these into account, it is possible to plot a graph showing which wavelength will propagate at a particular internal waveguiding angle for a film of thickness w using:

$$\lambda(\theta) = \frac{2\pi\ W \cdot n_s \cos(\theta)}{\pi\ m + \Phi_a(\theta) + \Phi_g(\theta)} \qquad (4-4)$$

Where m is the order of the mode starting with m=0 for the mode of longest wavelength. Figure 4.2 gives an example of the mode structure for a sample film. θ is the internal waveguiding angle. λ_0, λ_1 and λ_2, are the wavelengths of the first three modes that could propagate at this angle. This formula is used in chapter six, where the waveguiding angle is defined as θ_w.

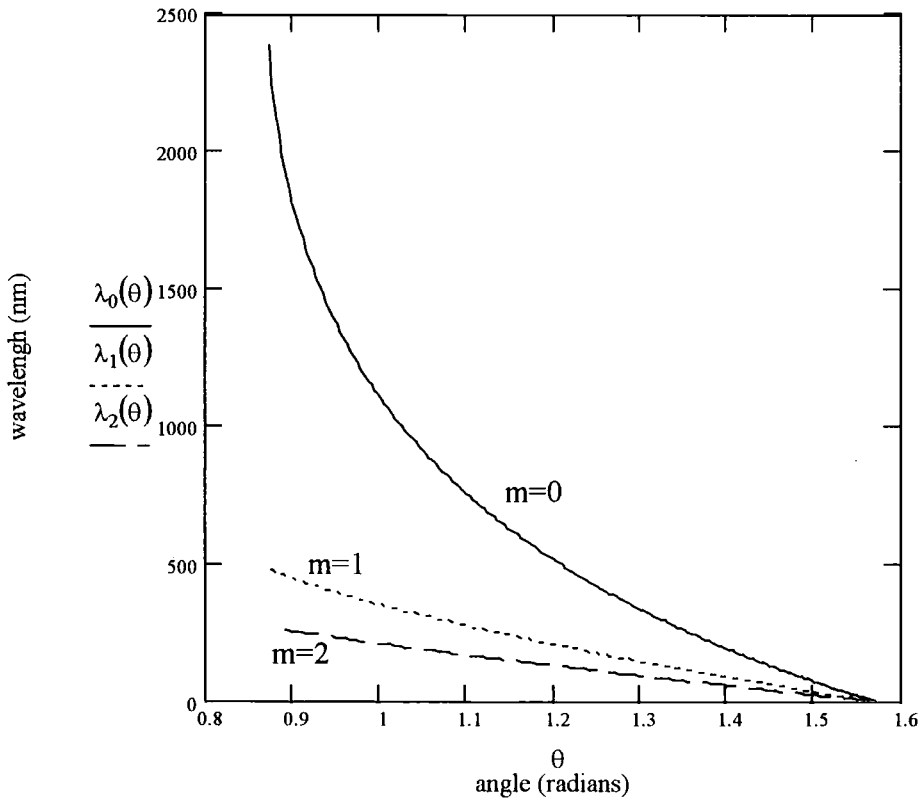

Figure 4.2 *Wavelength vs Internal angle (plotted using Mathcad 2000), for film thickness 250 nm, film Index 1.9, showing 3 waveguide modes.*

From figure 4.2 it can be seen that in order for more than one waveguide mode to exist for wavelengths over 500nm, a film with index 1.9 would need to be thicker than 250 nm. The use of multiple modes to make accurate measurement of refractive indices is discussed in chapter five.

4.4 Modelling Arbitrary Planar Structures

The model for waveguide modes considered so far is an approximation that does not allow for layers with complex refractive index such as metals in contact with the polymer. It also does not model leaky waveguide modes. If these are to be taken into account, a more general model needs to be considered.

To model the effects that can occur in any planar structure consisting of multiple thin films, a computer program was written. The standard method of analysing a stack of thin films applies the boundary conditions for electric and magnetic fields at every interface within the stack, and is able to provide values for the total reflectivity and transmisivity of the whole stack for any angle of incidence of light of any wavelength[4,5]. This technique is most often used when designing thin film coatings to be applied to lenses or other optical devices, often to minimise reflection at interfaces. It is possible to include the effects of absorption within the stack by allowing the layers to have complex refractive indices. Similarly, it is possible to include the effects of evanescent waves, by allowing the propagating waves to have complex amplitudes (i.e. an interface that is totally internally reflecting light incident upon it does not a have a transmissivity of zero, but rather a complex transmissivity at that angle to account for the evanescent wave). The computer program was able to account for absorptive layers, and also able to estimate the effect on lifetime that an optical microcavity would have on an excited state. The key subroutine used to calculate the reflection and transmission for light incident upon a stack of thin films with complex refractive index is listed in the Appendix of this thesis.

In this work, the technique was modified to analyse the effect of interference on a light emitting layer within the stack, achieved by summing the effects from all the layers above and below the emissive layer. This allows the change in emission rate to be calculated for a layer of luminescent material emitting at specific wavelengths and angles. A subroutine was also written in order to optimise a dielectric stack to maximise a mode propagating at any desired angle.

Figure 4.3 shows an analysis of the mode structure for the same example film used in figure 4.2. In order to generate this diagram, the reflectivity of the film is calculated working on the assumption that light is incident from a material of high refractive index that is brought close to the film being investigated. The reflectivity is calculated for a range of incident light wavelengths (y axis), and a range of angles of incidence (x axis). When this technique is used in practice, the high index material is usually a prism that allows a full range of waveguiding angles to be investigated, as discussed in the next chapter.

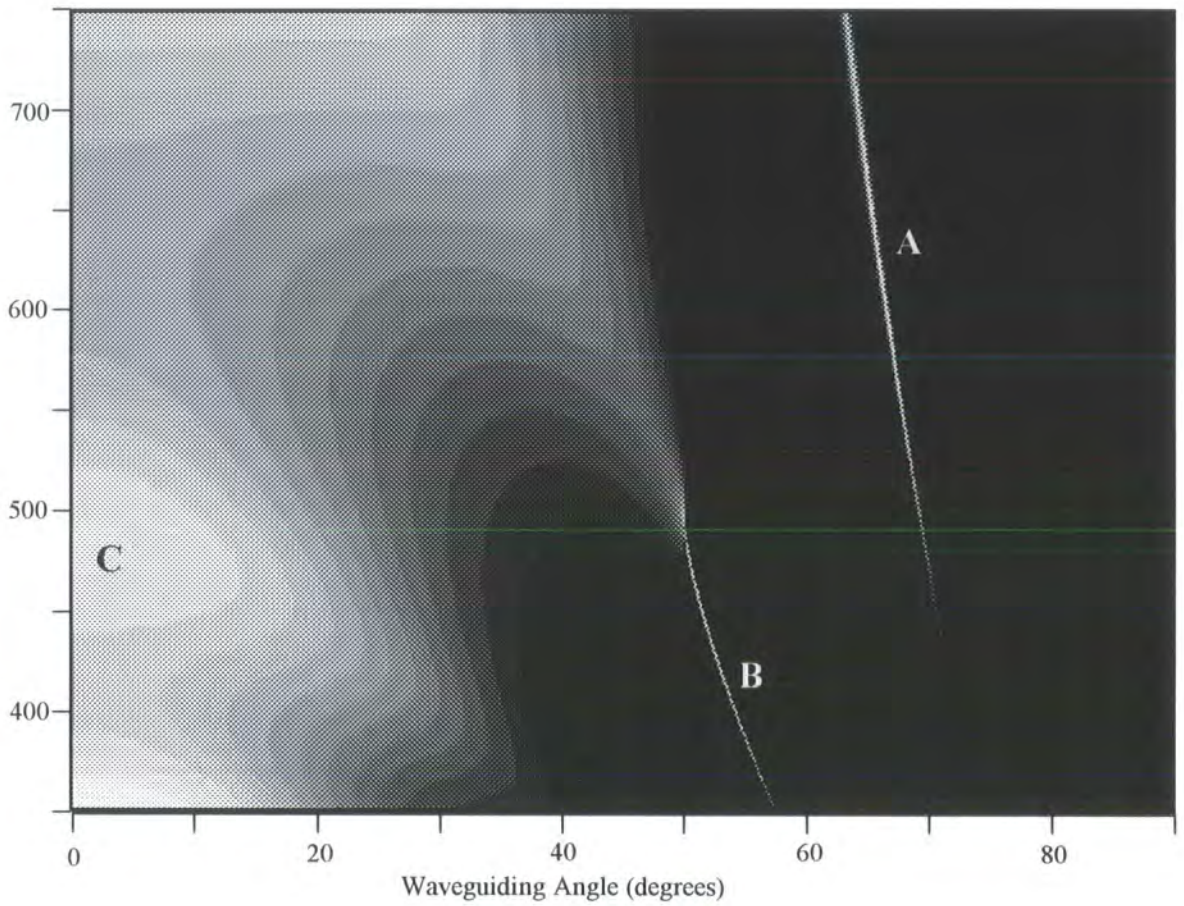

Figure 4.3 *Calculated TE reflectivity from a structure consisting of a top medium with index 1.9 (from which the light is incident), an air gap of thickness 150 nm, and a film of refractive index 1.9 with thickness 250 nm on a substrate of index 1.45. The y axis shows the wavelength in nanometers of the incident light, and the x axis the angle of incidence. The lighter shades show lower reflectivity, with a fractional reflectivity of close to zero plotted pure white and a reflectivity of close to one being plotted in black. The thin white lines marked A and B show regions where light can couple to a*

waveguide mode and reflectivity drops dramatically. Mode A is a true waveguide mode across the visual spectrum, whereas mode B becomes a leaky mode at wavelengths longer than 500 nm. C shows a region where reflectivity is lowered for light at normal incidence.

In this diagram, high reflection is plotted dark and low reflection is plotted in lighter shades. The plots shown here are for TE modes, responsible for most of the phenomena observed in the practical work discussed in this thesis. When light can couple into a waveguide mode, the calculated reflectivity is observed to drop, and this appears here as a white line. It can be seen that for light of wavelength longer than 500 nm, there is a single waveguide mode available in the film, just as was shown in figure 4.2, and a second waveguide mode available for light with wavelength shorter than 500nm. However, unlike the method discussed in section 4.3, this modelling method shows the transition of the second waveguide mode into a 'leaky' mode at wavelengths above 500 nm, for which the waveguiding angle is less than the critical angle between the film and the substrate. The previous simpler model only shows full waveguide modes, as shown in figure 4.2, and cannot account for absorption.

One of the advantages in using this method of modelling thin film structures is that the effects of including metal layers in the structure can be calculated. Figure 4.4 shows the reflectivity from a film with the same thickness and index as that shown in figure 4.4, but with the addition of a layer of gold 2 nm thick on one side of the film and a layer of aluminium 2 nm thick on the other side of the film.

From figure 4.4 it can be seen that the addition of even thin layers of metal (of just 2 nm thickness) has a considerable effect on the mode structure of the film. There is no longer the clear distinction between the 'leaky mode' at waveguiding angles below the film/substrate critical angle, and 'true' waveguide modes beyond this angle that was observed in figure 4.3. The encapsulation of the film in metal effectively makes all the modes 'microcavity' modes. Figure 4.6 shows the effect of increasing the thickness of the metal layers to 15 nm thick, making the structure similar to that which would commonly be used in a LED.

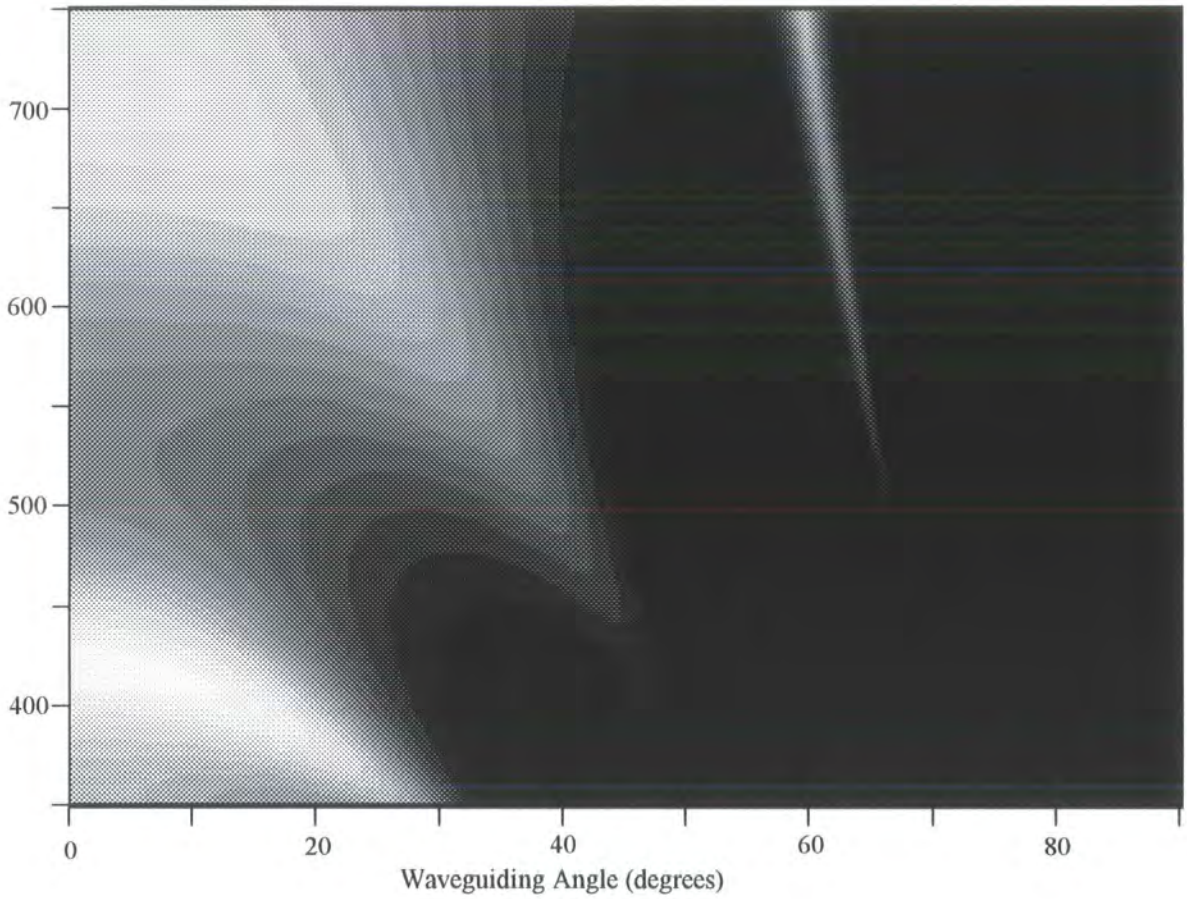

Figure 4.4 *Calculated TE reflectivity from a structure consisting of a top medium with index 1.9 (from which the light is incident), an air gap of thickness 150 nm, a layer of gold 2 nm thick (with complex refractive index taken as 0.47+2.8i) then the film of refractive index 1.9 with thickness 250 nm, followed by a layer of aluminium 2 nm thick (with complex refractive index taken as 1.2+7.3i), on a substrate of index 1.45. The y axis shows the wavelength of the incident light, and the x axis the angle of incidence. The shade plotted varies between white when the fractional reflectivity is close to zero and black where the reflectivity is close to one.*

This example demonstrates the importance of this method of modelling, since it allows the identification of waveguide modes and microcavity modes in multilayer structures, that include layers with finite absorption giving them a complex refractive index.

Comparing figures 4.3, 4.4 and 4.6, it can be seen that the cavity modes gradually shift to smaller waveguiding angles as the metal thickness increases. Modes propagating in the film are able to penetrate less distance into the metal layers than is the case with dielectric boundary layers. Thus in effect, the metal layers can be interpreted as making the effective thickness of the cavity smaller.

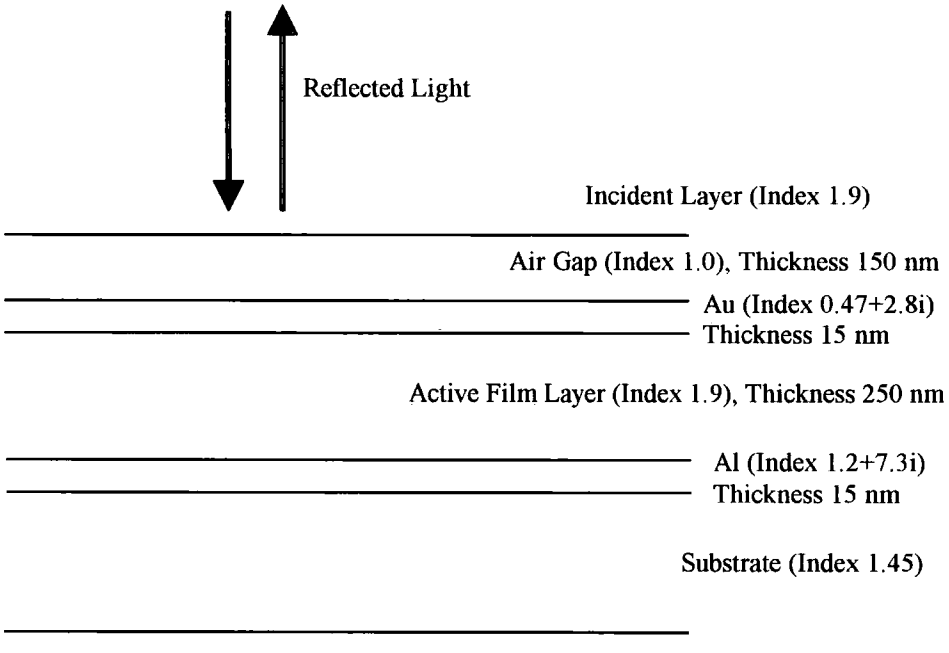

Figure 4.5 *Structure for which reflectivity is analysed theoretically in figure 4.6.*

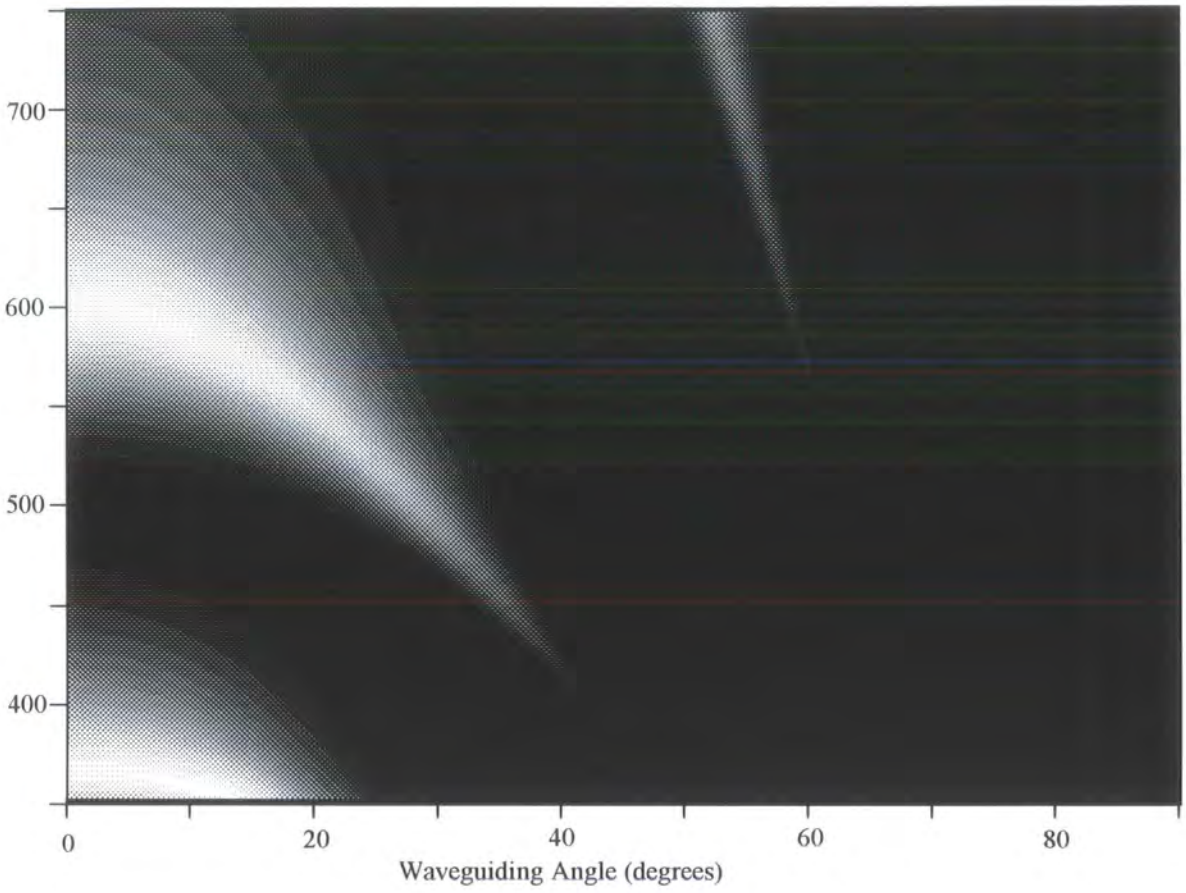

Figure 4.6 *Calculated TE reflectivity from a structure consisting of a top medium with index 1.9 (from which the light is incident), an air gap of thickness 150 nm, a layer of gold with thickness 15 nm (with complex refractive index taken as 0.47+2.8i) then the film of refractive index 1.9 with thickness 250 nm, followed by a layer of aluminium with thickness 15 nm (with complex refractive index taken as 1.2+7.3i), on a substrate of index 1.45 (See figure 4.5 for a diagram of this structure). The y axis shows the wavelength of the incident light in nanometers, and the x axis the angle of incidence. Regions of low reflectivity are plotted in white.*

The subroutine written to optimise layered structures to maximise cavity modes at specific angles was originally written with the intention of designing optically optimised planar LED structures. It was later found that investigating non planar structures was providing more novel results. Structures built up on sinusoidal gratings are the focus of most of the work in this thesis. These structures are difficult to model, however it is reasonable to assume that when the sinusoidal grating is weak, then it can be considered as a slight deviation from the planar case, and thus the same

methods of modelling can be used to understand some of the effects. The modelling program described here is successfully used in chapter seven to model emission from a conjugated polymer film on a weak metal grating.

Two specific uses of gratings when applied to structures that contain waveguide modes are to provide band gaps (or feedback using the band edges in laser applications), or to scatter waveguided light from the film. It is found that the scattering effect allows waveguided light to be scattered into the normal direction when the effective wavelength of the waveguide mode is identical to the period of the grating. The bandgap effect, which has the potential to block emission into waveguide modes, occurs for grating periods of half the wavelength of the propagating mode that is to be blocked. Clearly, in both cases, it is important to be able to design a structure that has modes with effective wavelengths appropriate for the grating that is available.

The optimisation routine was found to be suitable for designing structures that maximise cavity modes for the desired effective modal wavelength for any desired free space wavelength of light. In other words, the program can be used to design LEDs with weak corrugations that scatter the desired colour into the forward viewing direction. The program could also be used to design corrugated structures that inhibit the emission of certain colours using bandgap effects.

The most important subroutine from the modelling computer program, used to calculate reflection and transmission from a stack of thin films with complex refractive index, is listed in the appendix of this thesis.

---

[1] P. K. Tien, Applied Optics 10, 11, 2395 (1971)

[2] N. C. Greenham, R. H. Friend, D. D. C. Bradley, Advanced Materials 6 (6): 491-494 (1994)

[3] J. S. Kim, P. K. H. Ho, N. C. Greenham, R. H. Friend, Journal of Applied Physics 88 (2): 1073-1081 (2000)

[4] Born & Wolf, Principles of Optics, Pergamon (1980)

[5] H. A. Macleod, Thin Film Optical Filters (2nd edn), Adam Hilger (1986)

Chapter 5

Refractive Index Measurement

5.1 Introduction

In chapter four it was shown that it is vital to know the refractive index of all the materials used in an optical device in order to predict its photonic properties. In particular it was shown that a planar LED with an emissive layer that has an unusually high refractive index can suffer a considerable loss of efficiency due to wave guiding effects. The conjugated polymers that are investigated in this thesis are quite novel materials, and although estimates of refractive indices have been made for some materials[1,2], prior to this work no definitive measurement of refractive index had been made across the entire optical wavelength range for all the materials. It should also be noted that the refractive index of these materials might be expected to vary somewhat depending on the method used to deposit the material on a substrate.

It is found that measurement of refractive index of conjugated polymers that have been spin coated onto substrates is not straightforward. Although the techniques that are used in this work are established techniques, it should be noted that there are experimental complications that make the measurements discussed in this chapter non trivial. In particular, the very limited supply of material available for testing combined with its unusual complex refractive index and birefringence complicate matters.

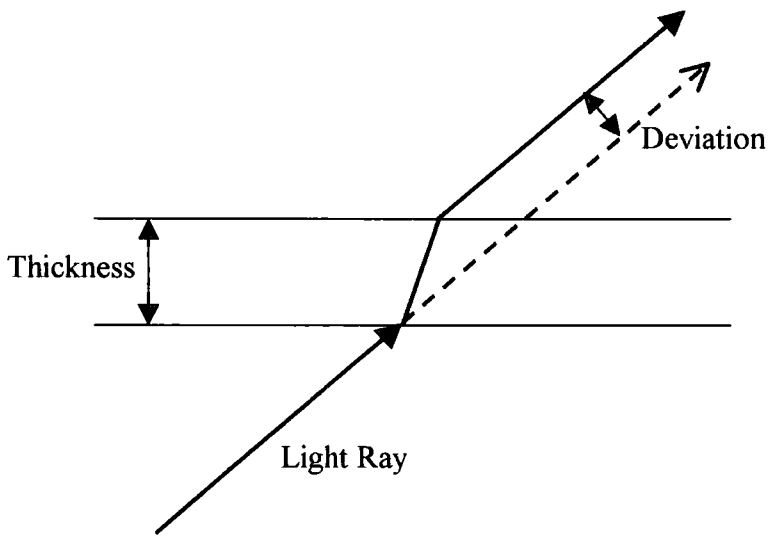

Figure 5.1 *A Light ray passing through a thin film is deviated only by a small amount.*

The standard method of measurement of refractive index for a bulk sample of material is to measure the deviation in angle of a light ray as it passes through an interface. If a sample is available only as a thin film this method will not produce a measurable deviation of a light ray.

Since the samples investigated here are deposited as thin films with a usual thickness in the order of hundreds of microns, it would be almost impossible to measure the deviation of a light ray passing through them with any accuracy. Performing the measurement on a bulk sample, or at least a thicker film would be prohibitively expensive since the materials under investigation are produced only in small quantities at present.

It is intuitive to expect that the polymeric chains will tend towards being parallel to the surface of the substrate[3] in the same way that cooked spaghetti dropped onto a plate would tend to lie reasonably flat. Importantly, this would imply that delocalised electrons would be more mobile parallel to the substrate than perpendicular to the substrate, causing the sample to be birefringent. Since there is only one axis in which the electrons have reduced mobility (i.e. perpendicular to the substrate), the birefringence is negative uniaxial. Light passing through the polymer observes a lower refractive index if its electric field vector is perpendicular to the substrate (TM) and a higher refractive index if its electric field vector is parallel to the substrate (TE). In this chapter the methods used to measure the refractive index of conjugated polymer films will be discussed, and results compared. Methods used included prism coupling and the analysis of reflectivity data from a sample over a range of angles.

5.2 Prism Coupling to Waveguide Modes

An established method of measuring the refractive index and absorption of thin films is to analyse the modes of waveguided light that can propagate in the film[4]. From the theory discussed in chapter four it is known that a film with reasonably low absorption and thickness on the optical wavelength scale will support distinct waveguide modes. The internal waveguiding angle (and the effective wave vector) of each mode depends on the wavelength of the light coupled into the film, and the refractive index and thickness of the film. Identifying the waveguide modes thus

allows us to calculate the refractive index of the film for the specific wavelength of light that is coupled into the waveguide mode.

Coupling externally generated light into a waveguide mode requires a technique that will allow the wavevector of the free light to match the wavevector of the waveguide mode in the direction of propagation. One method of achieving this is to use a prism. When light is totally internally reflected from a surface of the prism, an evanescent field will extend slightly beyond that surface. If a thin film is held close to that surface, with an air gap of a fraction of a wavelength of light, the evanescent field will overlap with the film, allowing some of the light cross the gap and be channelled into the waveguide mode. This is the optical equivalent of the quantum tunnelling effect that is often discussed in the context of particles. If all the waveguided modes in a film are to be accessed, then a prism with a higher refractive index than the thin film under investigation is required. Prior to the work conducted here, it was believed that conjugated polymers were likely to have a refractive index[5] in the region of 2. This means that a prism with refractive index substantially higher than 2 was required. Transparent materials with a refractive index higher than 2 are not common (or cheap), however a prism made from rutile, was found to be suitable to couple laser light into sample films of various conjugated polymers.

5.2.1 Orientation of Birefringent Rutile Prism

Like the conjugated polymers under investigation, rutile is also a birefringent material. The birefringence of rutile is positive uniaxial, which means that it has one axis (the optic axis) along which its constituent electrons have unusually high polarisability. Polarized light that passes through rutile so that the electric field component of the light is parallel to the optic axis will be affected by the materials extraordinary refractive index (n_e) of 2.903. Light polarized with electric vector perpendicular to the optic axis will act according to the material's ordinary refractive index (n_o) of 2.616. The refractive indices n_e and n_o for the prism used in this work was checked by measuring the Brewster angle of reflection for an incident laser beam.

In order to be able to access all the TE waveguide modes that might be expected to be exist in a film which is expected to have a high TE refractive index, it makes sense to use the highest index available from the prism material for TE modes.

To this end the prism was cut so that its optic axis was parallel to all of its rectangular surfaces. If the experiment is set up so that the propagation direction of all the light rays are in the plane perpendicular to the optical axis of the prism (as shown in figures 5.2 and 5.3), then we only need to consider the extraordinary prism index n_e for TE modes and the ordinary index n_o for TM modes. For any light rays outside this plane the effective prism index will vary with angle, which would make the mathematical analysis rather more complicated.

In order to maximise the efficiency of the coupling into the waveguide modes, it is important to control the size of the air gap between the film and prism with reasonable sensitivity. In this experiment the prism was pressed lightly onto the film with a clamp. The clamp jaw pressing upwards on the substrate has a small area of contact with the substrate. The slight natural flexibility of the silica substrate means that the pressure of the clamp can be adjusted until there is small coupling spot in the centre of the film where the separation between prism and film is a fraction of a wavelength. The coupling spot appears as a slight darkening of film colour with a size on the scale of a couple of millimetres.

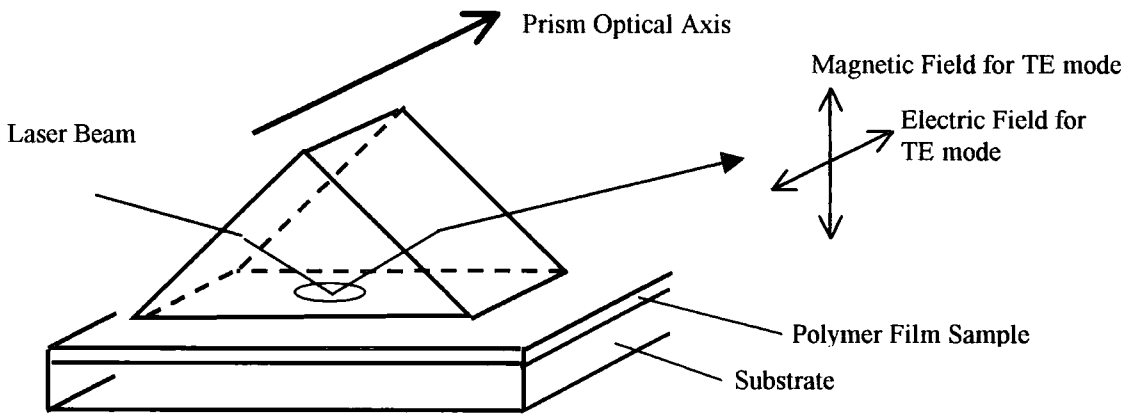

Fig 5.2 *Experimental orientation of rutile prism used to couple light into conjugated polymer film. The light entering the prism is aligned to strike the coupling spot.*

When light incident on the coupling spot is able to couple to a waveguide mode, the power of the reflected beam drops dramatically. Also in the case of the luminescent materials investigated here, the coupling spot will glow brightly. By varying the angle of incidence of the laser light ray systematically, it is possible to map out all the waveguide modes that exist within the film.

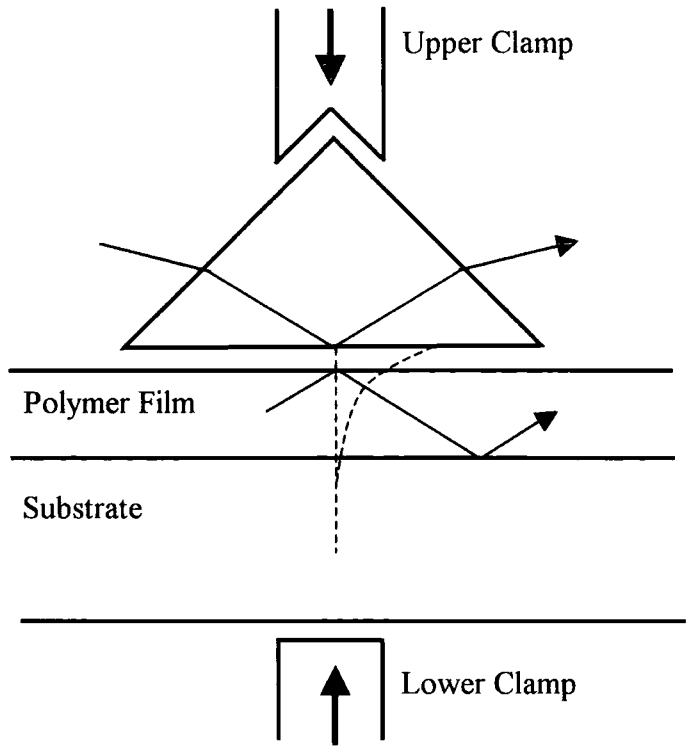

Figure 5.3 *Using a prism to couple light into a waveguide mode. A substantial fraction of light that would normally be totally internally reflected at the lower surface of the prism is able to 'tunnel' into the film below if the air gap is sufficiently small.*

5.2.2 Internal Reflections Within Prism

The prism used for the waveguiding experiments described here was a right angled prism, with an angle of 45 degrees between the base of the prism and the other two faces (as shown in figure 5.2). The base of the prism measured only 8mm, this limitation being entirely due to the high cost of Rutile. There are several difficulties involved in using a prism of such small size and high refractive index. When light is incident onto the surface of a standard glass prism (of index in the region of 1.5) at normal incidence, approximately 4% of the light will be reflected, an amount that can be ignored for many practical applications. For light incident on a rutile/air interface at normal incidence, the minimum amount of reflected light will be 19% (assuming the lowest index of the rutile of 2.6). For non normal angles of incidence the amount

of reflected light will usually be much higher. This means that light entering the prism and making multiple internal reflections within the prism cannot be ignored. Another interesting point to note is that due to the high refractive index, light cannot enter the prism though one of the rectangular prism faces and exit though another rectangular face without being totally internally reflected from one of the faces at least once (i.e. light cannot pass directly through the prim in normal usage).

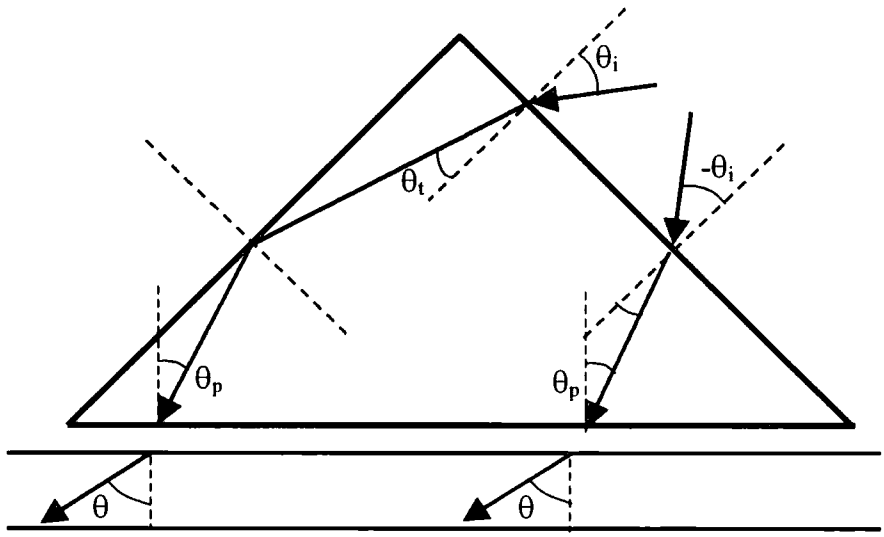

Figure 5.4 *By allowing a light ray to internally reflect from a prism face, it can be shown that light entering the prism at angles of θ or -θ to the normal of the prism face can both strike the prism base at the same angle.*

It was found that in order to ensure that the incident laser beam did not hit the clamp holding the prism (a problem enhanced by the small prism size), it was easier to allow the laser beam to make one internal reflection from a prism surface before striking the film coupling spot. Measuring the angle of incidence with respect to the prism surface normal and taking a clockwise rotation of the beam as a positive angle (as shown in figure 5.4) , it can be seen that this allows us to reverse the sign of the angle of incidence θ_i while keeping the angle that the beam strikes the prism base (θ_p) the same. It should be noted that no matter how many internal reflections of the light ray occur within the prism, the light ray can only strike that prism base at one of two possible angles. With some simple geometry it can be shown that if a light ray entering the prism at an angle θ_i that internally reflects from the side faces (not

counting reflections from the prism base) an odd number of times, it will always hit the prism base at the same angle θ_p, however after an even number of reflections it will hit the base at an angle of $(90-\theta_p)$ degrees. This situation is exactly reversed for a ray entering the prism at an angle of $-\theta_I$, requiring an even number of reflections to hit the base at θ_p. Clearly care is required in matching up angles for different orders of waveguided mode in situations where multiple waveguide modes exist.

5.2.3 Experimental Measurements for TE Modes

Having found a method of coupling light into a waveguide mode in a thin film for any waveguiding angle, we need a method of scanning through all angles, identifying waveguide modes, and also a method of using this data to determine the refractive index of the films. In the work described here, the prism, test film and clamp were all fixed onto an optical rotation stage, allowing full rotation in the horizontal plane (the prism being orientated so its optical axis would always be vertical), and also allowing small lateral movements of sample position to be made using screw mechanisms. A HeNe laser was shone through the prism, and the light was able to couple to waveguide modes when the sample was correctly orientated. A precise measurement of angle could then be made. In the measurements here, an angle of zero was defined as the position where the light reflected from the prism face would reflect straight back to the laser ($\theta_i=0$). A clockwise rotation is defined as positive as shown in figure 5.4, and it was also found that allowing one internal reflection was most practical for accessing most modes. Using a quarter wave plate and a polariser with the laser allowed the laser light to be set to TE or TM with respect to the sample.

A standard method of identifying angles that couple to modes is to use a second prism to couple light out the waveguide mode again at a distance further down the film. This method is suitable for studying samples that have a low absorption (and can be used to measure that absorption). It was found that the absorption of the conjugated polymers was too strong to allow light to propagate far down the film. A method more effective for samples with slightly higher absorption is to study the light reflected back from the coupling spot. Clearly when incident light is able to couple to a waveguide mode, the reflected light is expected to drop dramatically. This method

was used successfully to identify waveguide modes in this work. Also, since the samples were all luminescent, it was found that the coupling spot would glow when light was coupled into a mode, since the sample was able to absorb and re-emit the light. The HeNe laser used was able to emit red light at 632.8 nm, and orange light at 611.9 nm. The substrates used for all the experiments here were made from silica with an index of 1.45. Using a substrate with a reasonably low refractive index allows a maximum number of waveguide modes, as shown in chapter four.

To interpret the results, a graph was plotted for each film showing the possible thickness of film that would allow a waveguide mode at the angle measured experimentally, against possible refractive indices of the film. For each waveguide mode observed in the sample, one line could be plotted on the graph. For TE modes all lines should intersect at a point giving the correct refractive index and thickness of the film. The waveguide equation derived in chapter four was:

$$\lambda(\theta) = \frac{2\cdot\pi\cdot W\cdot n_s\cdot\cos(\theta)}{\pi\cdot m + \Phi_{gte}(\theta) + \Phi_{ate}(\theta)} \qquad (5-1)$$

Where λ is the wavelength of light that is able to waveguide with internal angle θ for a film of thickness W and the sample's refractive index n_s. We can rearrange this equation to give W as a function of n_s:

$$W(n_s) = \frac{1}{2}\lambda\,\frac{\left(\pi\ m + \Phi_{ate}(\theta, n_s) + \Phi_{gte}(\theta, n_s)\right)}{\left(\pi\ n_s\cos(\theta(n_s))\right)} \qquad (5-2)$$

Where Φ designates the Goos-Haenchen shifts at the surface interfaces of the film, as defined in chapter four. Φ is dependent on the index of the binding layers, and will be different for TE and TM modes. The internal waveguiding angle θ can be expressed as a function of the sample's refractive index n_s once the angle at which the incident light ray strikes the base of the prism has been determined by analysing the path of the light ray through the prism. Thus Φ can be expressed entirely as a function of n_s.

Measurements were taken for a range of samples of varying thickness. In general the most convincing results were obtained from fairly thick samples, since more modes can be observed. A slight difficulty with spinning thick samples is that a more concentrated solution was required to increase viscosity. Availability of materials placed an upper limit on solution concentration. Also it was noticeable that thicker films were usually thicker at the edges than in the centre, although this problem was reduced by using large substrates. For each substrate, measurements were made at several positions on the film. Some sample results for reasonably thick films are shown here.

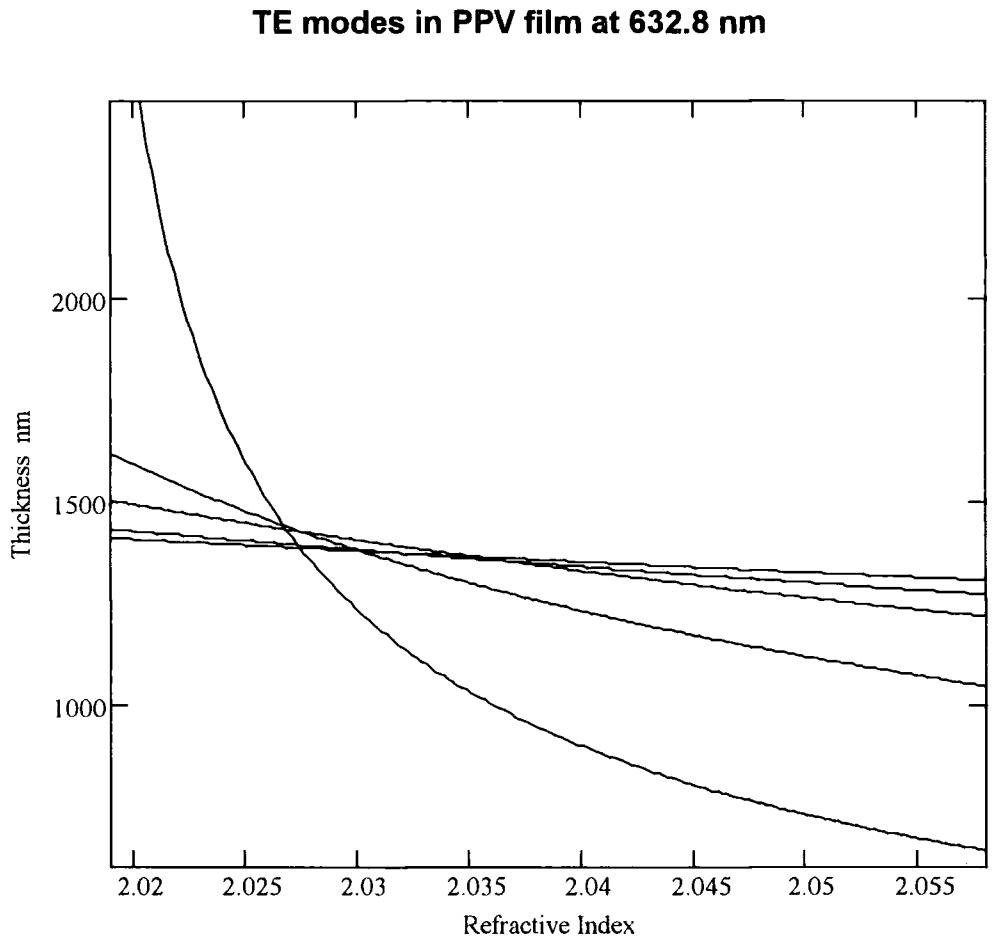

Graph 5.1 *This graph shows five waveguide modes that were observed in a film of PPV with a thickness measured on an alpha step to be 1.43μm. The modes were excited by the laser when the angle of incidence at the prism face (θ_i) was measured (in degrees) to be: 2.9, 5.3, 9.4, 15.8 and 24.1. The laser wavelength was 632.8 nm. The true TE refractive index of the film appears to lie in the region between 2.027 and 2.034 (The intersection of the lines). The graph is plotted using formula (5-2).*

In general it was found that a film thickness of approximately half a micron was ideal for waveguiding experiments. This thickness allows at least three waveguide modes to be observed so that the intersection of the three plotted lines provides extra evidence that the data has been correctly interpreted. Although thicker films can provide more data, it proved difficult to get a reliable intersection for the higher order waveguide modes. Conjugated polymer films thicker than a micron are not commonly used in LED applications. Graphs 5.1 and 5.2 show results from one of the thickest PPV films measured using red and orange light. The limit to the accuracy of the measurement can be estimated by observing the range of positions for the points of intersection of the lines

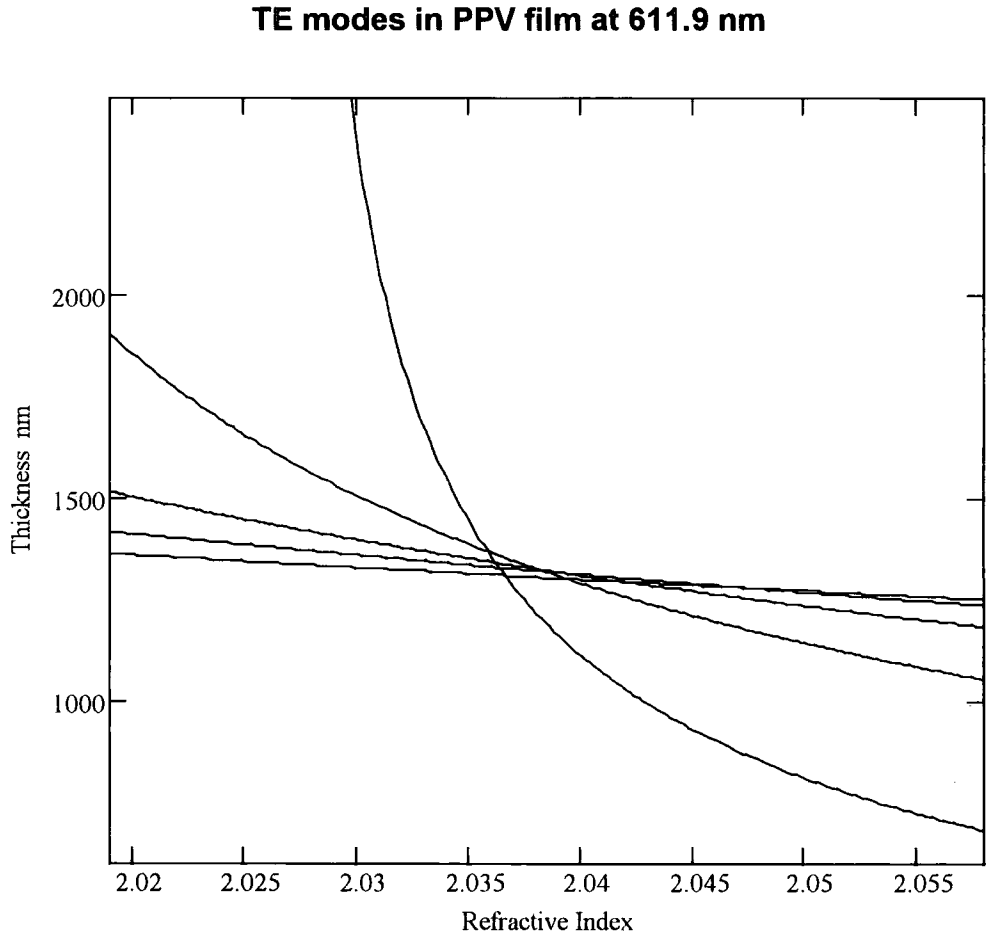

Graph 5.2 *This graph shows five modes coupled into the same film of PPV shown in graph 5.1, but using an orange laser line from the HeNe laser (611.9 nm). Some idea of the dispersion of PPV can be gained since the refractive index here appears to lie in the region between 2.036 and 2.04 (the region where the lines intersect).*

TE waveguide modes were analysed for a series of samples of various thickness using the materials PPV, MEH-PPV, and PPY. The results are summarised below in table 5.1.

	Red 633 nm	Yellow 611.9 nm
PPV	2.03 (+/-0.02)	2.04 (+/-0.02)
MEH-PPV	1.90 (+/-0.02)	1.93 (+/-0.02)
PPY (polypyridine)	2.01 (+/-0.05)	1.99 (+/-0.05)

Table 5.1 *Refractive indices of various conjugated polymers as determined using waveguiding experiments.*

It had been intended to use this method to evaluate the refractive index of these materials over a larger range of wavelengths than given here. Coupling blue and green light into the films with the prism was attempted using an Argon Ion laser. However, it was found that at these wavelengths the light was absorbed by the film much too quickly for it to exist as a waveguide mode. Another alternative that was given consideration was to use light from a bulb passed through a monochromator (allowing a continuous spectrum of wavelengths) rather than a laser. However it was found that getting a narrow beam of sufficient power to allow accurate measurements was very difficult.

5.2.4 Analysis of TM Modes

Analysing data from TM waveguide modes is more complicated than for TE mode. For a p-polarised light wave propagating through a birefringent conjugated polymer film, the effective refractive index of the film will be dependent on the angle of propagation of the light. Light trapped in a TM waveguide mode propagating within a film will experience a different film refractive index dependent on the internal waveguiding angle θ. Graphs 3a and 3b show TE and TM modes plotted for a film of MEH-PPV. The thickness of this film was measured to be 900 nm (±10nm) on the alpha step. This agrees well with the thickness given by the mode intersections in graph 3a. The TE refractive index suggested by this graph is approximately 1.9. Graph 3b shows two TM modes, and their intersection with the line showing the thickness of the film that was previously measured (from the TE mode). The points of

intersection with the dashed line (the previously measured thickness) show the effective index of the film for the two modes.

3a) TE modes in MEH-PPV film at 6 32.8 nm

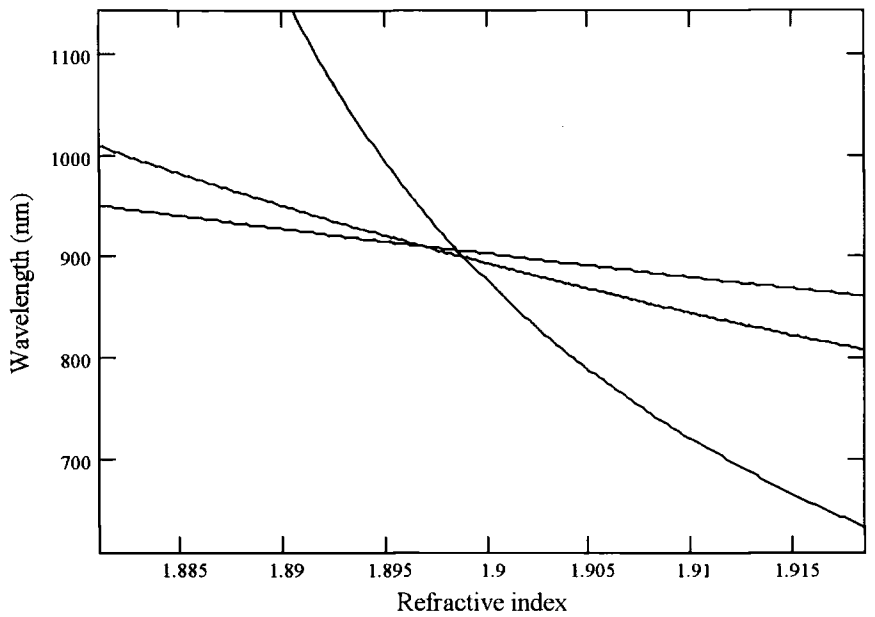

3b) TM modes in MEH-PPV film at 6 32.8 nm

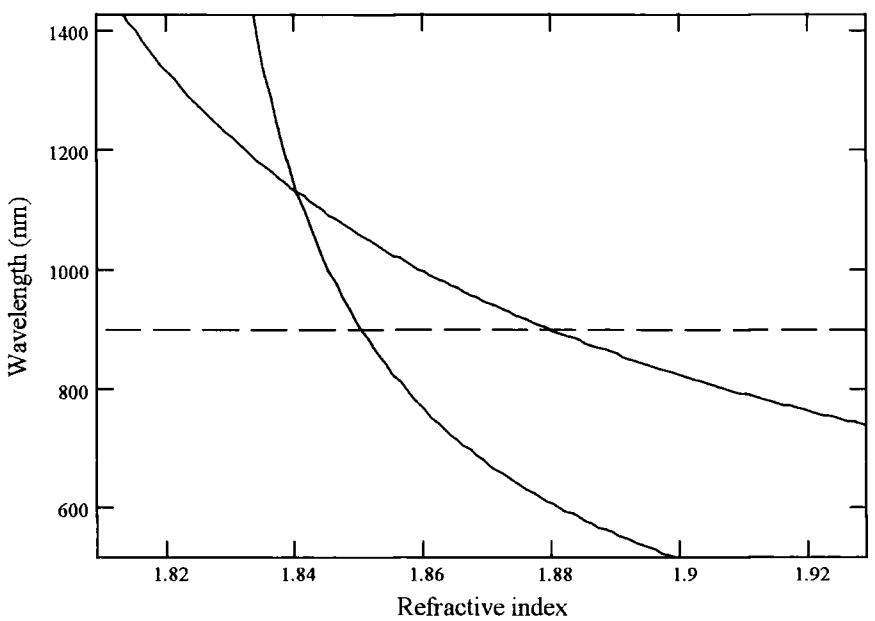

Graph 5.3a, 5.3b *These Graphs show TE and TM modes for a film of MEH-PPV 900nm thick. The angles of incidence (θ_i) on the prism were 14.0, 19.7 and 20.4 for the three TE modes in graph 3a. For the two TM modes in graph 3b* θ_i *was 18.1 and 22.5. The dashed line shows the film thickness found from the TE plot.*

The data in graph 3a gives a TE film index of 1.898 for the MEH-PPV film. Graph 3b gives a TM mode effective sample index of 1.85 for the first waveguide mode. The internal waveguiding angle (θ) for this mode was calculated to be 80°. The film index for the second TM mode for the film in graph 3b is 1.88, for a calculated internal waveguide angle (θ) of 70°. These results suggest that the TM index becomes closer to the TE index as θ becomes smaller, a result that would be expected intuitively. Repeating this process for the PPV film (TE index 2.037) shown in graphs 5.1 and 5.2 gives the results for TM modes: θ=83° gives a sample refractive index n_s of 1.846, θ=76.9° gives an index of n_s 1.855 and θ=70° gives n_s=1.861.

The variation of film refractive index with propagation direction for TM modes means that it is harder to confirm the accuracy results given here than is the case for TE modes. In general this method of analysis was found to be suitable for films that have reasonably low or moderate absorption. For the conjugated polymers tested here it provided reliable results for red and orange light. In order to get information about refractive index at blue and green wavelengths, where the absorption of these materials increases dramatically, alternative techniques were required.

5.3 Index Fitting to Reflectivity Measurements

Another method that can use waveguide modes to obtain information about the complex refractive index of materials in thin films is to perform detailed analysis of the reflectivity of a sample for a range of angles and wavelengths. The data can then be compared to values obtained from the boundary condition modelling discussed in chapter four. By using a iterative method of trial and error, it is possible to find values for refractive index and absorption of a sample that very closely fit the reflectivity data measured experimentally.

In general reflectivity data is easier to fit if it contains distinctive features. For example, if at certain angles of incidence light is able to couple to waveguide modes, we expect the reflectivity of the sample to drop substantially. Having one or more clear features like this makes fitting the complex index data easier and the results more precise.

In theory it ought to be possible to analyse all the data obtained using the rutile prism (as used in the experiments discussed in the first half of this chapter) by performing detailed reflectivity analysis in this way. However there is a problem with the prism coupling method in this situation. In order to model the reflectivity accurately it is vital to remove as many of the unknown variables as possible, leaving only those that we are trying to determine, in this case the complex refractive index of the conjugated polymer under investigation. When we couple light into a film using a prism and a small air gap, the size of the air gap between the prism and the film is very difficult to measure, usually being in the order of a fraction of a wavelength of light. The reflectivity of the sample measured through the prism would be highly sensitive to the size of this air gap. Furthermore the size of the air gap might well be expected to vary across the coupling spot due to any slight bending of the substrate, or unevenness of the film surface. Clearly it would be helpful to find a method of coupling light into a waveguide mode that avoids using an air gap.

5.3.1 The Analysis of Leaky Waveguide Modes

To avoid the problems discussed above, it is often easier to analyse leaky waveguide modes. By shining light directly onto a film that has been spun onto a flat substrate, we can analyse air modes only. By varying the angle of incidence of the light it would be possible to observe variations in reflectivity from the sample, but there will be no dramatic sharp features in a graph of reflectivity versus angle. It is possible to obtain more dramatic features by evaporating thin layers of metal on both sides of the polymer, effectively creating a microcavity between two metallic mirrors (Clearly one metal layer needs to be thin enough to allow light into and out of the film). However, this would not allow us to couple light into the sample at any angle greater than the critical angle between the polymer and air. In order to access a greater range of angles in the polymer film, it is necessary to return to using the prism. If we place a prism so that it is in contact with the substrate as shown in figure 5.5, rather than pressed onto the polymer film, then we can access a large range of angles (θ), but avoid the uncertainty involved in the size of the air gap that complicated the experiments described previously. As before, the higher the index of the prism, the greater the range of angles at which the light can be coupled into the film, but only if

the substrate material has a refractive index that is at least as high as the prism. Thus the prism and substrate are ideally made of the same material in order to have the same refractive index. This also means that by using index matching fluid between the prism and substrate, we can ensure that stray reflections from this interface are negligible. If the prism and substrate were both made of rutile, then we could be sure of accessing all possible propagation angles (θ) for light in the film. However in practice the high cost of this material means that buying multiple rutile substrates is not a feasible option. Thus the experiments described here were done using a cheaper silica prism and substrate.

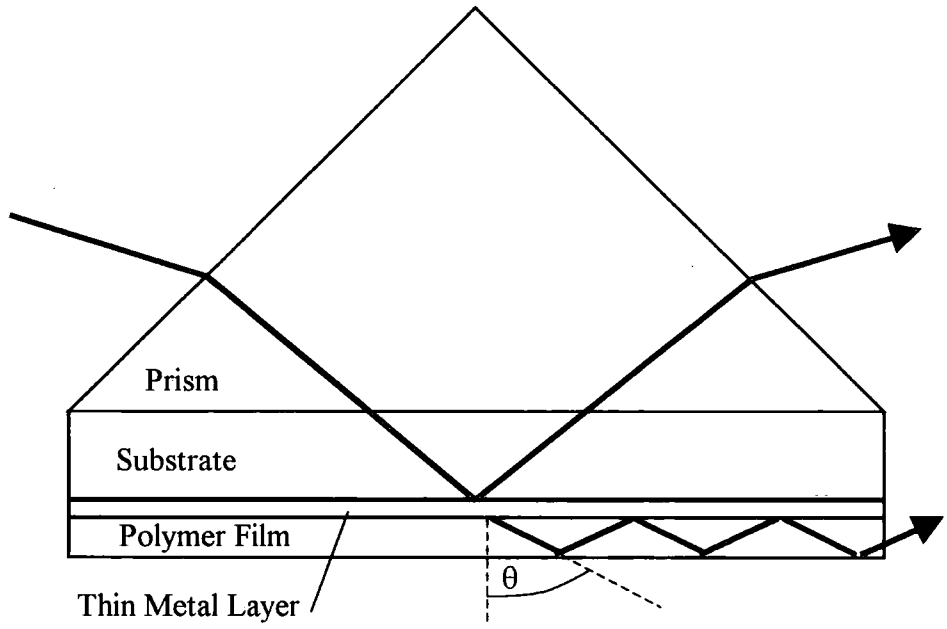

Figure 5.5 *Coupling light into a leaky waveguide mode using a prism in contact with a substrate.*

The structure shown in figure 5.5 was the first structure to have its reflectivity analysed over a range of angles. In this structure there is one metal layer that is deposited onto the silica substrate by evaporation, before the sample polymer film is spun on top. This layer acts as a partially reflecting mirror that helps to confine light in slightly leaky modes within the film. In effect the layer is performing a similar role to the air gap in the earlier experiments, but with the advantage that the metal thickness can be precisely measured and controlled during the evaporation process,

unlike the air gap which was difficult to measure or control. This structure is ideal for examining modes where the waveguiding angle θ is greater than the polymer/air critical angle, but less than the polymer substrate critical angle.

5.3.2 Apparatus for Measuring Reflectivity

In order to make reflectivity analysis an efficient method of obtaining information on materials or structure, it is helpful to make the measurement process automatic. The work described here was carried out during a visit to the University of Exeter, in collaboration with Dr W.L.Barnes.

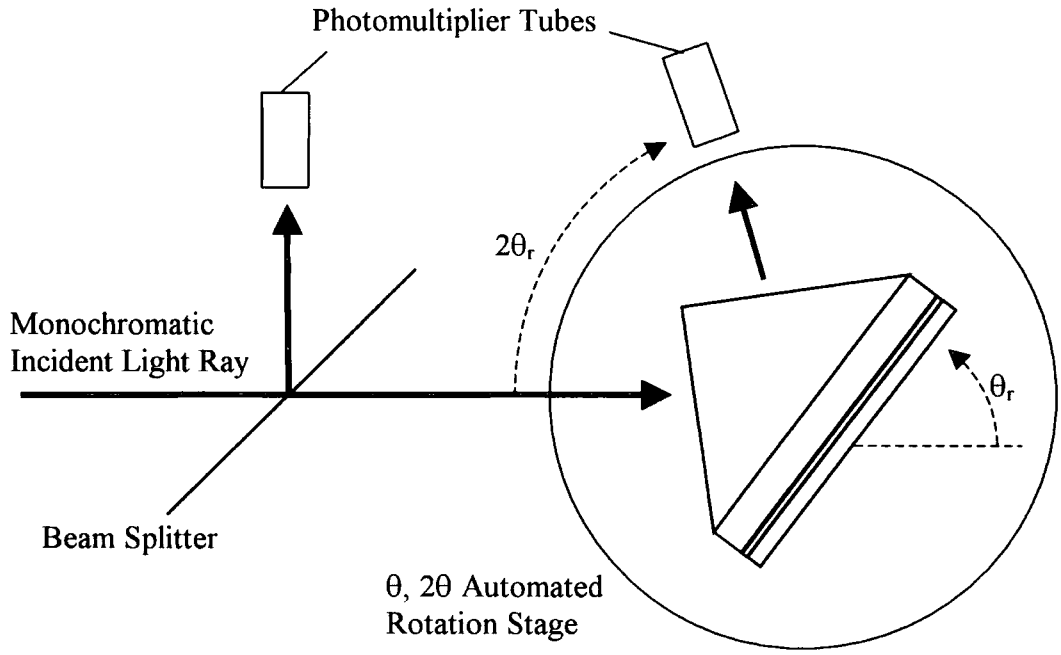

Figure 5.6 *Apparatus for measuring the reflectivity of a sample over a range of angles*

The apparatus used for these measurements is illustrated in figure 5.6. Monochromatic light of various wavelengths was reflected from the sample and detected using a photomultiplier tube, held in the correct position using a θ, 2θ rotation stage. The incident light was split at a beam splitter, allowing a reference beam to be detected at a separate photomultiplier tube. Monitoring the power of the reference beam allowed measurements to be adjusted to account for any fluctuations in power of the incident light. The rotation stage was controlled by a computer which

also logged the variations in power of the reflected light for the different angles of the sample rotation (θ_r). The apparatus was designed so that the light incident on the sample could be generated by a bulb, and then passed through a monochromator. However, the clearest results were obtained using light generated with a laser, allowing much greater power, although limiting the wavelengths at which measurements could be made.

5.3.3 Analysis of Reflectivity Measurement Results

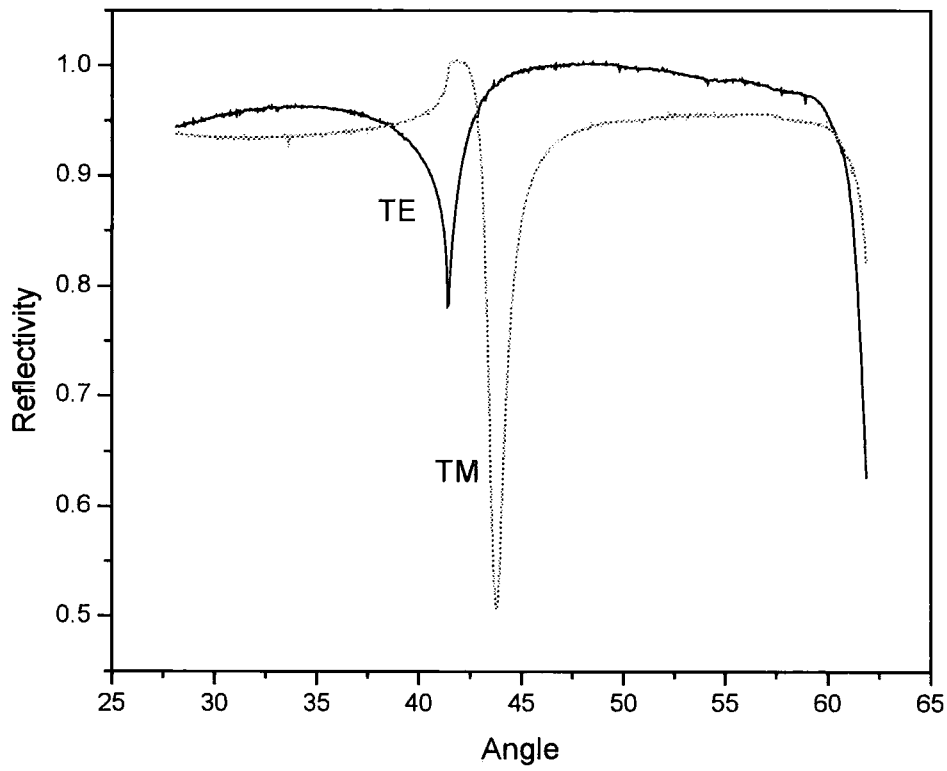

Figure 5.7 *Reflectivity from a film of PPV 250 nm thick on 40 nm Al layer using a 612 nm HeNe laser. The reflectivity is given as a fraction of the light that enters the substrate. The angle is the propagation angle within the silica substrate measured with respect to the normal.*

A reflectivity plot from a typical film is shown in figure 5.7. The light was coupled using the prism behind the substrate as shown in figure 5.5. There is one waveguide mode apparent for TE orientation and one for TM orientation in this plot.

In general the troughs that appear in reflectivity graphs when incident light is able to couple into a waveguide mode will have a position that is strongly dependent on the thickness and index of the film, and a width that is strongly dependent on the absorption on the film. Thus in theory, for a film of known thickness, one waveguide mode is sufficient to evaluate the real and imaginary components of the film index (n and k). In practice however it is preferable to have multiple waveguide modes visible in a reflection plot in order to get a reliable fit for all the parameters of a film under test. For the PPV film shown in figure 5.7 the modes that are visible are consistent with the refractive index values at 612 nm shown in table 5.1, however for this film it was not possible to show more that one TE mode. The reason for this limitation was that the thickness of the substrate limited the angles at which the light rays that had passed through the prism were able to strike the polymer film.

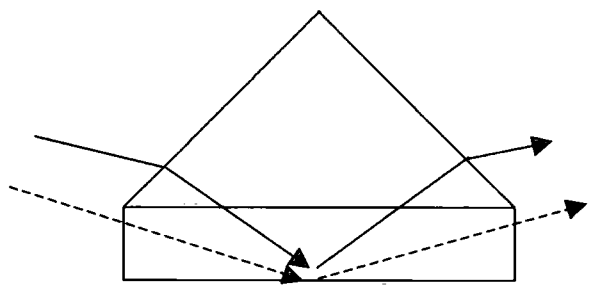

Figure 5.8 *The range of angles that can be accessed using the prism is limited by the thickness of the substrate.*

In order to access as many possible waveguide modes in the films as possible it was decided to spin polymer films directly onto a reasonably high index prism (n_p~1.8). High index prisms had one face coated with a thin layer of gold using evaporation. Films of MEH-PPV were spun onto the gold coated face, with thickness of 250 nm and 175 nm. By using the same iterative process of fitting the reflectivity spectra of the samples to the theoretical model, values of the refractive index and absorption of MEH-PPV were found for a range of wavelengths[6]. The results are shown in figure 5.9.

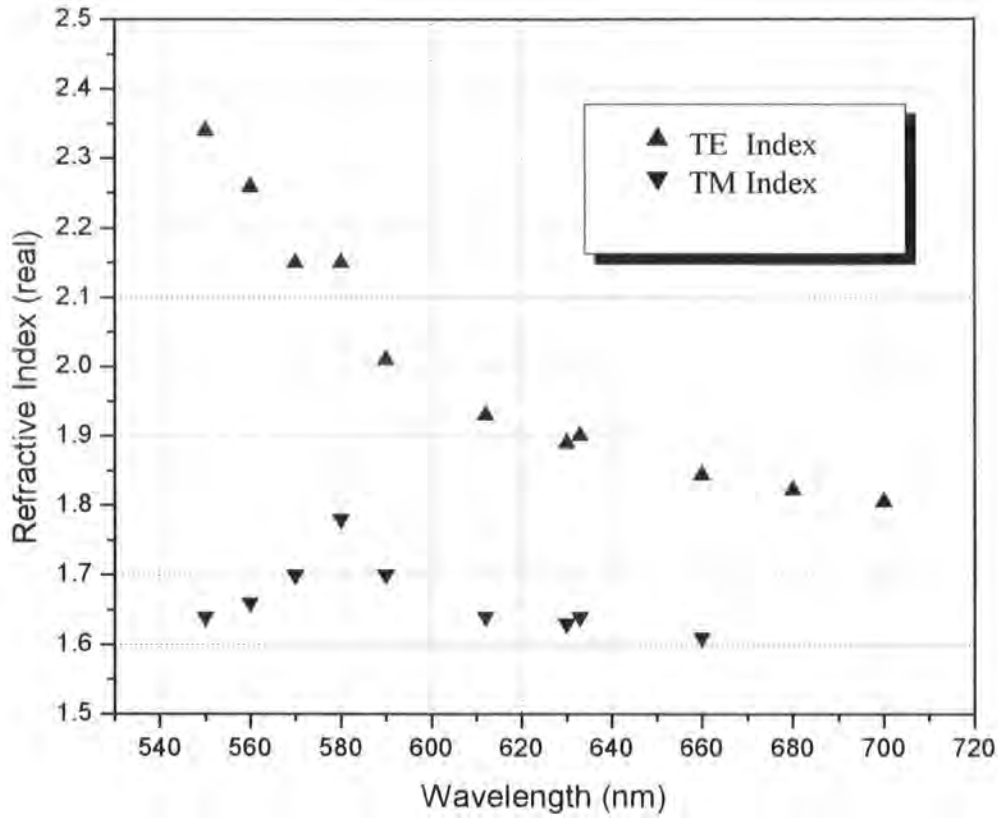

Figure 5.9 *TE and TM indices of MEH-PPV measured using reflection spectra of films spun onto a gold coated prism.*

5.4 Conclusion

From figure 5.9, it can be seen that MEH-PPV in film form is birefringent and highly dispersive. The TE refractive index is higher than 1.8 at the red end of the visual spectrum, and rapidly increases to higher than 2.3 in the green region of the spectrum. Testing the refractive index in the red region of the spectrum proved difficult to perform due to the increased absorption of the films at longer wavelengths (There is further discussion of film absorption in section 6.3.7). The full spectral analysis was performed only for MEH-PPV, while PPV only had its refractive index measured at a couple of wavelengths. However, since the chemical structure of PPV is so similar to MEH-PPV, it is reasonable to assume that it will have similar dispersive properties. The results from the different experiments gave good agreement for refractive index values.

Since the work in this section of the thesis was completed, there has been more investigation carried out on measuring the refractive index of MEH-PPV using ellipsometry[7].

The experiments in this chapter were surprisingly time consuming to perform, but accurate measurements of refractive index is important for LED design. The results gained in this chapter were also important for the analysis of light emission from MEH-PPV films on gratings that is discussed in chapters six and seven.

The MEH-PPV that was used in the work described in this chapter was also used in the experiments described in the remainder of this thesis. It had a purity in excess of ninety nine percent, and was provided by Dr Heinrich Becker at Covion.

---

[1] A. Mathy, K. Ueberhofen, R. Schenk, H. Gregorius, R. Garay, K. Mullen, C. Bubeck, Phys. Rev. B 53, 1 (1996)

[2] H. F. Wittmann, J. Gruner, R. H. Friend, G. W. C. Spencer, S. C. Moratti, A. B. Holmes, Advanced Materials, 7, 6 (1995)

[3] C. Y. Yang, F. Hide, M. A. Diaz-Garcia, A. J. Heeger, Polymer, 39 (11), 2299 (1998)

[4] P. K. Tien, Applied Optics, 10 (11), 2395-2413 (1971)

[5] S. E. Burns, N. C. Greenham, R. H. Friend, Synthetic Metals 76 205-208 (1996)

[6] A. Boudrioua, P. A. Hobson, B. J. Matterson, I. D. W. Samuel, W. L. Barnes, Synthetic Metals 111: 545-547 (2000)

[7] M. Tammer, A. P. Monkman, Advanced Materials 14, 201 (2002)

Chapter 6

Lateral Microstructure

6.1 Introduction

In chapter three, it was shown that the light emission from a film of luminescent material is influenced by the optical properties of the layers that surround it. Examples included the effect of metal layers in LEDs causing reflections and hence interference, which inevitably modifies emission characteristics of these devices. More dramatic microcavity effects have been observed when an emissive layer is bounded on both sides by mirrors, allowing emission to be strongly channelled into particular directions[1].

It is impossible to avoid modifications of light emission caused by interference effects in any planar structure, since wherever there is an interface between two layers with different refractive indices, there will be some reflected light. An important result related to these effects is that a luminescent film of high refractive index will usually have more than half of its light emission channelled into waveguide modes. In designs for simple organic LEDs, waveguided light can often be responsible for a loss of efficiency[2] greater than ninety percent.

In chapter five, measurements of refractive indices of conjugated polymers were made. It was established that they tend to have refractive indices considerably higher than most organic materials, and standard substrate materials such as silica. When films of these materials emit light, whether excited optically, or electrically in an LED structure, reflections at the interfaces will be substantial, causing strong interference effects, and causing a considerable amount of light to be channelled into waveguide modes and substantially absorbed and lost to emission. Although the amount of light channelled into waveguide modes can be modified by using different layered designs, such as microcavity structures, it is impossible to avoid a substantial fraction of emitted light being waveguided, as long as a planar structure is used[3].

A possible method of reducing the amount of light channelled into waveguide modes in a luminescent film is to abandon planar symmetry, and instead use a structure that has been textured. In this chapter, the effect of lateral microstructure on the photoluminescence of conjugated polymers will be investigated.

6.2 Textured Substrates

An alternative that can increase the amount of control that can be exercised over the generated light is to design a structure with at least one interface that has been inscribed with a regular grating. In general, a grating is expected to have a strong effect on light with a wavelength of the same order of magnitude as the grating period.

In order to maximise the effect of a textured interface on the light emission from a layered structure, the interface should be between two layers that have a high index contrast (their refractive indices must be substantially different), and the interface should also be positioned where the optical field is strong for any emission mode that is to be affected. These conditions can be met when luminescent conjugated polymers are deposited onto substrates that have been textured.

6.2.1 Manufacture of Substrates with Gratings

To create a regular textured surface on a substrate, with a period of the same order of magnitude as the wavelength of visible light, is not a trivial task. Indeed such a length scale is shorter than the limit achievable using conventional photolithography. The first method used to generate texture on this length scale, for the substrates used in the work described here, was to coat the top surface of the substrate with photoresist, and expose it to an optical interference pattern. Shipley S1805 photoresist was deposited onto silica substrates by spinning to give a film thickness of 500 nm. The samples were then exposed to an interference pattern generated by splitting and recombining a 457.9 nm laser beam from an argon ion laser. The spatial frequency of the interference pattern was adjusted by setting the angle between the recombining beams, thus allowing the period of the resulting gratings to be accurately controlled. The samples were then developed, exposed to UV radiation, and baked several times in air at temperatures up to 240°C. To generate planar reference samples, an identical process was followed, but without exposing the photoresist to the interference pattern. The first corrugated samples created using this technique were designed to have a roughly sinusoidal surface with a period of 400 nm. The period and quality of the gratings were first checked by measuring the

reflectivity of the grating as a function of angle. The manufacture of the photoresist based gratings was carried out by M. G. Salt and W. L. Barnes at the University of Exeter[4].

6.2.2 Examination of Gratings

Visual examination of the gratings in sunlight or room light allowed the characteristic 'rainbow' pattern associated with a diffraction grating to be observed, when the grating was held in a suitable orientation with respect to the light source and the observer. Since the gratings used here are of shorter period than diffraction gratings often used in optics, it is harder to observe the diffracted light than might be expected. For light at normal incidence with a wavelength longer than the period of the grating, there are no orders of diffracted light to be observed. Only when the grating is rotated about an axis perpendicular to the grating lines (analysed in section 6.4), can scattered orders be observed (Figure 6.1), causing the grating to appear coloured.

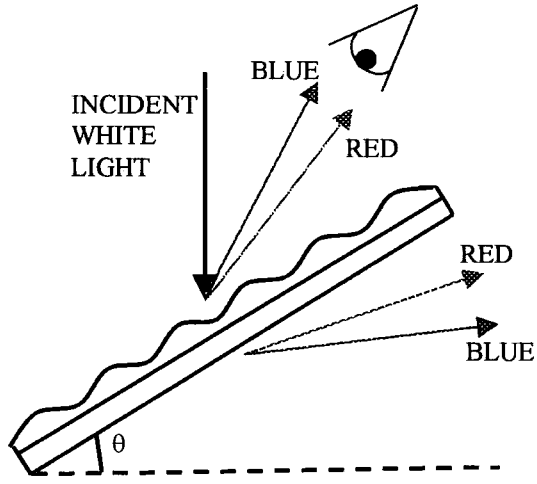

Figure 6.1 *Light scattered by a 400 nm grating causes a 'rainbow' appearance of the grating only when the light source, grating and observer are appropriately positioned. Holding the grating with the light source behind one's shoulder, and then adjusting the grating orientation until scattering is observed allows a rough determination of grating quality.*

6.2.3 Spherical Co-ordinate System

Light rays that are emitted from or incident upon a surface with a grating need to have their propagation direction specified by two angular co-ordinates. For all the results listed here, angles will be given using the spherical co-ordinate scheme shown in figure 6.2. The direction of the grating lines defines the direction of the z axis (ϕ=0), where ϕ is the azimuthal co-ordinate. The x axis is defined to be normal to the substrate (θ=0, ϕ=90°), where θ is the polar co-ordinate. ψ is defined as 90°-ϕ, and thus specifies the angle between a light ray and the xy plane. In the remainder of this thesis, unless otherwise specified, angles referred to in the format (a,b) refer to the angles θ and ψ as defined in this section.

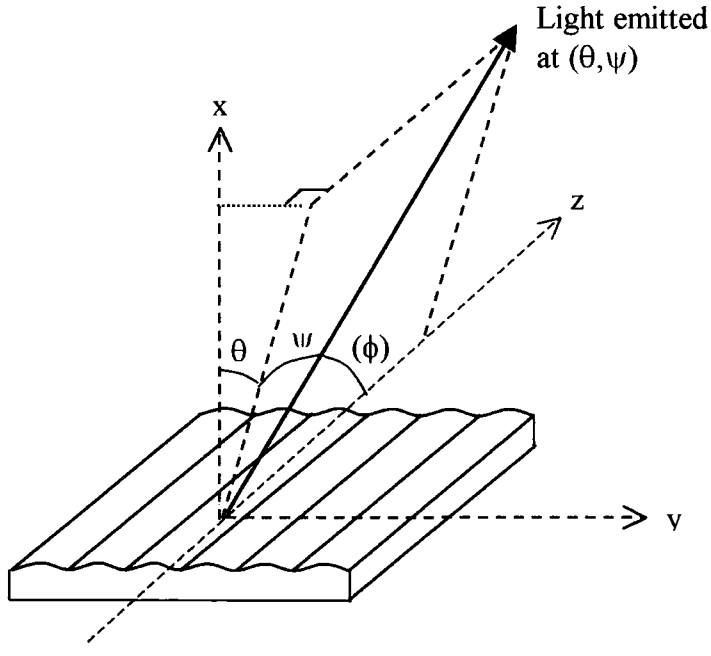

Figure 6.2 *The definition of the spherical co-ordinate system used to specify angles for textured samples with a single grating structure.*

6.2.4 Basic Diffraction conditions

A light ray of wavelength λ, propagating in the ψ=0 plane that is incident on the grating with period p, at an angle θ, will give rise to a first order diffracted light ray if it meets the conditions:

$$\lambda < 2p \qquad (6-1)$$

$$\theta \geq \operatorname{asin}\left(\frac{\lambda}{p} - 1\right) \qquad (6-2)$$

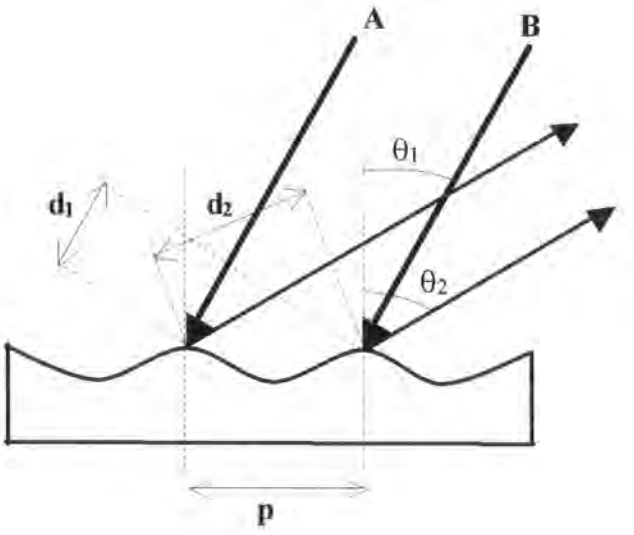

Figure 6.3 *The distances d_1 and d_2 must add to a whole number of wavelengths ($n\lambda$), for the light incident at angle θ_1 to be diffracted into angle θ_2.*

Figure 6.3 shows the geometry used to calculate the diffraction angle for a light ray of wavelength λ that is propagating in the xy plane (ψ=0). On diffraction, the light ray marked A, will be lagging behind ray B by a distance d_1+d_2, where:

$$d_1 = p \sin(\theta_1) \qquad (6-3)$$

$$d_2 = p \sin(\theta_2) \qquad (6-4)$$

The total phase lag d_1+d_2 equals the wavelength of the light for the first order diffracted mode, giving:

$$\sin(\theta_1) + \sin(\theta_2) = \frac{\lambda}{p} \qquad (6-5)$$

Higher order modes would normally scatter in directions for which the phase lag calculated in this way equals a whole number of wavelengths. For visible light and the grating periods used here, they are not present. It should also be noted that a grating with a perfectly sinusoidal surface will only produce a first order diffracted light ray (A sinusoidal surface can be considered as the holographic image of a point). The strength of higher orders of refraction is dependent on the grating surface containing the required Fourier components.

The result (6-4) also holds for light rays not travelling in the xy plane (i.e. $\psi \neq 0$). For a general light ray incident in direction (θ_1, ψ_1), the first order diffracted ray will have direction (θ_2, ψ_2), where:

$$\theta_2 = -\text{asin}\left[\frac{(\sin(\theta_1)\, p - \lambda)}{p}\right] \qquad (6-6)$$

$$\psi_2 = -\psi_1 \qquad (6-7)$$

6.2.5 Measuring Grating Period and Amplitude

A simple method used to check the period of the gratings is to find the angle for which an incident laser beam is diffracted back into the incident polar angle ($\theta_1=\theta_2$), most easily checked by using a very small azimuthal angle ($\psi_1 \approx 1°$). When the grating is positioned with the grating lines in the vertical plane, the diffracted laser beam will scatter into a path slightly above the incident beam. Measuring this polar

$$p = \frac{\lambda}{2\sin(\theta)} \qquad (6-8)$$

angle θ allows the grating period to be calculated as:

The first grating to be used was designed to have a period of 400 nm. A rough check of grating period using the method described above was consistent with this value. A more detailed check of grating quality was performed for the first two samples using atomic force microscopy (AFM). This technique allowed the period and amplitude of the gratings to be measured directly and accurately, and double check the accuracy of the optical techniques used to infer these values for the remaining gratings. Figure 6.4 shows an image of a sample generated using AFM. All further samples had grating period and depth calculated by measuring sample reflectivity over a full angular range. This was performed using the same apparatus described in section 5.6, using a similar technique.

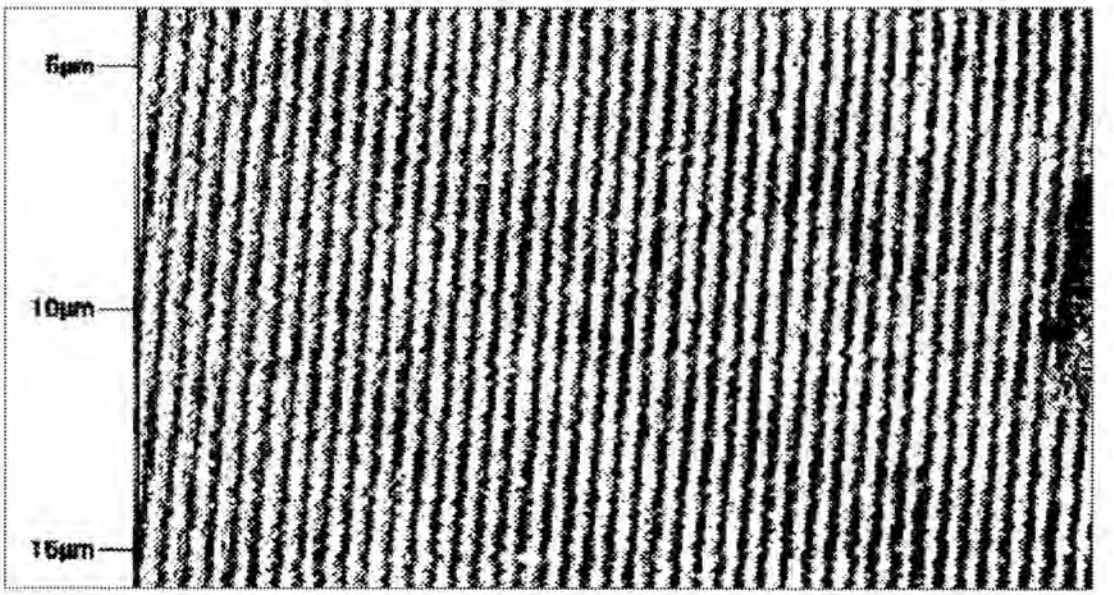

Figure 6.4 *An image of a 400 nm grating created using an AFM scan, measured by J. Badyal.*

6.3 Photoluminescence from a Polymer on a Textured Substrate

Conjugated polymers were deposited onto textured substrates using standard spinning techniques. The effect of the solvents used in the spinning process on developed photoresist was checked using sample substrates. It was found that none of the standard solvents used for this purpose were able to dissolve the photoresist on a timescale that would cause them to change the grating structure during the spinning process. Films were also spun onto planar reference samples in an identical manner. The results given in this section are a representative sample. A considerable amount of data was taken, during which time the apparatus was refined to allow a more accurate analysis of the earlier results.

6.3.1 Photoluminescence Apparatus

An important experiment performed on a textured conjugated polymer film was to see if the total light emitted from the optically excited film was increased by the texturing. To measure this, it is necessary to collect the light emitted from the sample in all directions, a task most easily performed in an integrating sphere. The integrating sphere allows the measurement of the absolute external PL efficiency of polymer films, by comparison of the total light emitted with the power of the excitation source (an argon ion laser). Filters were used to separate the emitted light from the laser light used to excite the sample. The results need various correction factors to be taken into account, such as the spectral response of the sphere and detector, and the effect of light that is not absorbed the first time the laser strikes the sample.

In addition to checking the possible modification to the total emission from a film, it is also important to know the effect of the texturing on the photoluminescence angular emission pattern for a sample. Again, the sample was excited using an argon ion laser, and the measurement of the emission spectrum at a range of different angles was done using a CCD spectrometer. Light was collected and channelled to the CCD spectrometer using optical fibre, ensuring that each reading collected only a small cone of light, and allowing the collection angles to be positioned and measured accurately. For the angular PL results in this chapter, the optical fibre was positioned

to collect a cone of light with a full angle of 1.6 degrees. The incident laser beam was aligned to avoid laser light directly entering the collection optical fibre and a filter, designed to block the 488 nm laser was placed in front of the collection fibre to avoid any stray laser reflections affecting the CCD. Despite the extra speed of measurement achievable using the CCD, collecting data for a full range of angles is quite time consuming, and continuous exposure of the sample to laser light while in air would cause photo-oxidation of the polymer. In order to avoid sample degradation, the sample was kept under high vacuum for the duration of the experiment. The apparatus used for this experiment needed to keep the sample under vacuum, while avoiding distorting the measured emission pattern due to reflections from the glass used to enclose the sample.

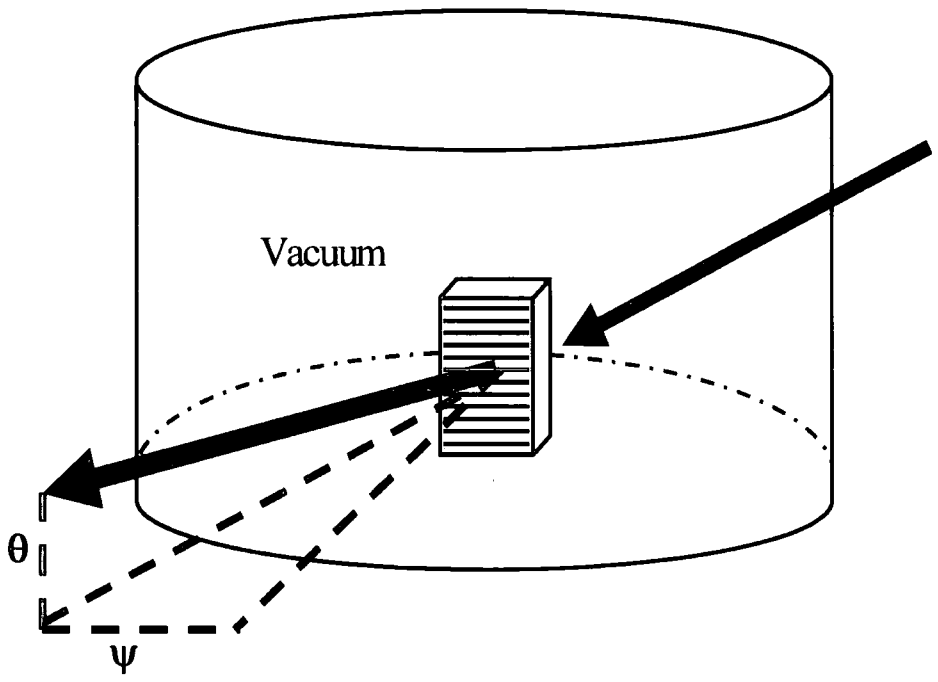

Figure 6.5 *Apparatus to measure angular dependent PL. The orientation shown here is suitable for measuring PL at small angles of θ. If ψ is small and θ large then the sample is best rotated by ninety degrees (making the grating lines vertical in this diagram) to minimise distortion at the vacuum chamber walls.*

6.3.2 PL modification by grating

Films of MEH-PPV and PPV were deposited onto substrates with gratings of period 400 nm. The MEH-PPV layer was deposited by spin coating directly from chlorobenzene solution, giving a thickness of 160 nm. The PPV was deposited by spinning a precursor onto the grating, and using the thermal conversion process to give a final thickness of approximately 90 nm. The amplitude of the gratings was checked using AFM, and found to be roughly 100 nm, although there was a certain amount of variation across the surface. When the polymers were allowed to dry after the spinning process, it was found the surface of the polymer followed the corrugations of the substrate, giving a structure shown schematically in figure 6.6.

Photoluminescence quantum yield experiments were performed first on the films, using the integrating sphere, before there was sufficient time for the samples to degrade significantly. When excited using the 488 nm argon Ion laser line, the corrugated MEH-PPV sample was found to have a slightly increased quantum yield compared to its planar reference sample (9% yield corrugated, 7% yield uncorrugated). However, the PPV showed no significant modification of yield for the corrugated and uncorrugated samples.

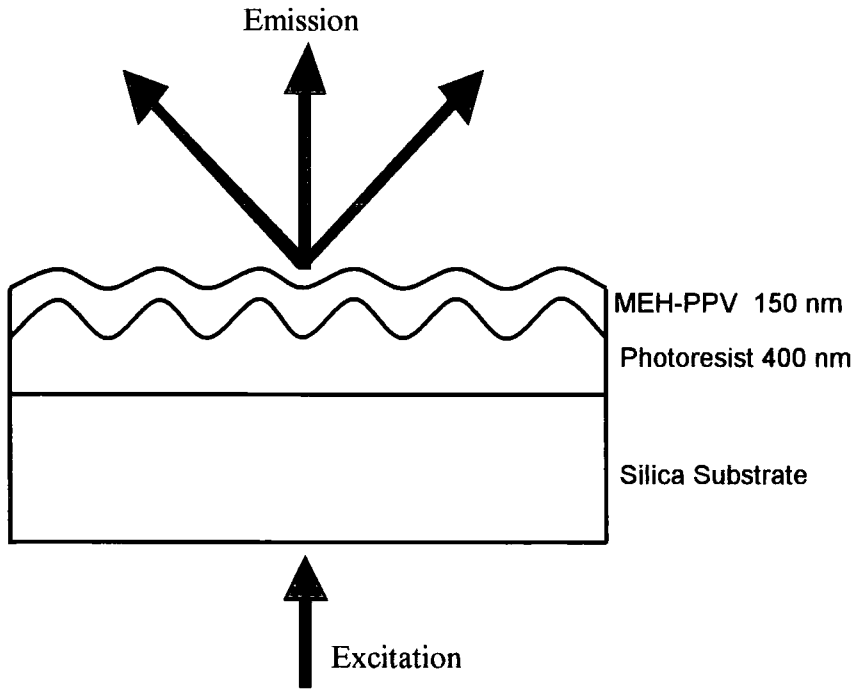

Figure 6.6 *Cross section of corrugated structure of the MEH-PPV film studied for angular dependent PL measurements, and total quantum yield measurements.*

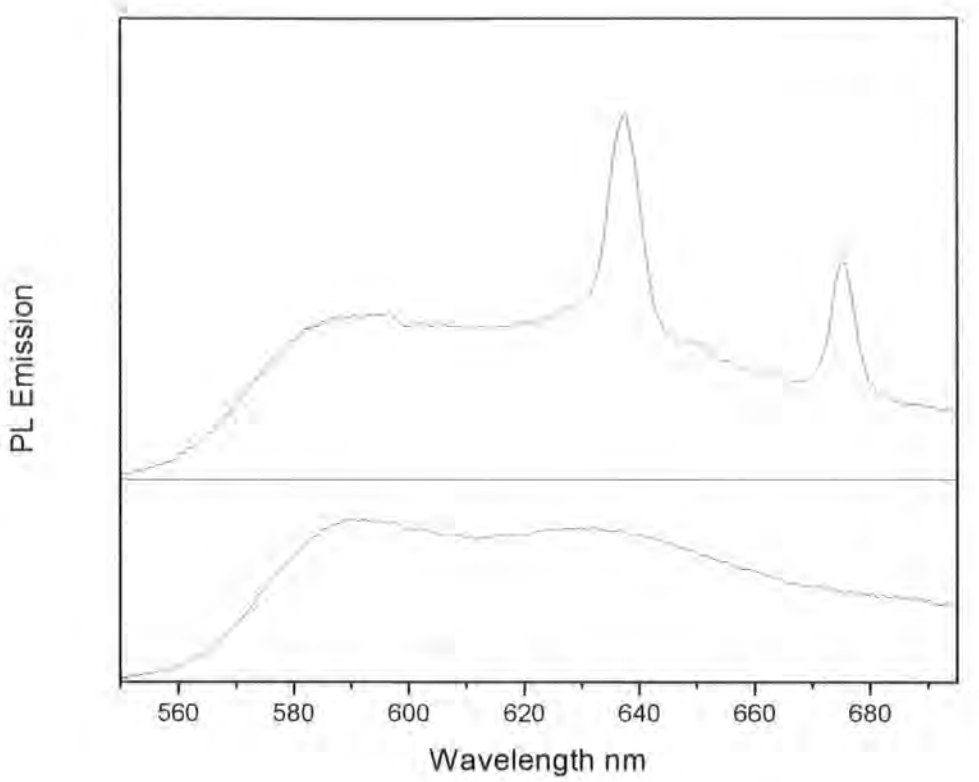

Figure 6.7 *Comparison of PL spectra from corrugated MEH-PPV (upper curve) with PL from a planar reference film (lower curve), excited using a 488 nm laser line. The light was collected at an angle of approximately* θ=5°, ψ=0. *Light was collected for a (full) angle of 1.6 degrees. The grating amplitude was 100 nm.*

When the photoluminescence emission spectrum of the corrugated MEH-PPV was examined in various emission directions, the modification of the spectra compared to the planar reference sample was quite dramatic[5]. Figure 6.7 shows the large peaks generated by the microstructure compared to the spectra from a planar reference sample, while under excitation at 488 nm. The position of the peaks was found to be highly dependent on viewing angle. The PL spectrum of the PPV film was not modified. The large peaks that are observed in the PL spectrum form the corrugated MEH-PPV sample are believed to be caused by the scattering of light that would otherwise be confined in a waveguide mode. The lack of modification from the PPV sample can be explained by the different scattering conditions associated with its lower thickness.

6.3.3 PL measurement over full angular range

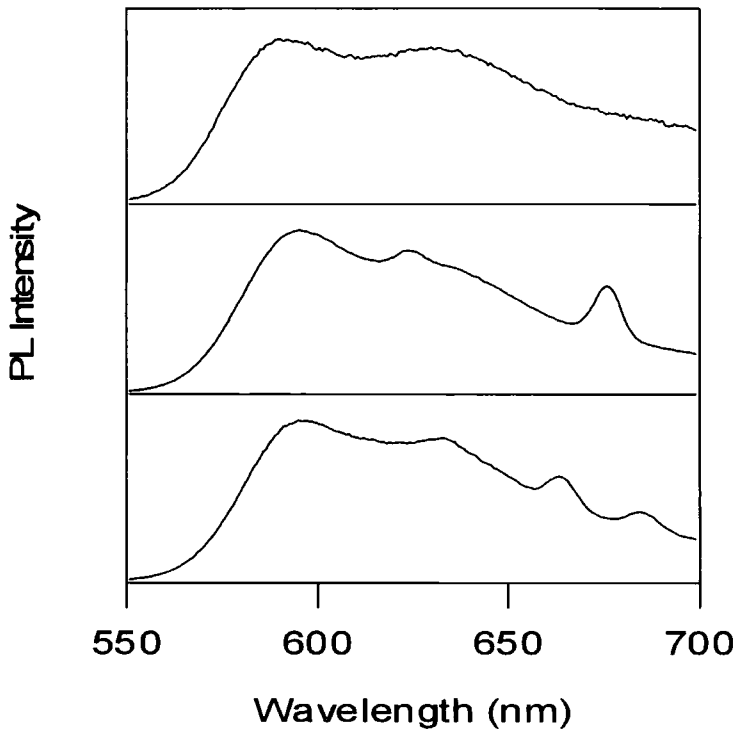

Figure 6.8 *Emission spectra for a corrugated MEH-PPV sample with grating amplitude 30 nm, measured for angles (0,0) –middle graph, (2.5°,0) –lower graph, compared to a planar reference sample (top graph).*

A second MEH-PPV film of similar thickness was spun onto a grating with weaker amplitude (approximately 30 nm), in order to analyse the PL emission over a full range of angles. The sample was excited in a similar manner, using a 488 nm argon ion laser line. In order to ensure that all possible modes were excited in the film, a quarter wave plate was placed in front of the laser to circularly polarise the incident light (using linearly polarised light directly from the laser would excite modes propagating perpendicular to the electric vector direction preferentially). It was found that the peaks caused by the texturing were smaller, but moved with viewing angle in a similar manner to the first grating examined. At normal incidence (0,0), a scattered peak was observed at a wavelength of 675 nm (Figure 6.8). When the

viewing angle is moved to (2.5,0), this peak is observed to split into two peaks, at 663 nm and 684 nm. The peak positions for other viewing angles in the θ direction are shown in figure 6.9. Peak positions for variable ψ angles are shown in figure 6.10.

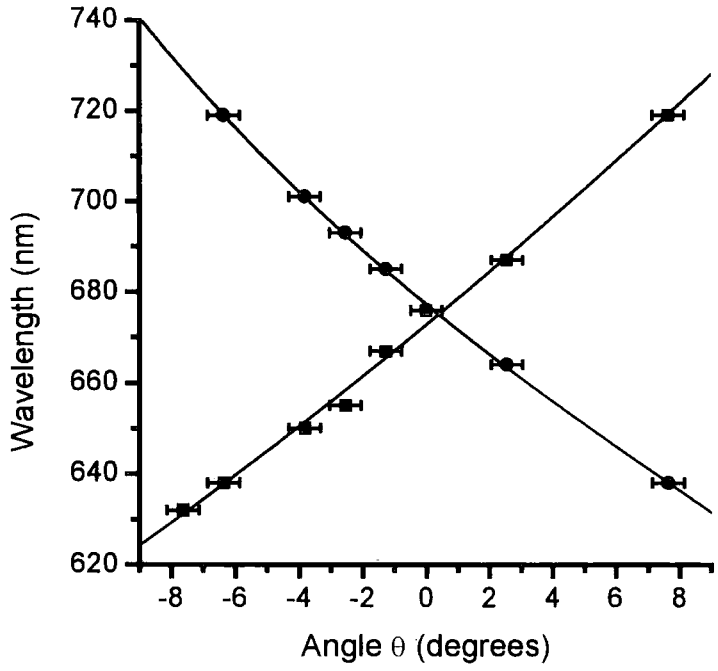

Figure 6.9 *Dependence of peak position on viewing angle θ, with ψ kept fixed at zero (detector kept in the xy plane).*

When the optical fibre collecting the emitted light was rotated outside the xy plane ($\psi \neq 0$), while the angle θ was kept constant, any peaks caused by scattering were observed to gradually shift to shorter wavelength as ψ was increased. Figure 6.10 shows this effect.

The results in this section can be explained by assuming that the grating is able to scatter waveguided light out of the film. The next section presents a detailed mathematical explanation of this. It must be assumed that the scattering length is shorter than the absorption distance for a waveguide mode within a film.

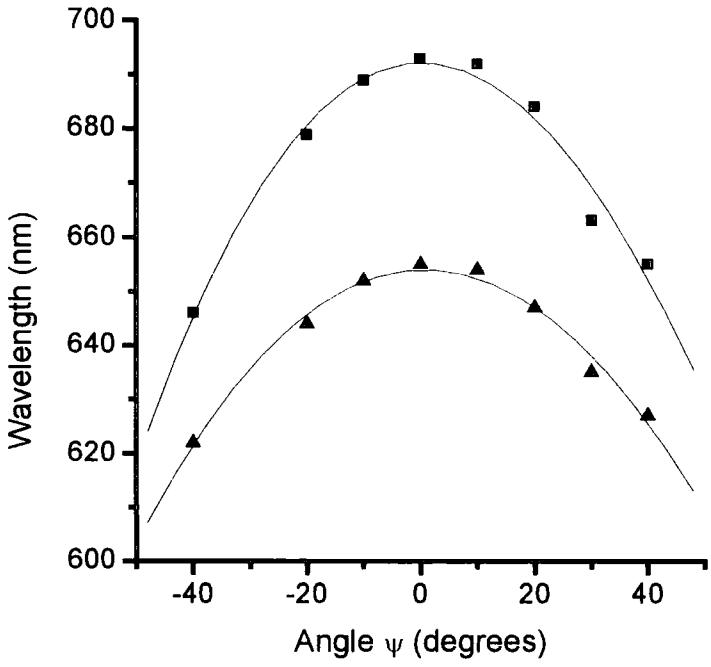

Figure 6.10 *Dependence of scattered peak position on viewing angle ψ, with θ kept constant at 2.5°.*

6.3.4 Waveguide Scattering Theory

The modified PL spectra of conjugated polymer films spun onto gratings can be explained by the scattering of waveguided light out of the film. The simplest way to model the scattering of waveguided light is to assume that the waveguide equations derived in chapter four remain valid. This seems to be a reasonable approximation for fairly weak gratings, for which there will be only a slight perturbation from the planar layer approximation. If a single monochromatic TE waveguide mode is propagating within a polymer layer with a weak grating such that its propagation direction is at an angle of ξ to the y axis and the wavefronts of the mode form an angle of ξ to the direction of the grating lines then a simple calculation can be done to find the direction in which the light will be scattered. The scattering direction will be expressed in terms of θ and ψ as shown in figure 6.11.

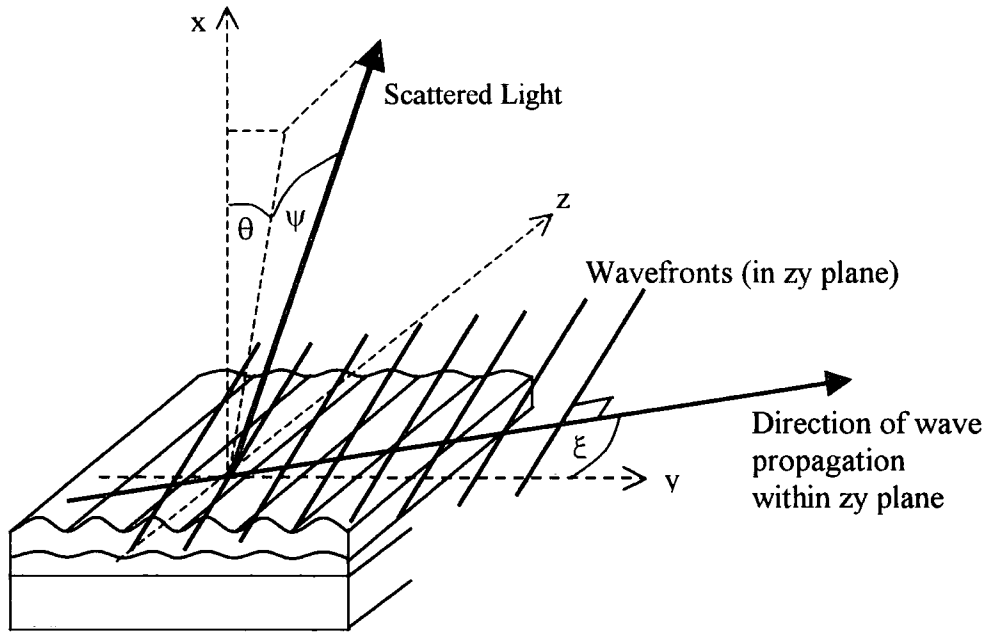

Figure 6.11 *A TE waveguide mode propagating in a polymer film at an angle of ξ to the y axis, with light scattering out in a direction (θ, ψ). The wavefronts lie in the zy plane, as does the electric field vector of the light.*

Light with a vacuum wavelength of λ that is trapped in a waveguide mode in a medium with refractive index n_f such that its internal waveguiding angle is θ_w (as defined in chapter 4), then the effective wavelength of the light within the medium λ_w will be:

$$\lambda_w = \frac{\lambda}{n_f \sin(\theta_w)} \qquad (6-8)$$

If it is assumed that the waveguided light is propagating through the film at an angle ξ to the y axis (as shown in figure 6.11), then we can calculate the effective wavelength of the light in the form of components in the direction of the z and y axes, defined as λ_z and λ_y. If the phase of the evanescent field above the polymer film was mapped out at a fixed time, λ_z would be the distance between two points of identical phase as measured along a line parallel to the grating lines. λ_z and λ_y are calculated as:

$$\lambda_z = \frac{\lambda_w}{\sin(\xi)} \qquad \lambda_y = \frac{\lambda_w}{\cos(\xi)} \qquad (6-9)$$

If a guided mode is travelling directly along the y axis and has a film wavelength λ_y equal to the grating period (p), then the wavefronts and grating lines will match up exactly. In this circumstance, energy from the waveguide mode will be scattered out in the normal direction ($\theta=0, \psi=0$).

The scattering process can be understood by considering the evanescent field above the polymer film. For all waveguiding systems, the electric field of a guided mode extends outside the guiding medium. Thus there is an optical frequency oscillating electric field in the air above the polymer layer. Clearly an oscillating electric field is normally expected to generate freely propagating light. However as the waveguide structure tends towards being planar, the radiation field generated by the oscillating electric field summed over the entire surface exactly cancels out. Thus for a waveguide in normal operation, the evanescent field does not allow energy to escape the waveguide. However if the polymer surface has a sinusoidal depth profile, as we assume here, energy can escape the film. The propagation direction for the free wave can be calculated by considering the phase of the electric field only at the peaks of the sinusoidal surface (for simplicity the 'grating lines' can be considered to be the lines along the peak of the sinusoidal surface). For a free wave to propagate the phase of the evanescent field at the grating lines must add coherently in the direction of the freely propagating wave. If the grating depth is shallow, then the electric field along the troughs of the sinusoidal surface will be almost out of phase with the electric field along the grating lines, thus largely cancelling out the radiation field and making the scattering weak. As the grating is made deeper, the field from the troughs is less able to cancel the electric field along the grating lines, and the scattering becomes stronger. Theoretically the strongest possible scattering in the normal direction that could be obtained would require the depth of the grating (peak to trough distance of the sinusoidal surface) to equal the free wavelength of the light, under which circumstance the field from troughs and peaks would add coherently, although such a grating would probably not be very practical to manufacture.

It should be noted that the conditions required for light to be scattered in the normal direction (λ_y=p) will be met for two guided modes, travelling in each direction

along the y axis. Due to the symmetry of the situation, each guided mode will have the same wavelength, and therefore cause a single peak in a photoluminescence graph that is obtained when the detector is positioned normal to the excited film. When the detector is moved slightly in the xy plane, so that it is capturing light scattered for an angle where θ is small but non zero, the detector will still receive light from two scattered waves travelling up and down the y axis. However, since the symmetry is now broken, the wavelengths for each of the waves matching the scattering conditions are slightly different and give two peaks on the PL graph. This explains the peak splitting phenomena observed in figure 6.8.

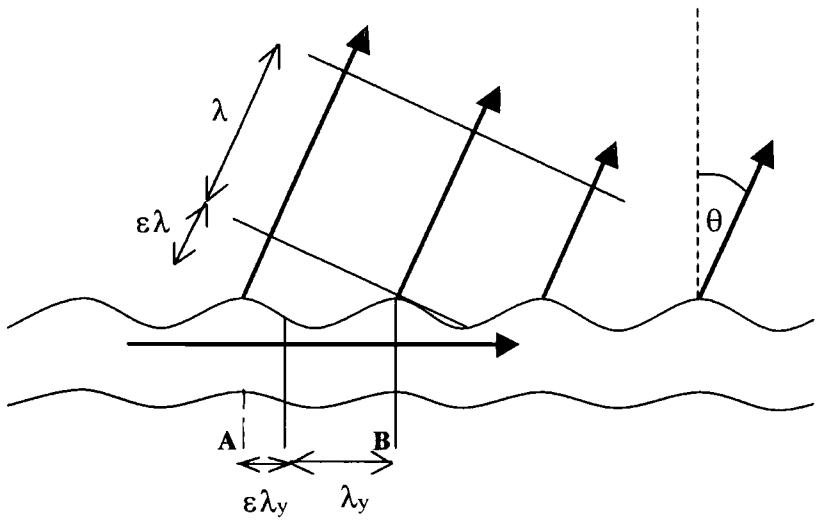

Figure 6.12 *Scattering conditions for a non zero value of θ are met when the phase lag (ε) from rays emitted from grating lines at A and B is the same as the phase difference of the guided mode between these points.*

For a waveguided mode scattering at an angle θ as shown in figure 6.12 it can be shown geometrically that for a grating with period p:

$$\sin(\theta) = \lambda\left(\frac{1}{\lambda_y} - \frac{1}{p}\right) \qquad (6-10)$$

In a similar way, it can be shown that when ξ is non zero, and λ_z is finite, the emission angle ψ is given by:

$$\sin(\psi) \equiv \frac{\lambda}{\lambda_z} \qquad (6-11)$$

By using the TE waveguide equations derived in chapter 4, assuming a zero order mode (m=0), all the available internal waveguiding angles θ_w can be analysed. By fixing ψ to be a small angle, we can calculate the values of θ that light of specific wavelengths is able to scatter into, and attempt to model the PL results of the MEH-PPV film shown in figure 6.9. The refractive index of the photoresist grating (n_g) is taken as 1.68, the MEH-PPV index (n_f) 1.85, the grating period (p) as 400 nm, and the film thickness (w) as 160 nm. Varying θ_w between $\pi/2$ radians and the film substrate critical angle θ_{wc} allows us to calculate the emission angles (θ_1, θ_2).

$n_g = 1.68 \qquad n_f = 1.85 \qquad n_a = 1$

$w = 160 \cdot 10^{-9} m \qquad p = 400 \cdot 10^{-9} m \qquad m = 0$

$\theta_{wc} = \operatorname{asin}\left(\frac{n_g}{n_f}\right) \qquad \frac{\theta_{wc}}{2\pi} 360 = 65.245$

θ_{wc} is the critical angle. Waveguiding at a smaller angle than the critical angle (in this example being 65.2 degrees) will be leaky.

$$\theta_w = \frac{\pi}{2}, \frac{39.99\,\pi}{80} .. \theta_{wc} \qquad \psi = 0.0001$$

ψ is kept small but non zero so that we can use the general formula while avoiding a divide by zero. A series of values of θ_w is taken across the range of available waveguiding angles.

$$\phi_0(\theta_w) = \operatorname{atan}\left[\frac{\sqrt{\left(n_f^2 \sin(\theta_w)^2 - n_g^2\right)}}{n_f \cos(\theta_w)}\right] \qquad \phi_1(\theta_w) = \operatorname{atan}\left[\frac{\sqrt{\left(n_f^2 \sin(\theta_w)^2 - n_a^2\right)}}{n_f \cos(\theta_w)}\right]$$

$$\lambda(\theta_w) = \frac{2\,\pi\, w\, n_f \cos(\theta_w)}{\pi\, m + \phi_0(\theta_w) + \phi_1(\theta_w)} \qquad (6-12)$$

The wave guiding equation derived in chapter four (6-12) can be used to find the wavelength as a function of internal waveguiding angle. From equations (6-10) and (6-11) we can also derive the emission angles θ_1, θ_2 as a function of internal waveguiding angle θ_w assuming that ψ is small:

$$\lambda_w(\theta_w) = \frac{\lambda(\theta_w)}{n_f \sin(\theta_w)}$$

$$\lambda_z(\theta_w) = \frac{\lambda(\theta_w)}{\sin(\psi)} \qquad \lambda_y(\theta_w) = \sqrt{\frac{\lambda_w(\theta_w)^2\, \lambda_z(\theta_w)^2}{\left(\lambda_z(\theta_w)^2 - \lambda_w(\theta_w)^2\right)}}$$

$$\theta_1(\theta_w) = \operatorname{asin}\left[\left(\frac{\lambda_y(\theta_w) - p}{\lambda_y(\theta_w)}\right)\frac{\lambda(\theta_w)}{p}\right] \qquad \theta_2(\theta_w) = \operatorname{asin}\left[\left(\frac{p - \lambda_y(\theta_w)}{\lambda_y(\theta_w)}\right)\frac{\lambda(\theta_w)}{p}\right]$$

We can now plot a graph of emission angle versus wavelength:

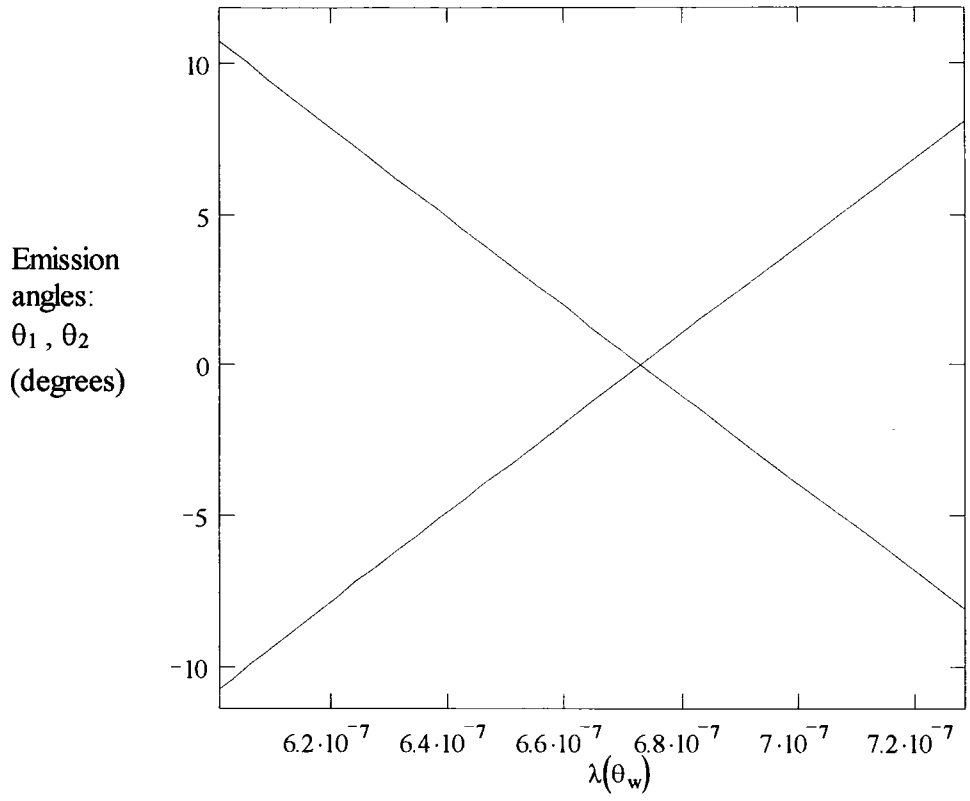

Figure 6.13 *Theoretical plot of scattering angle* θ *versus wavelength with* ψ *held constant close to zero.*

The theoretical plot in figure 6.13 can be compared to the experimental plot shown in figure 6.9. The simplified model used predicts that at normal angle a wavelength of 673 nm will be emitted (The point of intersection on the graph). This is close to the 675 nm feature in the PL emission spectrum shown in the middle graph in figure 6.8. The agreement is reasonable but not perfect. The equations used do not take the absorption or dispersion of the conjugated polymer into account, but are certainly sufficient to give a qualitative explanation of the observations in section 6.3.2.

It is possible to rearrange the equations to plot the emission wavelength with the angle ψ while θ remains fixed. Using the same data and basic waveguide equations as used in the previous section (6-12) and again varying the internal waveguide angle (θ_w), but fixing the detection angle θ at 2.5 degrees (working is in radians) obtains:

$$\theta = 2.5\left(\frac{\pi}{180}\right)$$

$$\lambda_w(\theta_w) = \frac{\lambda(\theta_w)}{n_f \sin(\theta_w)}$$

$$\lambda_{y1}(\theta_w) = \frac{p\,\lambda(\theta_w)}{\left(\lambda(\theta_w) - p\sin(\theta)\right)} \qquad \lambda_{y2}(\theta_w) = \frac{p\,\lambda(\theta_w)}{\left(\lambda(\theta_w) + p\sin(\theta)\right)}$$

$$\lambda_{z1}(\theta_w) = \sqrt{\frac{\lambda_w(\theta_w)^2\,\lambda_{y1}(\theta_w)^2}{\left(\lambda_{y1}(\theta_w)^2 - \lambda_w(\theta_w)^2\right)}} \qquad \lambda_{z2}(\theta_w) = \sqrt{\frac{\lambda_w(\theta_w)^2\,\lambda_{y2}(\theta_w)^2}{\left(\lambda_{y2}(\theta_w)^2 - \lambda_w(\theta_w)^2\right)}}$$

$$\psi_1(\theta_w) = \operatorname{asin}\left(\frac{\lambda(\theta_w)}{\lambda_{z1}(\theta_w)}\right) \qquad \psi_2(\theta_w) = \operatorname{asin}\left(\frac{\lambda(\theta_w)}{\lambda_{z2}(\theta_w)}\right) \qquad (6-14)$$

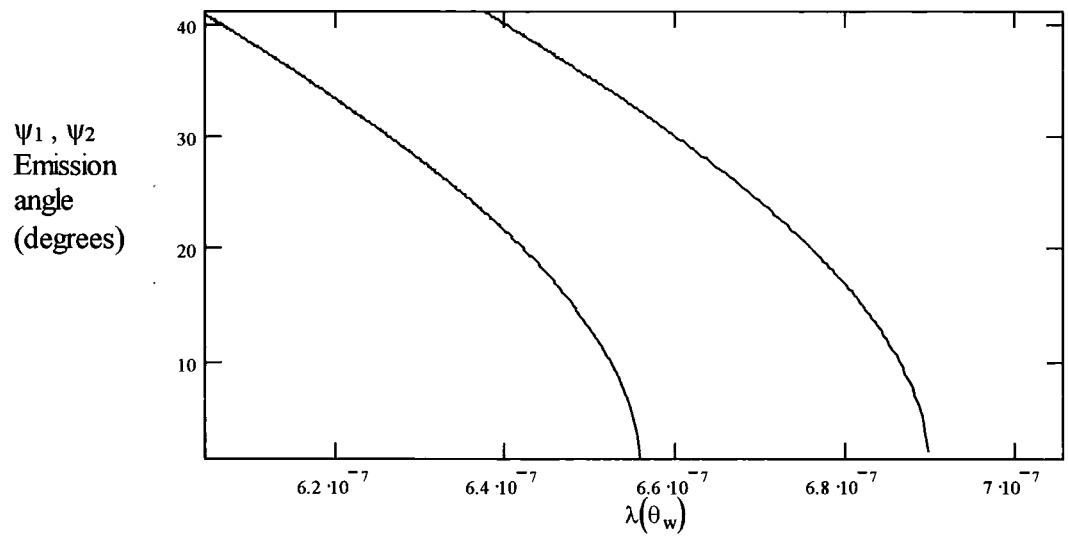

Figure 6.14 *Theoretical plot of scattering angle ψ in degrees versus wavelength with θ held constant at 2.5 degrees.*

In the theoretical plot shown in figure 6.14 the peak positions for negative values of ψ will be identical to the positive values (i.e. figure 6.14 is symmetrical in the ψ=0 axis). The theoretical results in this figure match up reasonably well with the experimental results shown in figure 6.10.

When the detection angle ψ is non zero, the waveguide mode scattering into this direction must have had a propagation direction across the film (ξ) that deviates away from the y axis. The direction that the waveguide mode is propagating in before scattering effects the polarisation of the scattered light. The propagation direction ξ for increasing values of ψ can be calculated using:

$$\xi_1(\theta_w) = \operatorname{atan}\left(\frac{\lambda_{z1}(\theta_w)}{\lambda_{y1}(\theta_w)}\right) - \frac{\pi}{2} \qquad \xi_2(\theta_w) = \frac{\pi}{2} - \operatorname{atan}\left(\frac{\lambda_{z2}(\theta_w)}{\lambda_{y2}(\theta_w)}\right)$$

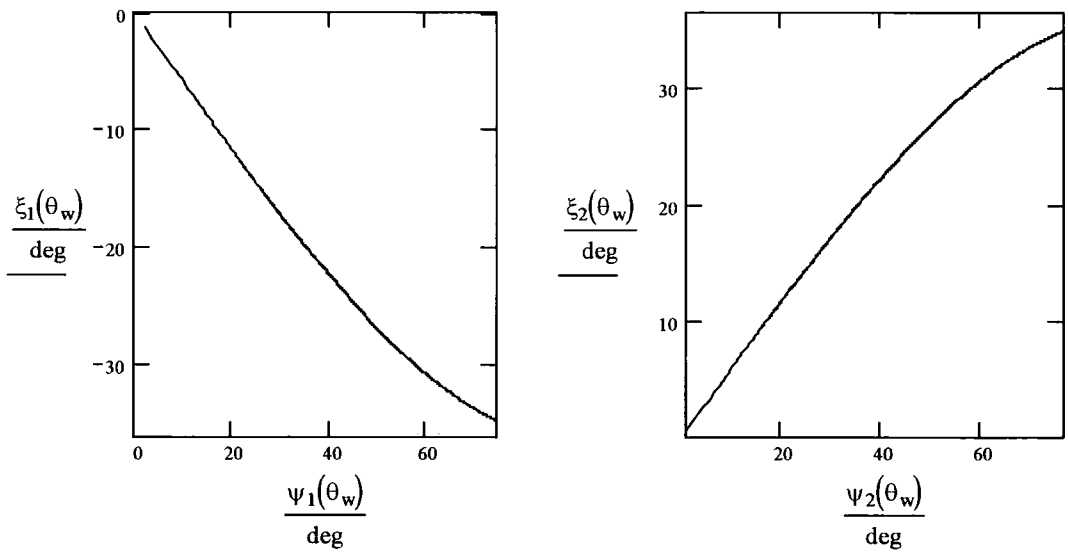

Figure 6.15 *The propagation direction ξ of the waveguide modes scattering to cause the scattered features plotted in figure 6.14.*

From figure 6.15 it can be seen be seen that the waveguide mode propagation direction (ξ) for the two modes scattering into large angles of ψ, becomes increasingly different for each mode as ψ is increased. This means that for large ψ, the polarisation of each scattered peak is expected to be different. This effect was checked experimentally, and it was confirmed that the polarisation for the two peaks

was dramatically different when the detection angle ψ was large (a nonzero value of θ was used so that two peaks were visible). This contrasts with PL measurements made with the detector in the xy plane (ψ=0). For these measurements, the waveguide modes scattering into this plane are always travelling perpendicular to the grating lines (usually with one mode travelling in each direction along the y axis). All the features encountered experimentally so far can be explained using TE waveguide modes alone. This is not surprising, since TM modes are difficult to excite with a laser at close to normal incidence for the substrate. TE modes scattered within the xy plane will always have their electric vector lying along the z axis, and it was confirmed experimentally that the resulting features in the PL spectra were indeed polarised in this way.

6.3.5 PL Emission Enhancement from a Deep Photoresist Grating

Figure 6.16 shows the dramatic modification to a PL spectrum that can be obtained from MEH-PPV on a strong photoresist grating (period 388 nm, depth 160 nm). Figure 6.16a shows emission at normal angle (0,0) for the corrugated film (continuous line) and an uncorrugated reference portion of the same film. There is a large extra peak at 675 nm in the corrugated PL spectrum. Figure 6.16b shows a PL spectrum for a small angle in the θ direction (2.5,0), in which the peak has split into two peaks. Figure 6.17 shows the variation of the position of the large peaks for a various angles of θ with ψ kept constant.

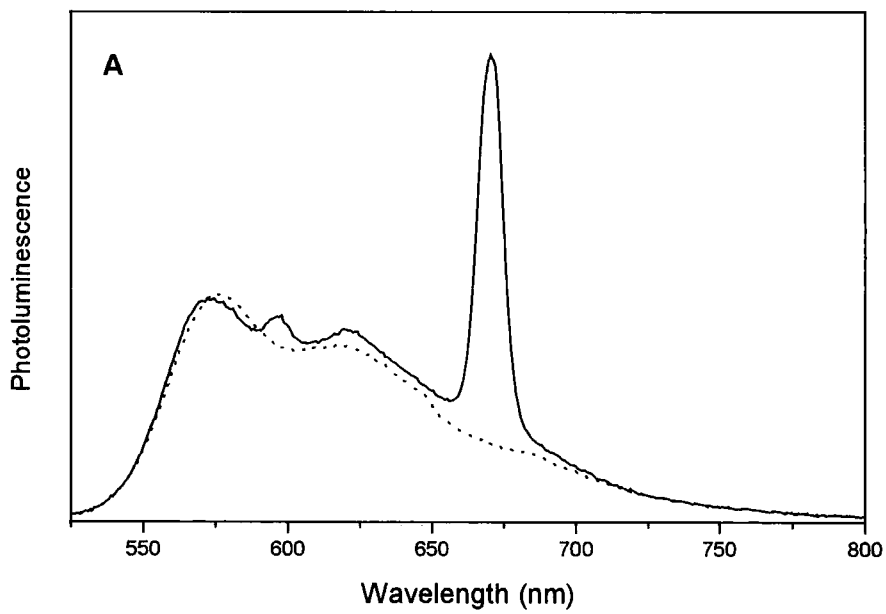

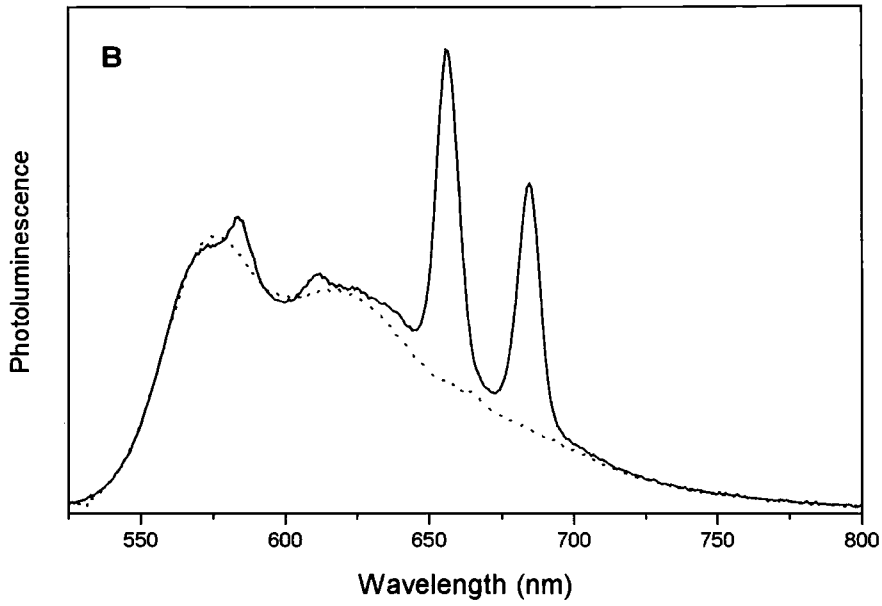

Figure 6.16 A *and B show PL spectra from MEH-PPV on a grating with period 388 nm, using detection angles at normal (0,0), and (2.5,0) appropriately. The dashed line shows the emission from uncorrugated area of the same film as a reference.*

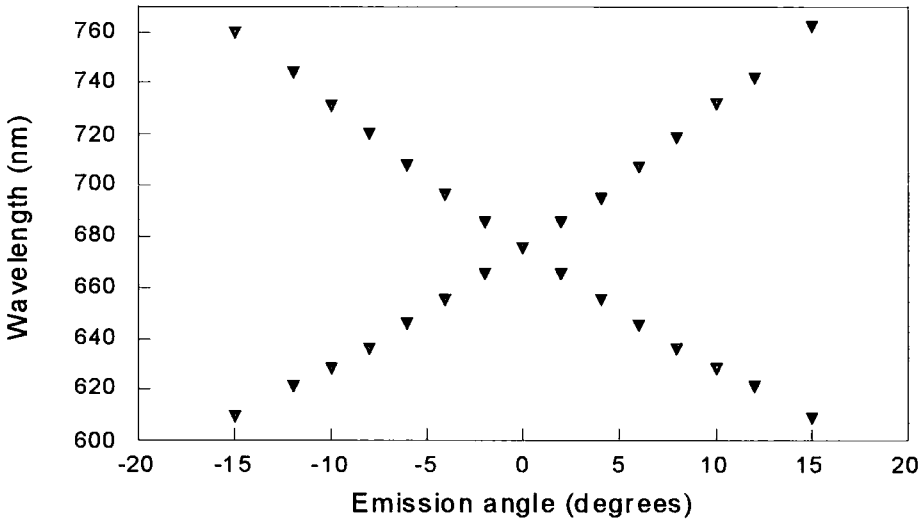

Figure 6.17 *Variation of peak positions for corrugated MEH-PPV film with variable angle θ for constant ψ (Detector kept in the xy plane).*

In figure 6.16a, in addition to the large peak, there is a second much smaller peak at 600 nm. The small peak is observed to split into two peaks in figure 6.16b in a similar manner to the large peak. This feature was observed in many spectra from strong photoresist gratings. The small peak is believed to correspond to a waveguide mode that is propagating through both the polymer film layer and through the

photoresist layer. Although the peak splits into two, the longer wavelength peak is not evident at wavelengths above 630 nm (despite adjusting the position of the detector). This suggests that at longer wavelengths the mode causing the small feature becomes increasingly 'leaky', as the internal waveguide angle becomes smaller.

In order to examine the effect of the grating on the total PL of the film, the film was excited in an integrating sphere. The PL from corrugated and uncorrugated areas is shown in figure 6.18. The PL is nearly double, in fact increasing by a factor of 1.9, integrating over all wavelengths and angles. The shape of the spectrum is only modified slightly. The only part of the spectrum that does not show increased PL due to the grating is the shorter wavelength area below 570 nm. In this spectral region, the absorption of MEH-PPV becomes quite high, so it is unlikely that waveguide modes could propagate far enough to be scattered.

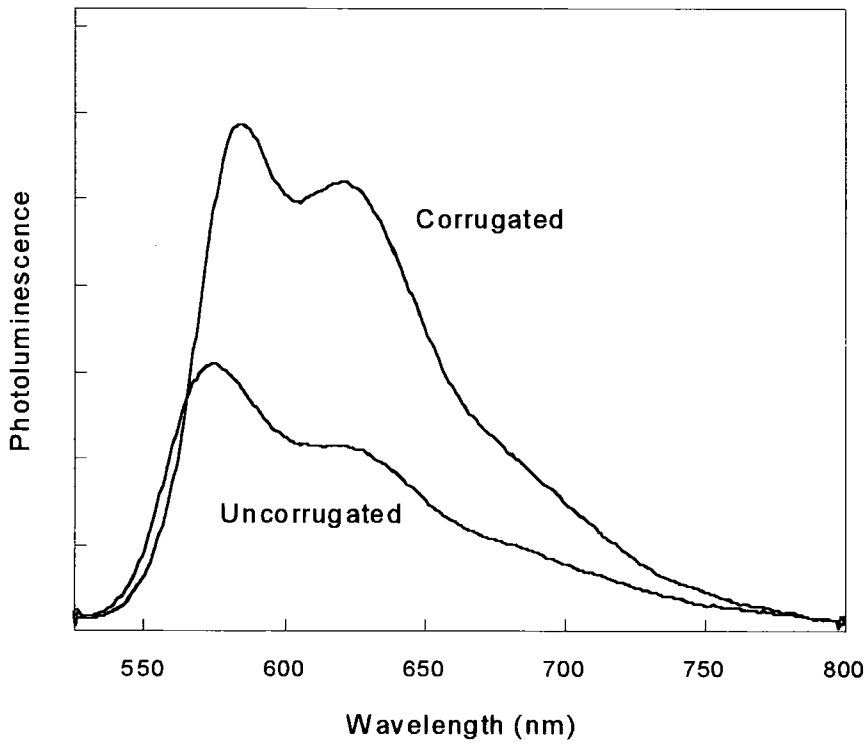

Figure 6.18 *Effect of corrugation on total PL. Using an integrating sphere, the modified emission of the film used in figure 6.16 was summed over all angles and compared to the uncorrugated reference area of the film.*

6.3.6 Grating Tunability Using Etched Silica Grating

There are several disadvantages in using photoresist gratings for texturing conjugated polymer films. Using the methods described in 6.3.4 to model scattering from films is complicated by the inclusion of a photoresist layer. The scattering conditions are very sensitive to the refractive indices of the layers that bound the polymer layer, and the refractive index of photoresist is a value that could well vary depending on the methods used to deposit it. Since the refractive index of the photoresist is higher than that of glass, some waveguided light might be expected to penetrate the photoresist layer. Photoresist has a relatively high absorption over much of the optical spectrum, especially shorter wavelengths. If gratings are to be used in any application that is intended to increase light output from luminescent films, it is best to avoid the absorption losses that would occur when the light passes though a photoresist layer. To avoid these problems, using a grating etched directly into a silica substrate would clearly be an advantage.

A method of generating a grating on a silica surface is to use electron beam lithography. This is used to create a patterned resist. The pattern can then be etched into a substrate before the resist is removed. This method allows very precise control over the pattern of the grating etched into the silica. In particular, it allows different grating regions of different periods to be etched onto the same substrate. This would be very difficult to achieve on a photoresist grating using the interference method. Since electron beam lithography is time consuming and expensive, it is not a realistic solution for mass producing substrates with gratings. However, two substrates were created using this method in order to investigate how changing the period of the gratings might be used to tune the wavelength of the scattered light. These gratings were manufactured by Professor T.F.Krauss at the University of St Andrews in Scotland.

The gratings were etched with a square wave depth profile, to a different depth on each substrate. Each substrate was etched with several strips of grating, across which there were various regions of grating period. Two strips were etched to have periods varying between 350 nm and 420 nm, increasing in steps of 5 nm. Two more strips were etched to have period regions varying between 160 nm and 440 nm in steps of 20 nm.

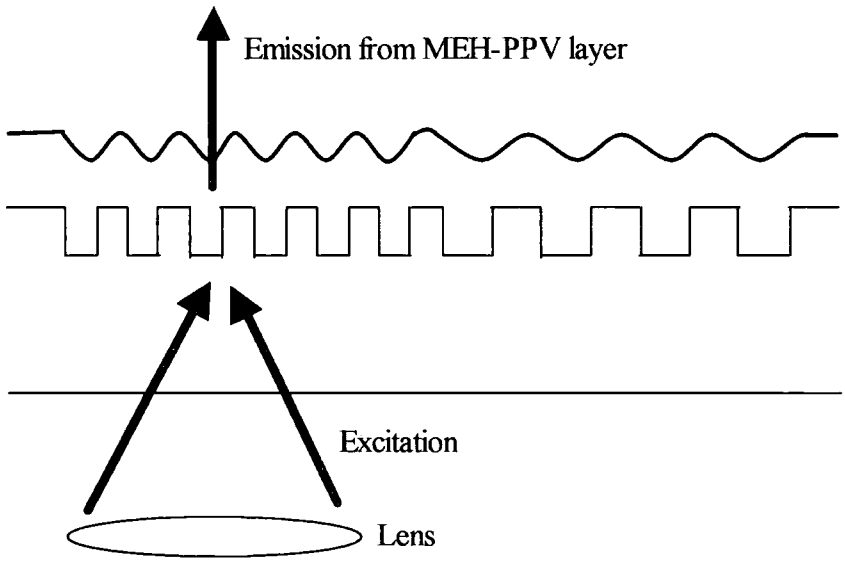

Figure 6.19 *Schematic diagram showing how excitation is focused into regions of different grating period. The focusing is required since each region of grating was a fraction of a square millimetre in size.*

A film of MEH-PPV was spun onto one of the etched silica substrates to a thickness of 190 nm. The grating depth of the substrate (peak to trough of the square wave surface) was 95 nm. The MEH-PPV film was excited at 488 nm, using a lens to focus the laser into regions of the substrate of all the available periods (shown in figure 6.19). The photoluminescence from the film was measured for a range of angles for each region of the grating. Figure 6.20 shows a superposition of several PL spectra obtained when the film was excited in various grating regions. It can be seen that the large peak caused by the grating can be moved to almost any part of the MEH-PPV photoluminescence spectrum by altering the grating period, while the detection angle is kept normal to the excitation spot on the grating.

It is clear that the large peak is similar to the features seen from photoresist gratings, and is caused by the Bragg scattering. This experiment provides a clear demonstration that the grating period can be changed to select a particular wavelength of light to be scattered in a desired direction.

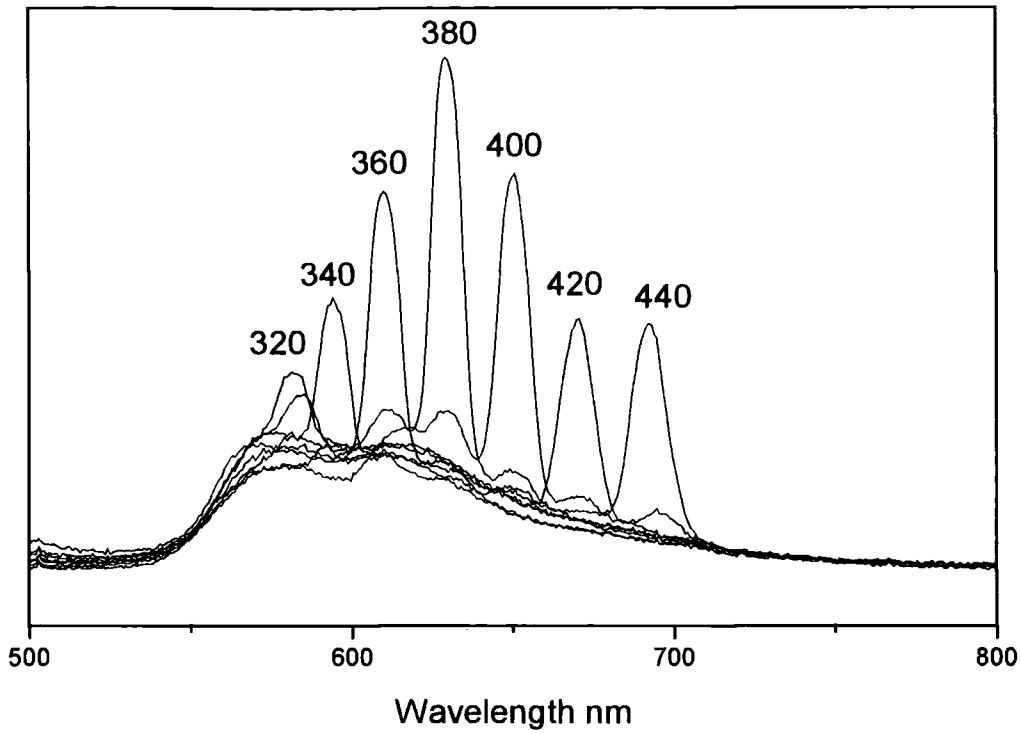

Figure 6.20 *A superposition of PL emission spectra from a 190 nm thick MEH-PPV film, on a substrate etched with regions of grating with periods of 320, 340, 360 380, 400, 420 and 440 nm. The spectra are detected at normal angle for each grating region. The peaks on the graph are labelled by the wavelength in nm of the grating region that they were obtained from.*

It is noticeable that the scattered peak become much smaller for regions of grating below 340 nm in period, where the scattered peak has a wavelength of less than 600 nm. This occurs despite the fact that the MEH-PPV is still highly luminescent in this region. The likely explanation for this reduction in peak size is the increase in absorption of MEH-PPV for shorter wavelengths. The high absorption allows waveguide modes to propagate only a short distance, giving them less time to scatter out of the film.

The peaks in the emission spectra measured for the etched grating regions at normal incidence were compared to the theoretically predicted positions using the formula in section (6-13). This modelling can only be considered a good approximation for weak gratings (since the waveguide equations become more

accurate as the planar approximation is approached). Nevertheless, the predicted peak positions are fairly close to those measured in practice, as shown in table 6.1.

Grating Period (nm)	Measured Peak Position (nm)	Calculated Peak Position (nm)
320	581	586
340	594	598
360	610	612
380	630	628
400	651	645
420	670	666
440	693	687

Table 6.1 *Comparison of measured and theoretically predicted peak positions for waveguide modes scattered in normal direction by regions of grating of varying period.*

6.3.7 Waveguide Mode Propagation distance

A very useful experiment that was also performed using the etched silica gratings was to investigate the propagation distance of waveguide modes in conjugated polymer films. This is not a trivial measurement to make. The standard method of measuring propagation distance within a film would be to couple light into a film with a prism, and then back out again at a distance with another prism. However in the case of conjugated polymers the light does not propagate far enough within the film for this method to work, since the absorption is too high. However, the absorption is actually too low (towards the red region of the spectrum) to make a measurement of the absorption with a standard spectrometer (since the measurement is confused by reflections and interference from the front and back film surfaces).

The etched gratings were useful for this experiment since they had a very clearly defined edge between the flat and grating areas on the substrate. The substrate was mounted on a micrometer screw gauge, allowing it to be moved small but precisely measurable distances along the y axis (perpendicular to the grating

direction). The excitation laser was once again focussed onto the substrate, onto the very edge of a grating area. The detector was positioned slightly off normal incidence to allow two peaks to be detected while the grating area was excited, corresponding to the two waveguide modes travelling in each direction along the y axis.

When the substrate was moved a small distance so that the excitation spot was no longer in the textured region of the substrate, but just outside it, it was found that one of the peaks in the PL spectrum vanished completely. This is due to the fact that one of the waveguide modes generated in the film was moving away from the grating region, and therefore did not interact with the grating at all. The single remaining peak in the PL spectrum was observed to gradually decay as the excitation spot was gradually moved away from the grating area using the micrometer screw mounting. The rate at which this peak decays as the distance between excitation spot and grating is increased gives an estimation of the distance which waveguide modes are able to propagate in the uncorrugated portion of the polymer film.

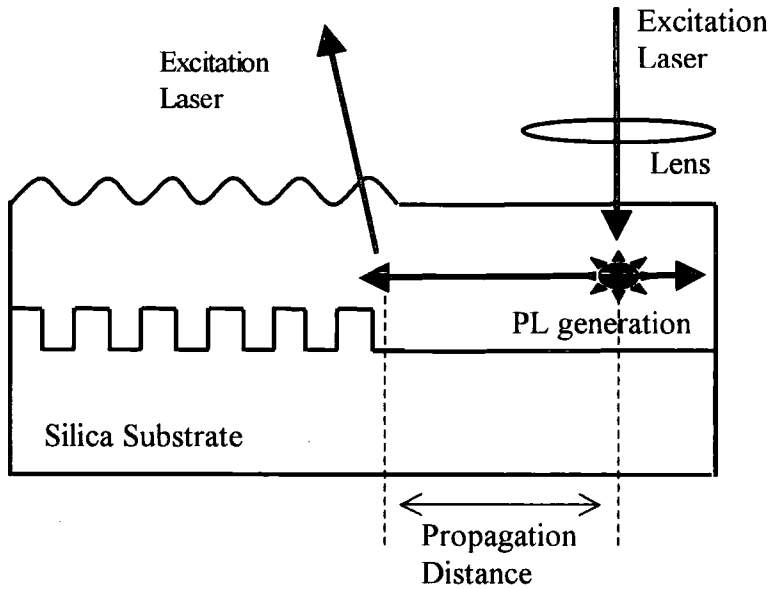

Figure 6.21 *Schematic diagram showing the method used to estimate the propagation distance of waveguide modes in Polymer films.*

By adjusting the position of the optical fibre detector, it was possible to set the wavelength of the peak under observation to any wavelength in the emission spectrum of the MEH-PPV. In theory, this technique could be used to make accurate measurements of the absorption of polymer in this part of the spectrum. In general measuring weak absorption in polymer films is difficult to do with accuracy since

most standard methods such as measuring transmission through a film have difficulty in distinguishing between absorbed and reflected light. This technique does not suffer from this problem. In practice, an accurate calculation of absorption using this technique would require modelling to calculate the spread in propagation direction of a waveguide mode excited by a focused laser, and this lies outside the scope of this project. Nevertheless the experiment did allow a rough determination of the distance a waveguide mode can propagate in a film of MEH-PPV. Figure 6.22 shows the decay of a scattered peak at 645 nm, as the excitation area is moved away from the grating. From this plot, we can say with certainty that at least half the generated light is able to propagate 80 μm along the film. The scattered peak is still clearly present at 500 μm separation, so it is certain that a small but significant amount of light is able to propagate half a millimetre within the film. This information is very important for the design of LEDs and to justify the interpretations of results in this thesis.

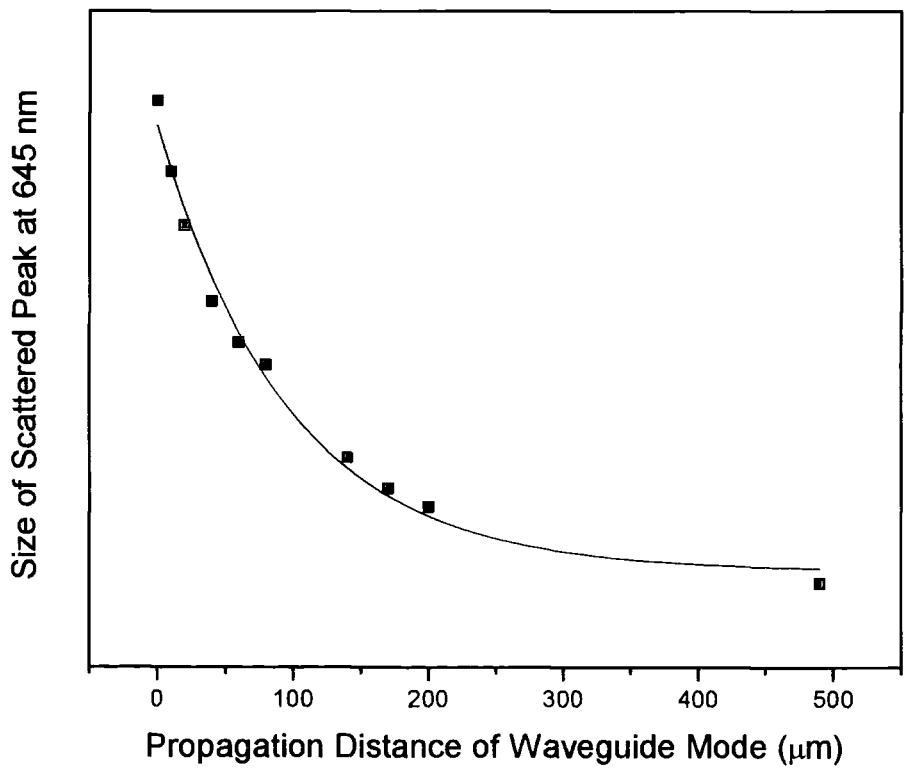

Figure 6.22 *Decay of scattered peak at 645 nm from waveguide mode as excitation spot is moved away from grating region.*

This experiment was repeated for several peaks at different wavelengths. It was observed that shorter wavelengths were able to propagate shorter distances, with the distances becoming hard to measure for wavelengths below 575 nm. The same experiment was also attempted using a metal layer on top of the polymer, deposited by evaporation. The propagation distance of the light in the uncorrugated MEH-PPV film region with a 40 nm Aluminium layer on top of the film (rather than air), was found be too short to measure accurately. This suggests that waveguide modes confined by a metal layer propagate substantially shorter distances than modes confined on both sides by dielectrics.

6.3.8 Multiple waveguide modes

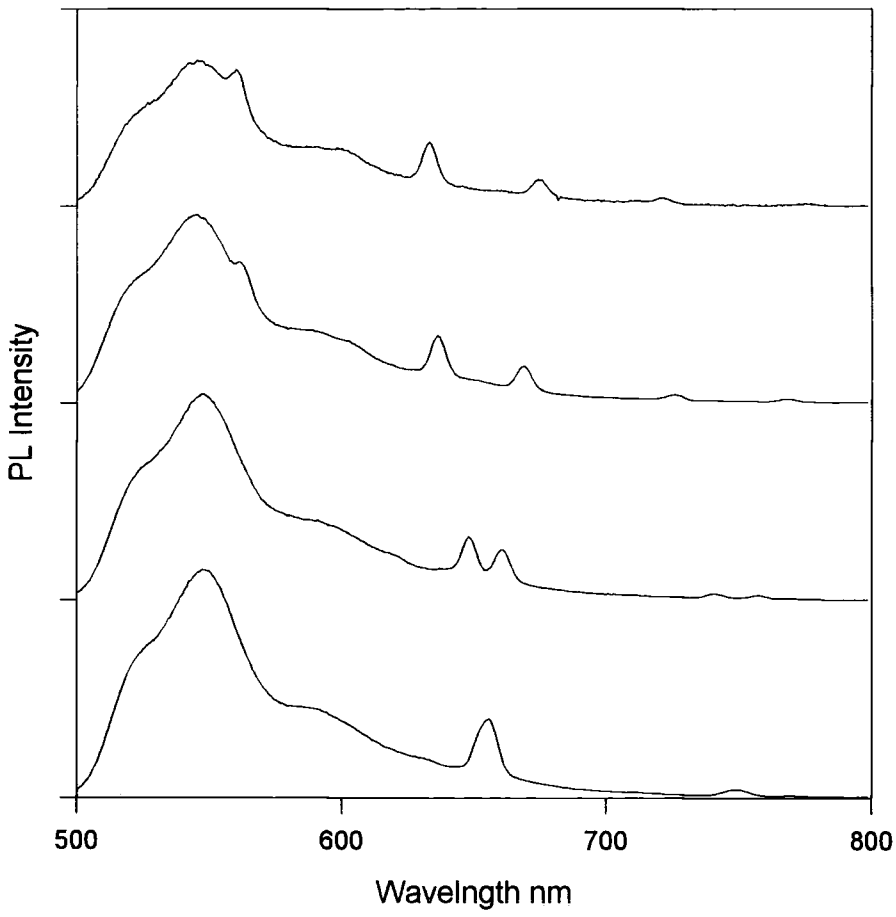

Figure 6.23 *Scattered waveguide peaks from corrugated PPV film 500 nm thick. The lower curve shows emission at normal incidence, with scattered peaks at 655 nm and 750 nm. The curve above this shows emission at an angle of (2,0), where both peaks have split. The curve above shows an angle (4,0), and the top curve (6,0).*

Most of the PL spectra using grating substrates considered so far have been for MEH-PPV films with thickness in the region 150 nm to 200 nm. Several samples were also made using PPV films on photoresist gratings. It was found that spinning undiluted PPV precursor and then thermally converting was suitable for depositing thick films. Figure 6.23 shows a PL spectrum from a PPV film sufficiently thick to show scattering from two modes at normal incidence. As the position of the detector is rotated in the xy plane to an angle of (6,0), another scattered feature from another modes becomes apparent at about 560 nm. In general it was found that in order to show scattering from multiple modes, conjugated polymer films (or indeed any samples with similar refractive index to these) needed to have a thickness in excess of 450 nm, when using photoresist gratings with a period of 400nm. Films thinner than 90 nm did not show any scattered modes at all using these gratings.

6.3.9 Conclusion

The work presented in this chapter has demonstrated that lateral microstructure can have a dramatic effect on the photoluminescence from conjugated polymer thins films. It has been shown that the spectra are changed substantially and that a large overall increase in photoluminescence quantum yield can be obtained. Furthermore, it has been shown that by altering the period of the grating, the photoluminescence can be tuned, allowing an increase in selected wavelengths in desired emission directions.

These results have been interpreted by considering the scattering of light within waveguided modes that would otherwise have been absorbed after propagating a fraction of a millimetre within the film. The scattering conditions have been analysed mathematically (considering the grating as a perturbation from the planar case), and the observed effects can be explained over all emission angles and for gratings with different periods. The analysis here is insufficient to model the effects of high amplitude gratings, or gratings that include a metal interface. The effect of stronger gratings on the light emission from conjugated polymer films is considered in the next chapter.

So far this thesis has only considered effects on photoluminescence caused by gratings. In simple LED designs, it has been shown that as much as ninety percent of generated light is lost to waveguide modes. If the results shown here are replicated in electroluminescence, then there is potential to create more efficient light emitting diodes by recovering waveguided light. This is demonstrated in the last chapter.

---

[1] J. Gruner, F. Cacialli, I. Samuel and R. Friend, Conference Proceedings NATO-ARW on Quantum Optics in Wavelength Scale Structures, Cargese, Corsica, Aug 26-Sept 2 (1995)

[2] M. G. Craford, in *High Brightness Light Emitting Diodes*, Vol. 48 (Eds: G. B. Stringfellow, M. G. Craford), Academic, San Diego, CA (1997)

[3] S. E. Burns, N. C, Greenham, R. H. Friend, Synthetic Metals, 76, 205 (1996)

[4] S. C. Kitson, W. L. Barnes, J. R. Sambles, IEEE Photon . Tech. Lett, 8, 1662 (1996)

[5] B. J. Matterson, M. G. Salt, W. L. Barnes, I. D. W. Samuel, Synthetic Metals, 101 (1-3): 250-251 (1999)

Chapter 7

Metal Gratings and Corrugated LEDs

7.1 Introduction

The previous chapter demonstrated that it was possible to use a grating to increase photoluminescent emission from a conjugated polymer film by scattering waveguide modes. So far, the gratings used have been made of dielectric materials. If this technique is to be extended to be of use for LEDs, then it is necessary to sandwich the polymer between materials that make suitable electrodes. LEDs using luminescent conjugated polymers usually have at least one metal electrode. It is therefore important to know how the scattering of waveguide modes is affected when a metal grating is used.

In general when light is incident on a corrugated interface, the effect of the corrugations is likely to be enhanced if there is big difference in refractive index between the layers (if both layers have the same complex refractive, then light would not be affected by the corrugations at all). Due to the complex refractive index of metals (due to their high absorption), there will always be a high contrast in complex refractive index between metal and dielectric layers. Thus it should be expected that scattering from metal gratings would be more dramatic than that observed from dielectric gratings[1].

This chapter starts by investigating the effect that metal gratings have on photoluminescence spectra of MEH-PPV. Strong mocifications of spectra are observed. It is found that the amplitude of the metal gratings affects the shape of the spectra in addition to the total intensity of the photoluminescence. It is determined that using gratings with high amplitude, it is possible to obtain dramatic increase in light output and hence photoluminescence quantum yield. Finally, it is demonstrated that this technique could be used in electroluminescence, and can provide a method for improving the efficiency of conjugated polymer LEDs[2,3,4].

7.2 Photoluminescence from Polymers on Metal Gratings

The effect of metal gratings on PL was found to be highly dependent both on the amplitude of the grating, and the thickness of the conjugated polymer film. Several PL spectra taken from films with weak gratings (<60 nm amplitude) and thin MEH-PPV layers (<80 nm) showed a reduction in total photoluminescence for corrugated regions coated in metal when compared to uncorrugated metal reference regions on the same substrate. For films of thicker MEH-PPV (>140 nm) it was found that corrugating the metal layer in contact with the polymer could be used to increase photoluminescence from the sample. The shape of the photoluminescence spectrum was found to vary considerably with the grating amplitude, suggesting that there might be more processes involved than the simple scattering model discussed in the previous chapter.

In order to analyse the effect of grating amplitude on the modification of photoluminescence spectra, several sets of gratings were manufactured with a range of grating amplitudes, but with a constant grating period. The sequence of plots shown here are photoluminescence spectra from a set of gratings with a period of 388 nm. The gratings were created in a layer of photoresist using the method described in the previous chapter. The gratings were manufactured so that each substrate had a corrugated region and a flat region. This allowed modified and reference spectra to be taken from the same substrate, simply by using the excitation laser to excite a different region of the film. Strips of aluminium and gold were evaporated on top of the photoresist in such a way that there would be a corrugated and flat region for each metal and also corrugated and flat regions with no metal on each substrate. The metal was 40 nm thick for the aluminium and 25 nm thick for the gold. Finally MEH-PPV was deposited by spinning to a thickness of 150 nm. The resulting structure is shown schematically in figure 7.0.

By taking modified and reference spectra from the same substrate it was ensured that the thickness of polymer and metal regions would be constant, and that there would be little chance for the polymer to degrade between measurements. The spectra were taken using the apparatus described in the previous chapter, again

keeping the sample in a vacuum, and using a 488 nm argon ion laser to excite the sample. The excitation laser was passed through a quarter wave plate adjusted to circularly polarise the light, so that no mode is preferentially excited in the sample.

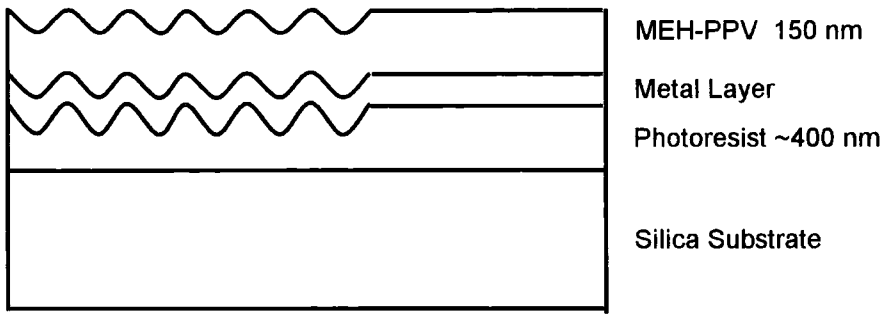

Figure 7.0 *Structure used to investigate the effect of corrugation amplitude on the photoluminescence of MEH-PPV.*

The following series of graphs (figure 7.1 to figure 7.6) shows a sequence of photoluminescence spectra taken at normal angle from gratings with gradually increasing amplitude (7 nm 13 nm, 35 nm, 50 nm, 90 nm, 140 nm), for both aluminium and gold gratings with a period of 388 nm. From figure 7.1, it can be seen that a metal grating with a weak amplitude of only 7 nm can still have a dramatic effect on the photoluminescence of the MEH-PPV film. The photoluminescence from the corrugated region is dramatically reduced when compared to the uncorrugated region, with the exception of a single peak at 587 nm for the aluminium grating, and a peak at 590 nm for the gold grating, where the luminescence is strongly increased in both cases. In figure 7.2, it can be observed that the grating with amplitude 13 nm gives a similar reduction in photoluminescence for the aluminium apart from the single peak. However the gold grating does not substantially reduce the photoluminescence for any wavelengths, but still causes a large peak at 584 nm.

The subsequent graphs showing gratings of 35 nm and upwards all show an increase in photoluminescence from the grating regions. The peaks appear to become broader as the gratings become stronger. For the strongest gratings with amplitudes 90 nm and 140 nm (figures 7.5 and 7.6), the photoluminescence across the entire spectrum is increased fairly evenly, with no narrow peaks evident.

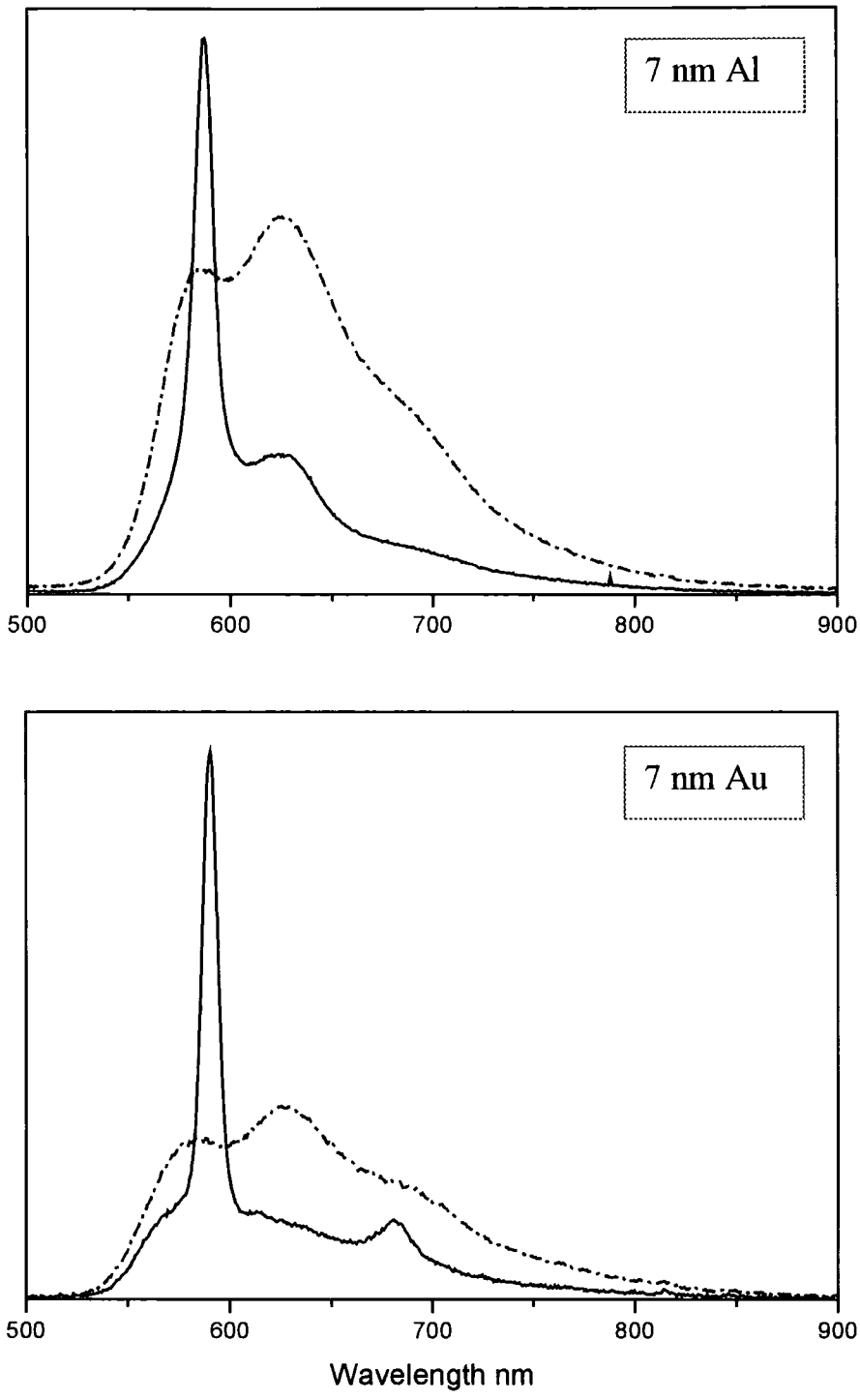

Figure 7.1 *Photoluminescence Spectra from MEH-PPV 150 nm thick on corrugated metal (continuous line) and flat metal (dashed line), at normal angle (0,0). The metal layer was aluminium in the top graph and gold in the lower graph. The corrugation amplitude (peak to trough) was 7 nm, with period 388 nm.*

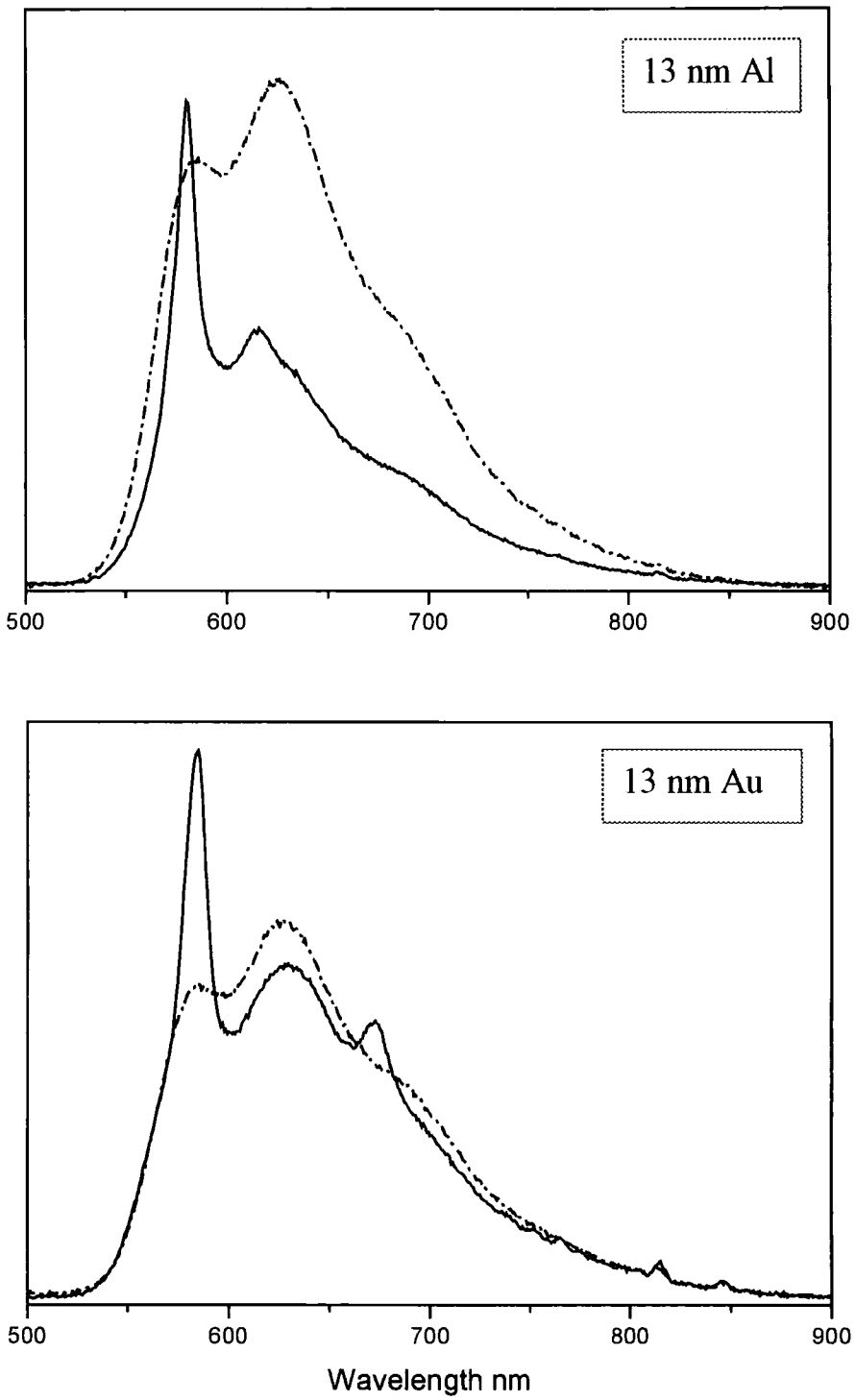

Figure 7.2 *Photoluminescence Spectra from MEH-PPV 150 nm thick on corrugated metal (continuous line) and flat metal (dashed line) at normal angle (0,0). The metal layer was aluminium in the top graph and gold in the lower graph. The corrugation amplitude (peak to trough) was 13 nm, with period 388 nm.*

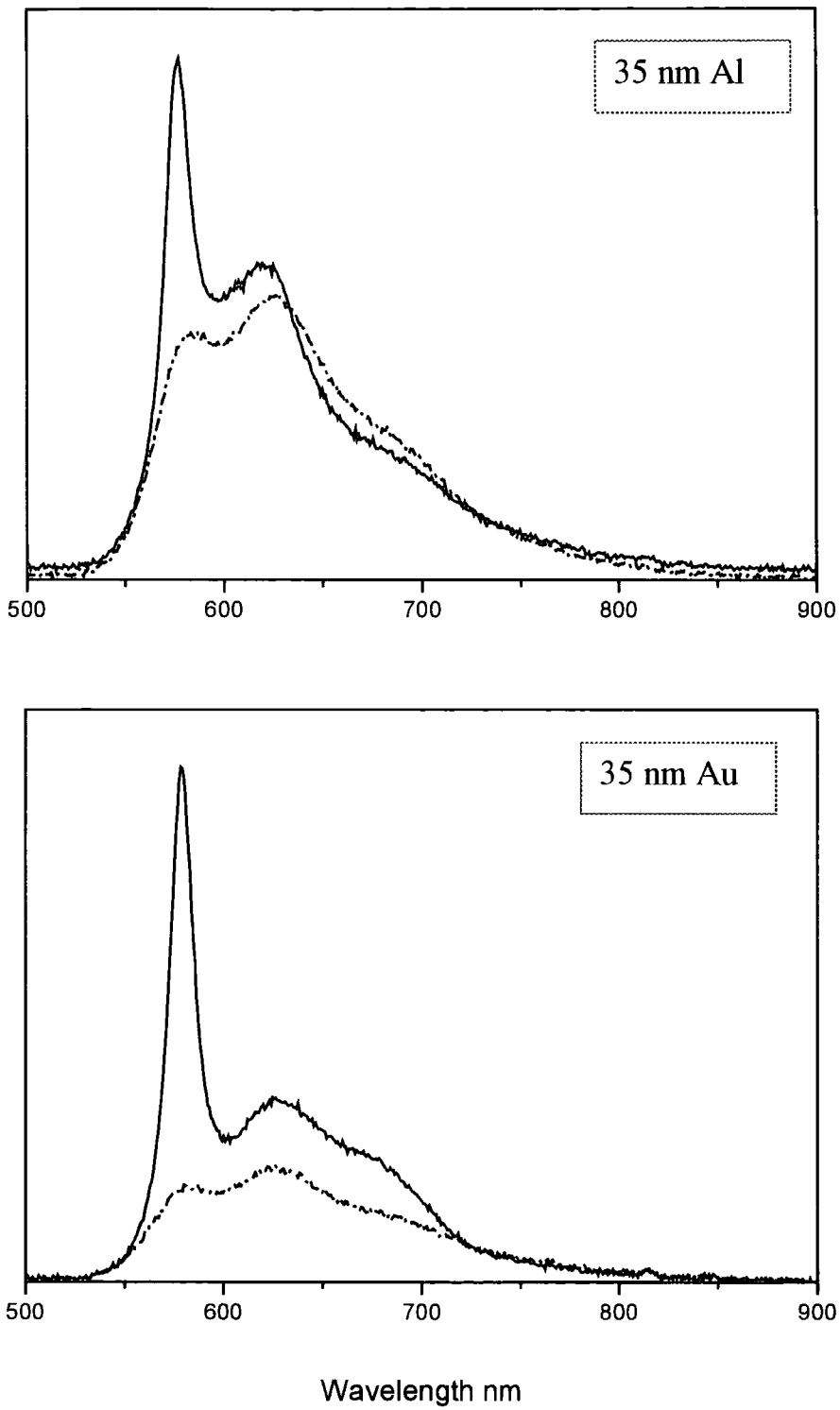

Figure 7.3 *Photoluminescence Spectra from MEH-PPV 150 nm thick on corrugated metal (continuous line) and flat metal (dashed line) at normal angle (0,0). The metal layer was aluminium in the top graph and gold in the lower graph. The corrugation amplitude (peak to trough) was 35 nm, with period 388 nm.*

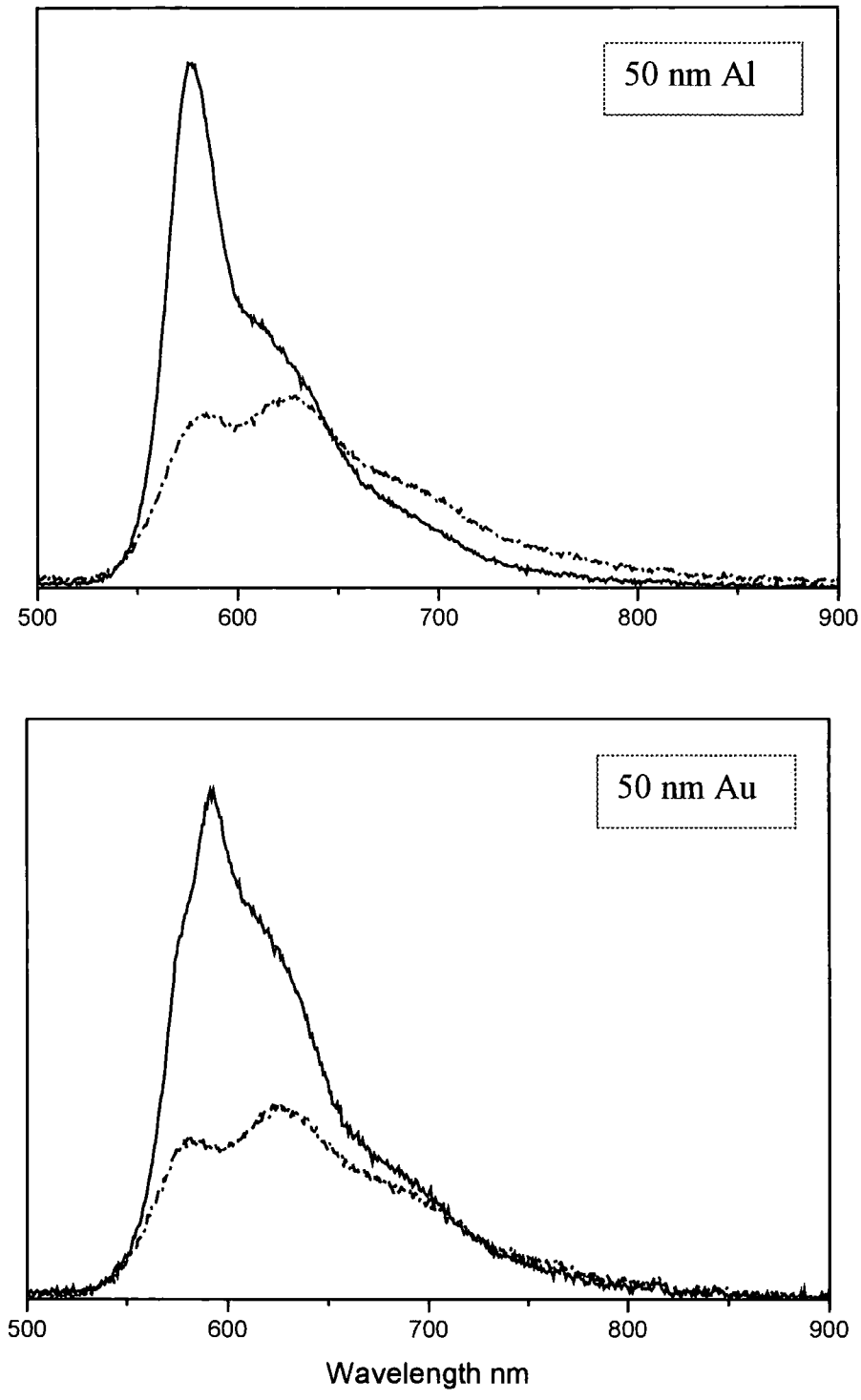

Figure 7.4 *Photoluminescence Spectra from MEH-PPV 150 nm thick on corrugated metal (continuous line) and flat metal (dashed line) at normal angle (0,0). The metal layer was aluminium in the top graph and gold in the lower graph. The corrugation amplitude (peak to trough) was 50 nm, with period 388 nm.*

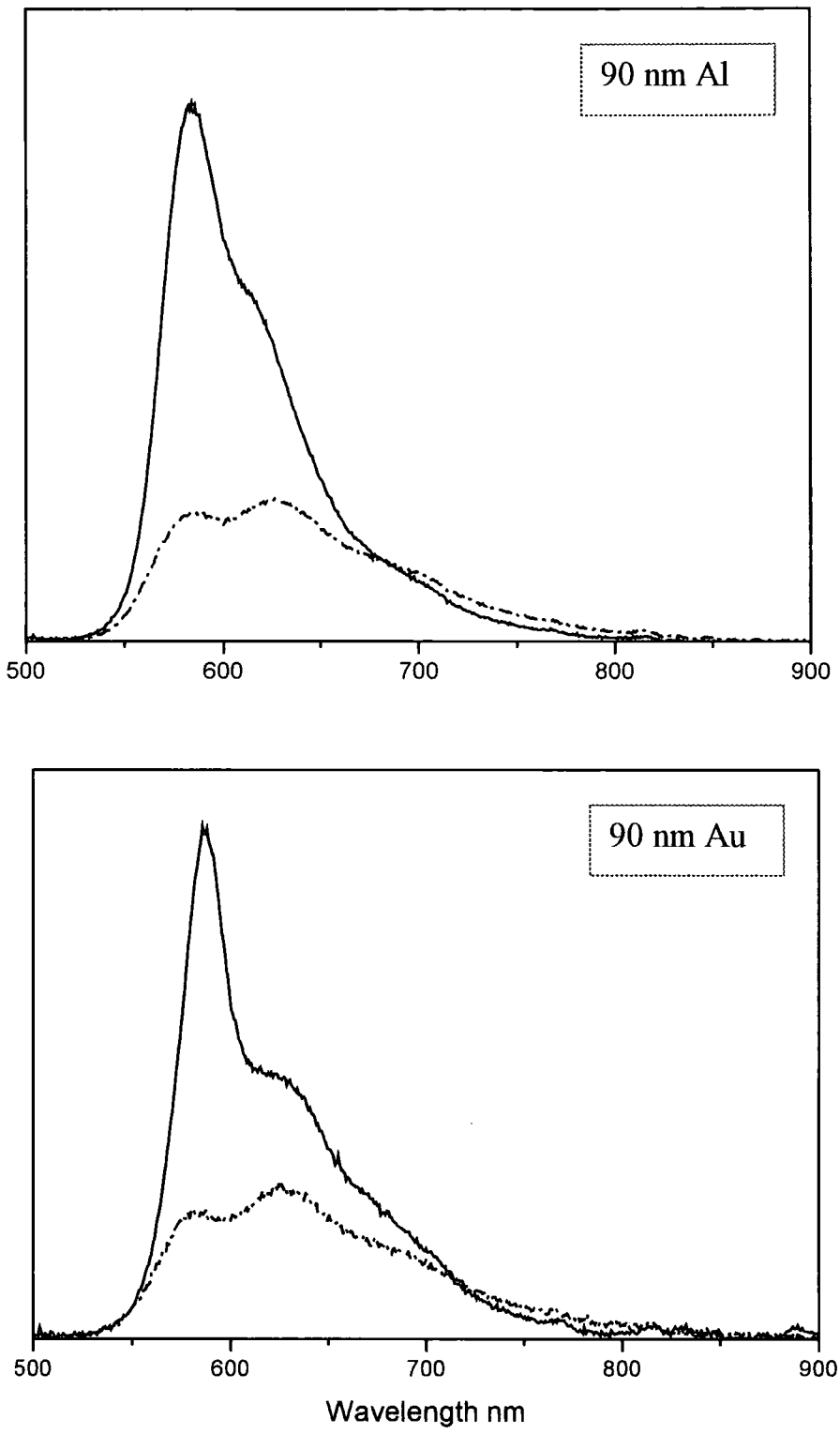

Figure 7.5 *Photoluminescence Spectra from MEH-PPV 150 nm thick on corrugated metal (continuous line) and flat metal (dashed line) at normal angle (0,0). The metal layer was aluminium in the top graph and gold in the lower graph. The corrugation amplitude (peak to trough) was 90 nm, with period 388 nm.*

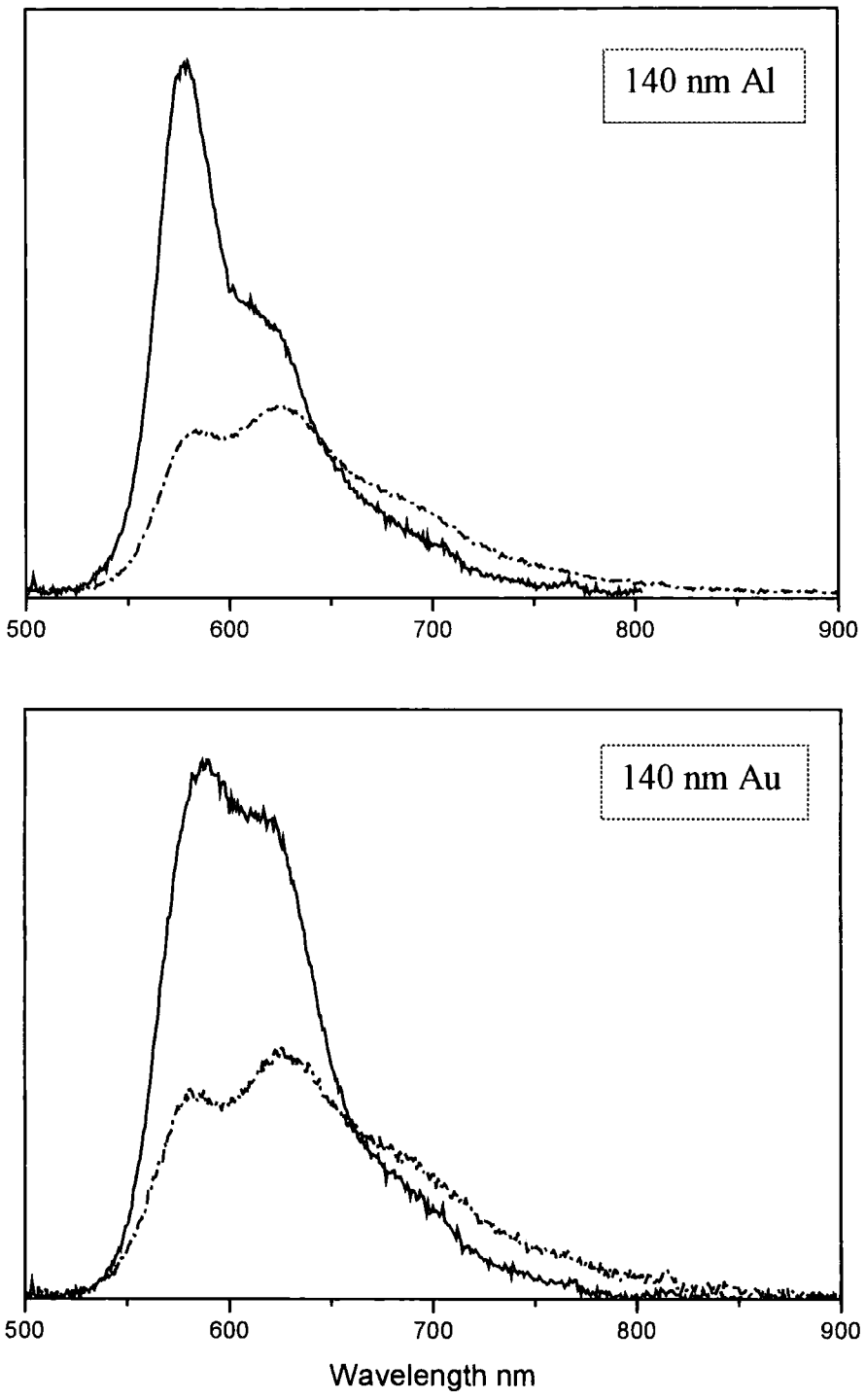

Figure 7.6 *Photoluminescence Spectra from MEH-PPV 150 nm thick on corrugated metal (continuous line) and flat metal (dashed line) at normal angle (0,0). The metal layer was aluminium in the top graph and gold in the lower graph. The corrugation amplitude (peak to trough) was 140 nm, with period 388 nm.*

It is possible to analyse the effects from the weaker gratings theoretically by considering the corrugation as a slight deviation from the planar case. If this assumption is reasonable, then it is expected that a grating with a period that is the same as the wavelength of a propagating mode will scatter that mode into the forward direction. In figure 7.1, the scattered peak is at 587 nm. If the grating with period 388 nm is able to scatter this wavelength into the normal direction, then it can be assumed that the effective wavelength of this mode in the plane of the substrate will match the grating period, taking the film index and waveguiding angle into account. The effective waveguiding angle θ can therefore be calculated using:

$$\sin\theta = \frac{\lambda_{real}}{n_f \lambda_{grating}} \qquad (7-1)$$

where n_f is the refractive index of the film at the 587 nm wavelength, λ_{real} is the wavelength of the scattered peak observed in the emission spectrum, and $\lambda_{grating}$ is the period of the grating, which must be assumed to match the effective wavelength of the propagating waveguide mode. This gives $\theta=\sin^{-1}(587/(2.0 \times 388)) = 49.2°$.

This can be compared with the theoretical prediction obtained using the computer program discussed in chapter four. The modal structure of a film 150 nm thick with refractive index 2.0 is shown in figure 7.7. Using the program, the waveguiding angle for light in this film with a wavelength of 587 nm is predicted to be 48.1°. This is in good agreement considering the errors in refractive index of the polymer and the metal layers.

The procedure can be reversed by using the optimisation routine of the computer program to find a suitable film thickness that will give the required waveguiding angle to a chosen wavelength in order to allow it to be scattered in a desired direction. The thickness of film that is predicted by the program to give a waveguiding angle of 49.2°, and hence allow a grating period of 388 nm to scatter light of 587 nm into the normal direction is found to be 144 nm. This is certainly close to the measured film thickness of 150 nm, and within the error limits of the measurement. Film thicknesses were measured experimentally using an alphastep,

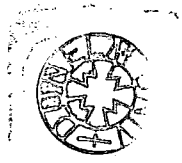

and it was found that variations of film thickness of 5-10 nm were not unusual from films of MEH-PPV deposited by spin coating.

When the photoluminescence spectrum from the stronger gratings are observed, it can be seen that the position of the large peak has not moved far from the 587 nm position when the grating peak to trough depth has been increased to 50nm, but the definition of the peak is somewhat reduced. It seems that there may be some value in analysing the planar mode structure when corrugations depths are less than 50 nm or so, but for corrugations stronger than this the 'near' planar analysis is perhaps of limited value.

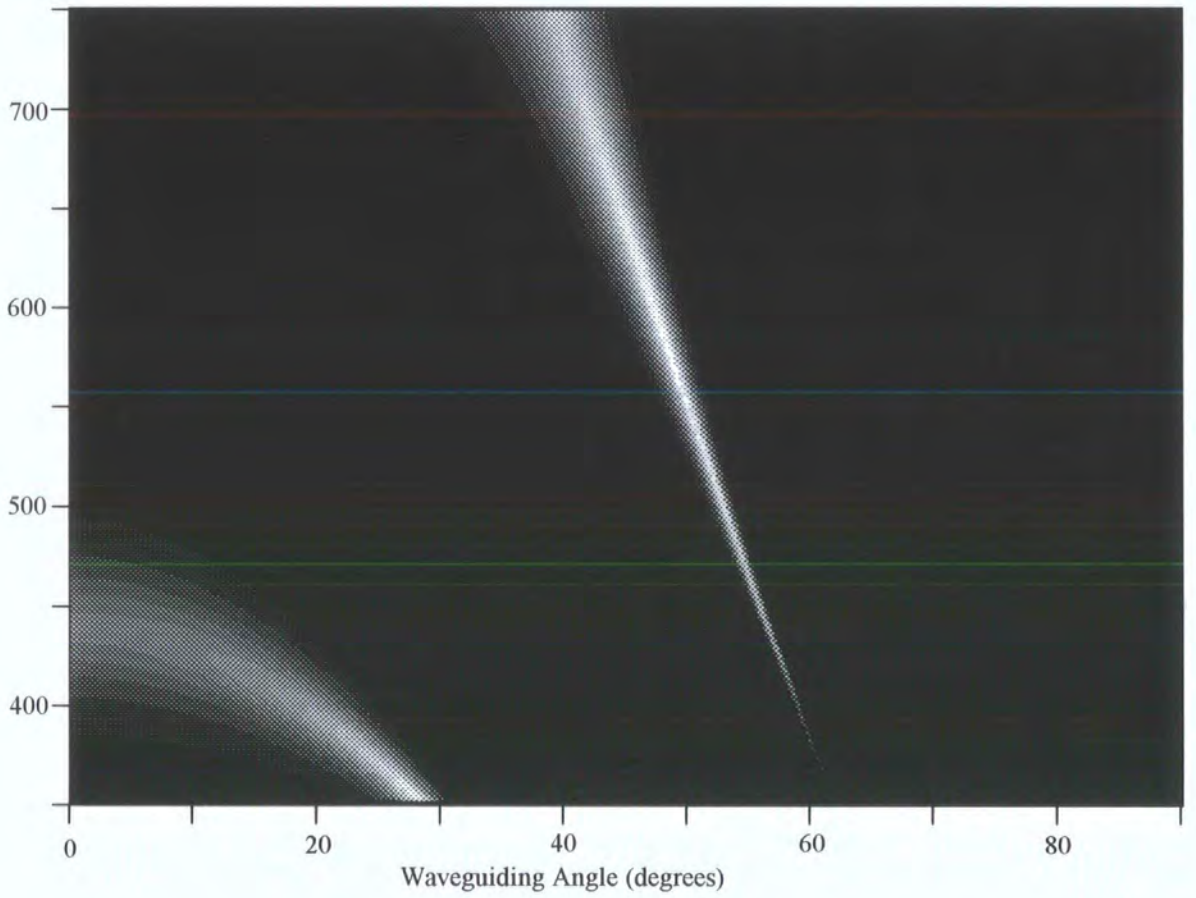

Figure 7.7 *Theoretically predicted TE modes shown in white, for film 150 nm thick with refractive index 2.0, on a thick aluminium layer. The index of aluminium is taken as 1.2+7.3i. The y axis gives the wavelength in nanometers of the mode propagating at the angle given on the x axis. This modelling predicts that at 587 nm the mode propagation angle will be 48.1, a reasonable agreement with the experimental observation.*

7.2.1 Angular Dependence of Photoluminescence from Metal Gratings

In figures 7.1 to 7.6, the photoluminescence spectra from the gratings at normal angle show a gradual change in features as the grating amplitude increases. Measurements were also made on these gratings at a range of angles. It was found that for the weaker gratings, the behaviour of the large peak was similar to the behaviour of the scattered peaks from corrugated photoresist discussed in the previous chapter, suggesting that a similar method of scattering is involved.

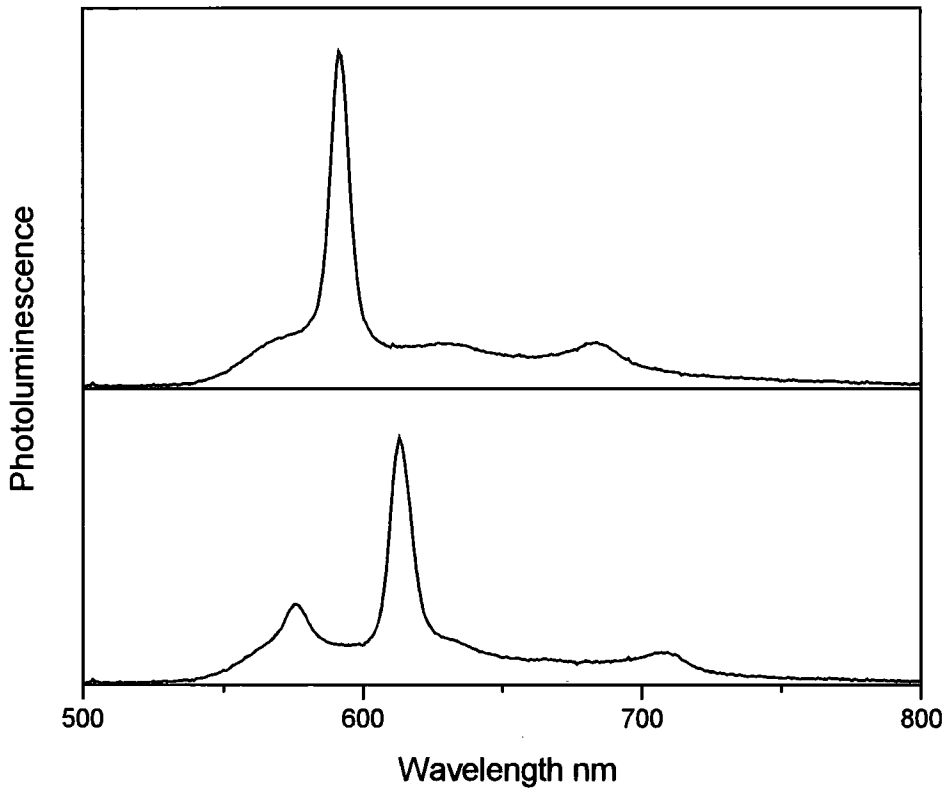

Figure 7.8 *Photoluminescence spectra taken from MEH-PPV (150 nm) on gold coated grating with period 388 nm and amplitude 13 nm. The top graph was taken at normal angle, the lower graph taken with the detector rotated ten degrees within the plane perpendicular to the grating lines (θ=10, ψ=0).*

Due to the different waveguiding conditions caused by the presence of the metal, the peak is positioned towards the shorter wavelength edge of the MEH-PPV spectrum. However, for some gratings the peak could still be observed to 'split' when

the detector was moved slightly away from the forward emission angle (0,0). An example of this, for the grating with amplitude 13 nm, is shown in figure 7.8. The large peak at 591 nm in the top graph taken at normal incidence splits into two at an angle (10,0), although the shorter wavelength peak at 576 nm is quite small. It is likely that this is caused by the scattering of two waveguide modes travelling in opposite directions perpendicular to the grating lines. The technique described in section 6.3.7 were used to try and confirm this, but it was found that it was not possible to measure the propagation distance of waveguide modes in samples of polymer deposited onto metal. This could be explained if the absorption associated with the metal makes the propagation distance of a waveguide mode very short. There is also a small peak at 684 nm for the forward angle (0,0), which gradually shifts to 707 nm for the (10,0) angle.

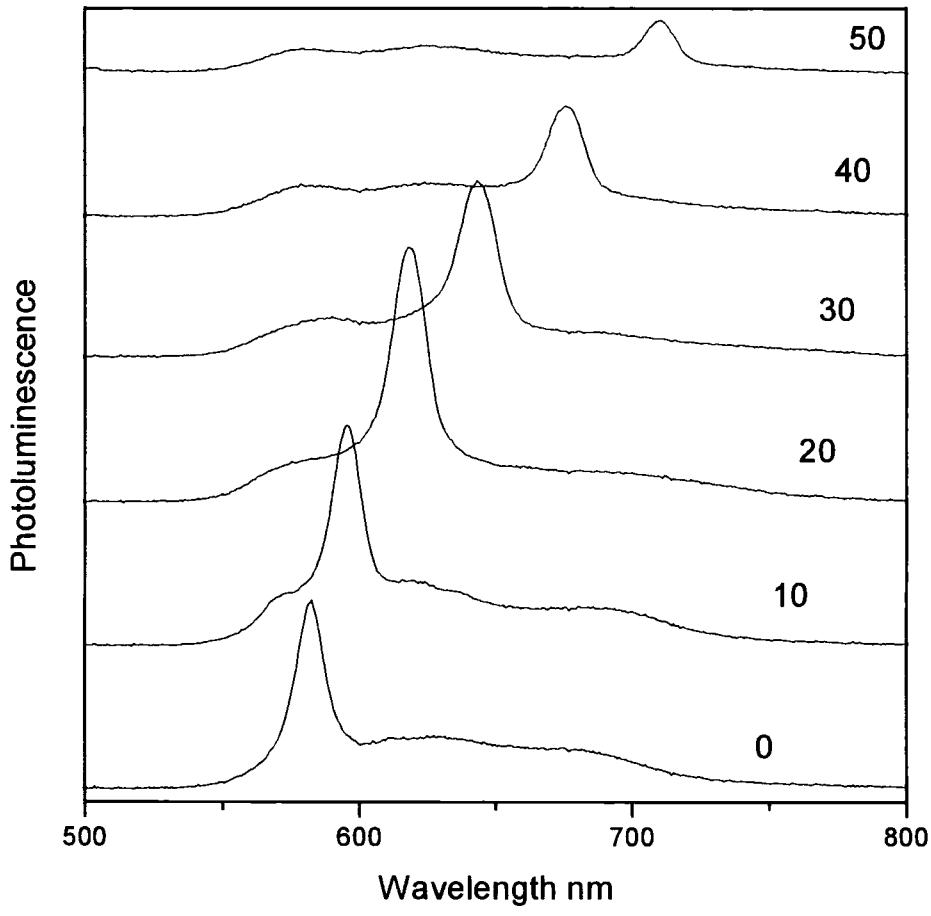

Figure 7.9 *Variation of photoluminescence spectrum of MEH-PPV (150 nm) on gold grating with amplitude 35 nm. Angle of detection normal for lowest curve, increasing by ten degrees at a time in the θ direction for each higher curve.*

From the data for emission normal to the substrate, shown in the previous section, it can be observed that the gratings with larger amplitudes tended to have much broader peaks in their emission spectra. Figure 7.9 shows spectra taken from a range of angles (rotating the detector in the xy plane) from the gold coated region of the 35 nm grating, and figure 7.10 spectra from the gold coated 90 nm grating. In both graphs, the peak shifts to longer wavelength as the angle is increased. It can be observed that the peaks in the angular spectra from the 90 nm grating are broader than the peaks observed in the spectra from the 35 nm grating, and both are broader than the peaks observed from the 13 nm grating. The broadening of peaks from stronger gratings was a feature observed from regions of corrugated aluminium and gold.

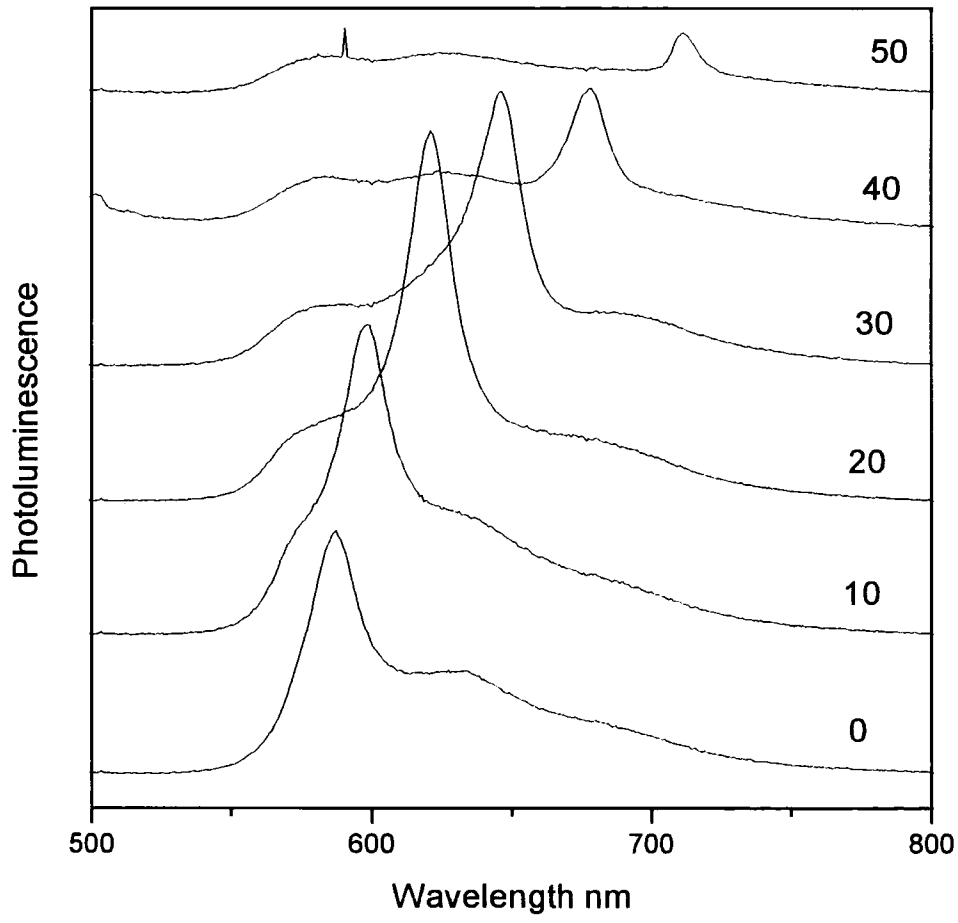

Figure 7.10 *Variation of photoluminescence spectrum of MEH-PPV (150 nm) on gold grating with amplitude 90 nm. Angle of detection normal for lowest curve, increasing by ten degrees at a time in the θ direction for each higher curve.*

Although the width of the peak in the angular photoluminescence spectra increases for the stronger corrugated gratings, the dependence of the position of the peak on detection angle remains approximately constant for grating amplitudes of less than 100 nm. For gratings with amplitude greater than 100 nm, the angular variation of the spectra becomes comparatively slight, although the spectra still have dramatically increased intensity compared to the reference spectra from the uncorrugated metal regions of the films. Figure 7.11 shows the angular dependence of the photoluminescence spectra from a strong grating, with amplitude 140 nm. The shape of the spectrum changes little with angle, although at an angle (40,0) the shoulder of the graph at 635 nm becomes more pronounced.

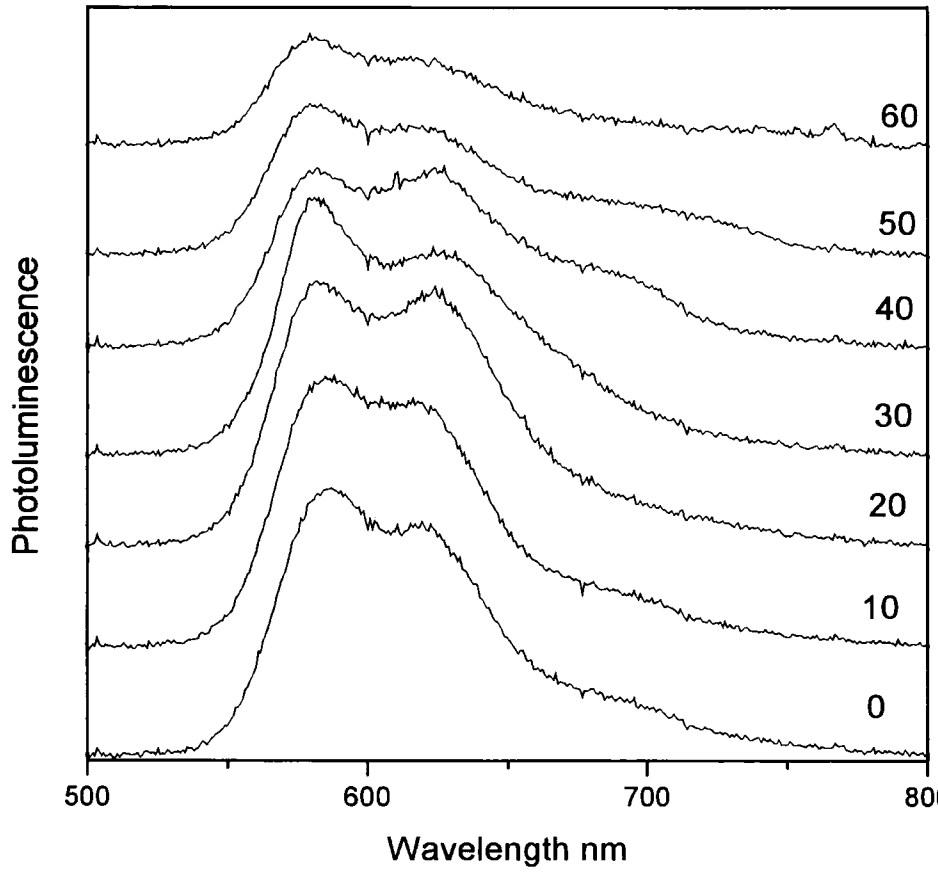

Figure 7.11 *Variation of photoluminescence spectrum of MEH-PPV (150 nm) on gold grating with amplitude 140 nm. Angle of detection normal for lowest curve, increasing θ by ten degrees at a time for each higher curve.*

A possible explanation for the increase in the width of the peaks in the photoluminescence spectra from metal gratings is that the increase in grating

amplitude causes any waveguide modes to be scattered more strongly, and thus propagate a shorter distance within the film. If the propagation distance of a waveguide mode is short, then the area of the evanescent field above the film that generates the freely propagating light is also small, and would thus be expected to diffract into a large area. This is similar to the effect that light passing through a narrow slit diffracts into a larger angular range than light passing through a wider slit.

7.2.2 High Amplitude Gratings

In the results analysed so far, the photoluminescence spectra from conjugated polymer films on metal gratings have been fairly simple, and it has been possible to find viable explanations for most of the features observed. However, when strong gratings with an amplitude of the order of 200 nm were used, it was found that the resulting spectra were considerably more complicated, and some of the features observed in the spectra were less easy to explain.

A deep photoresist grating, with an amplitude of approximately 200 nm (peak to trough distance) and a period of 400 nm was coated with a strip of aluminium along one edge to a depth of 40 nm using evaporation. MEH-PPV was deposited using spin coating to a depth of 220 nm. Finally another strip of aluminium 30 nm thick was evaporated on top, along an edge adjacent to the bottom aluminium layer, so as to leave four areas of the film, one with no metal, one with metal on top, one with metal underneath, and one with metal above and below.

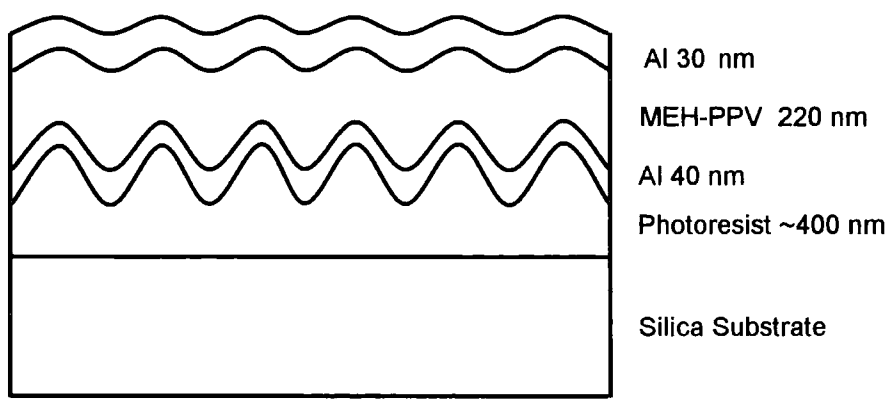

Figure 7.12 *Corrugated structure with MEH-PPV bound by layers of aluminium. Diffraction from the top layer of aluminium demonstrated that all the layers on top of the photoresist retained strong corrugation.*

It might be expected that the polymer deposited by spin coating would cover the corrugations so that its top surface was flat. However it was found that while the polymer dried, its top surface became corrugated like the grating below (this even occurred for gratings with a low amplitude). When the metal on top of the polymer was examined, it was found to diffract light strongly, showing that all layers of the structure remained corrugated, as shown in figure 7.12.

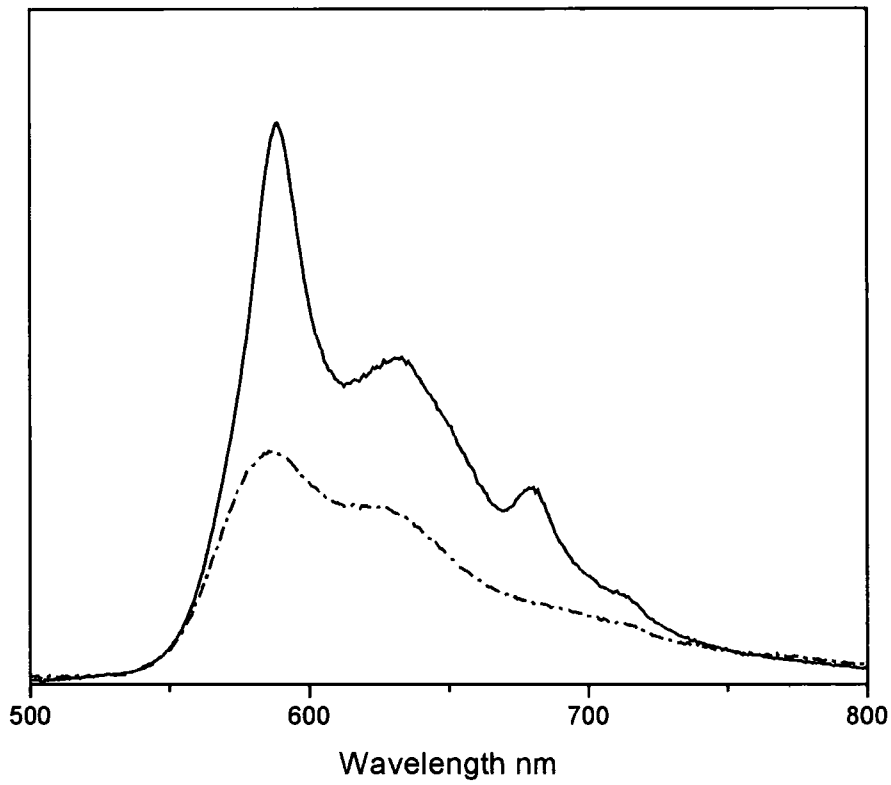

Figure 7.13 *Modified photoluminescence from MEH-PPV on strong photoresist grating at normal angle (continuous line). The grating amplitude is approximately 200 nm. The MEH-PPV thickness is 220 nm. The dashed line shows photoluminescence from an uncorrugated photoresist region.*

When the photoluminescence of the MEH-PPV on the photoresist was measured, it was found that the strong corrugations increased the free light generation across the entire spectrum, rather than just causing extra peaks in emission. However, there was still an extra peak generated for emission in the direction normal to the substrate (0,0) that split into two for non zero angles of θ, behaving in a similar way to the scattered peaks from weak gratings. Figure 7.13 shows a spectrum at normal

incidence from a strong photoresist grating, with the angular dependent peak present at 680 nm.

When the photoluminescence spectra from the aluminium coated region of the high amplitude grating were taken, it was found that the corrugations caused a dramatic increase in the light escaping from the sample, and shape of the spectra became more complicated, as shown in figure 7.14. The peak at 619 nm was found to be completely polarised, with the electric component of the feature lying parallel to the z axis (parallel to the direction of the grating lines). The peak at 582 nm was found to be unpolarised.

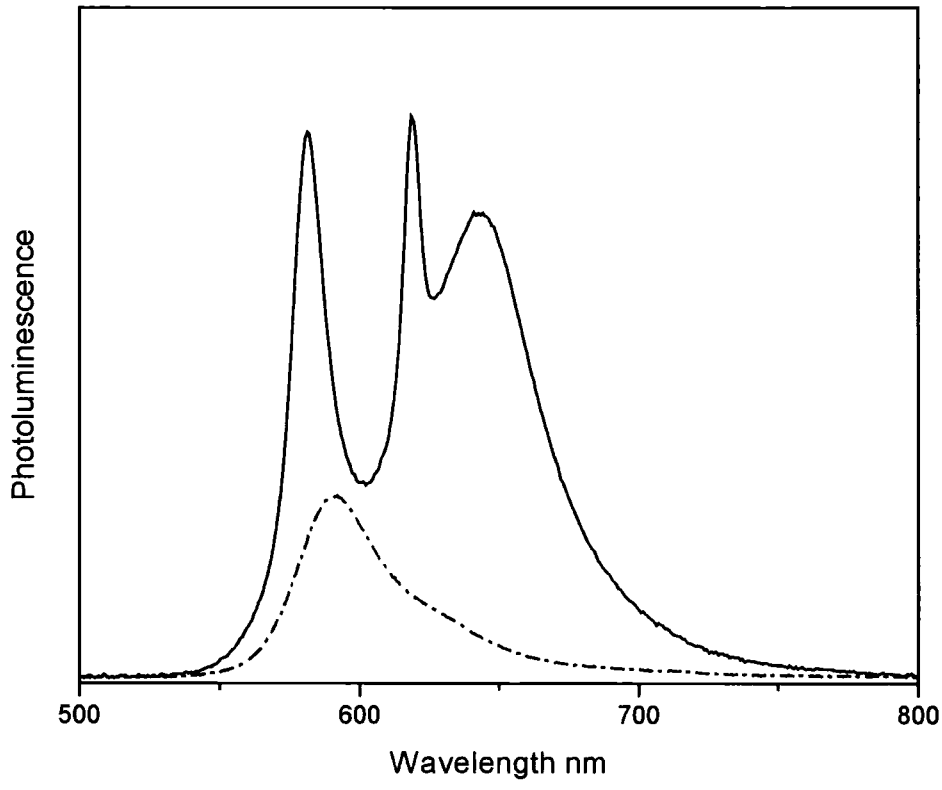

Figure 7.14 *Modified photoluminescence from MEH-PPV on strong aluminium grating, detected at normal angle (continuous line). The grating amplitude is approximately 200 nm. The MEH-PPV thickness is 220 nm. The dashed line shows photoluminescence from an uncorrugated aluminium region.*

The dependence of the photoluminescence spectra on viewing angle was also investigated for the high amplitude aluminium grating. It was found that the spectra

varied considerably with angle, and in a more complex manner than any the weaker gratings examined so far.

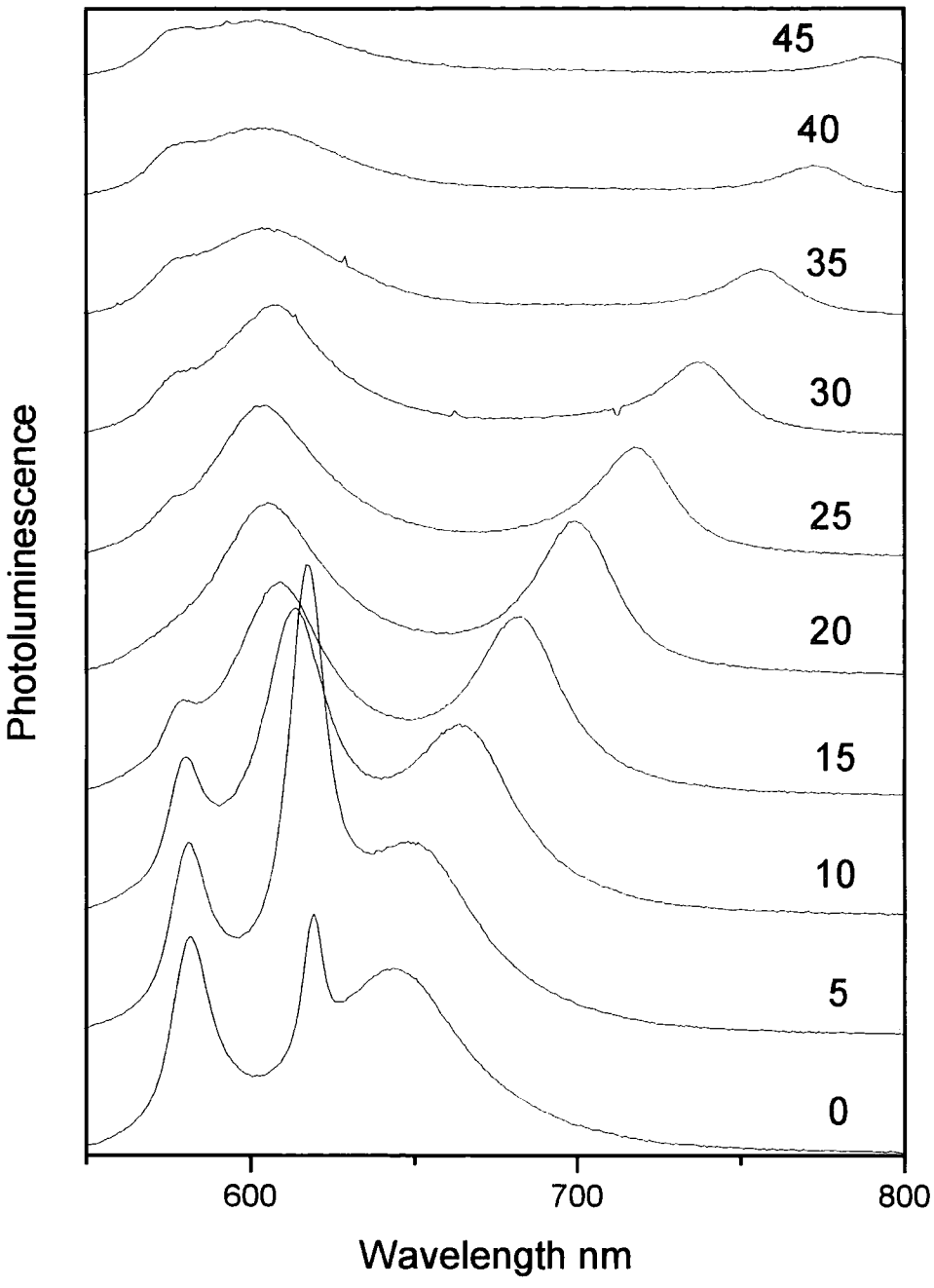

Figure 7.15 *Variation of photoluminescence spectrum of MEH-PPV film 220 nm thick on aluminium grating with amplitude 200 nm. Angle of detection normal for lowest curve, increasing by 5 degrees at a time in the θ direction for each higher curve.*

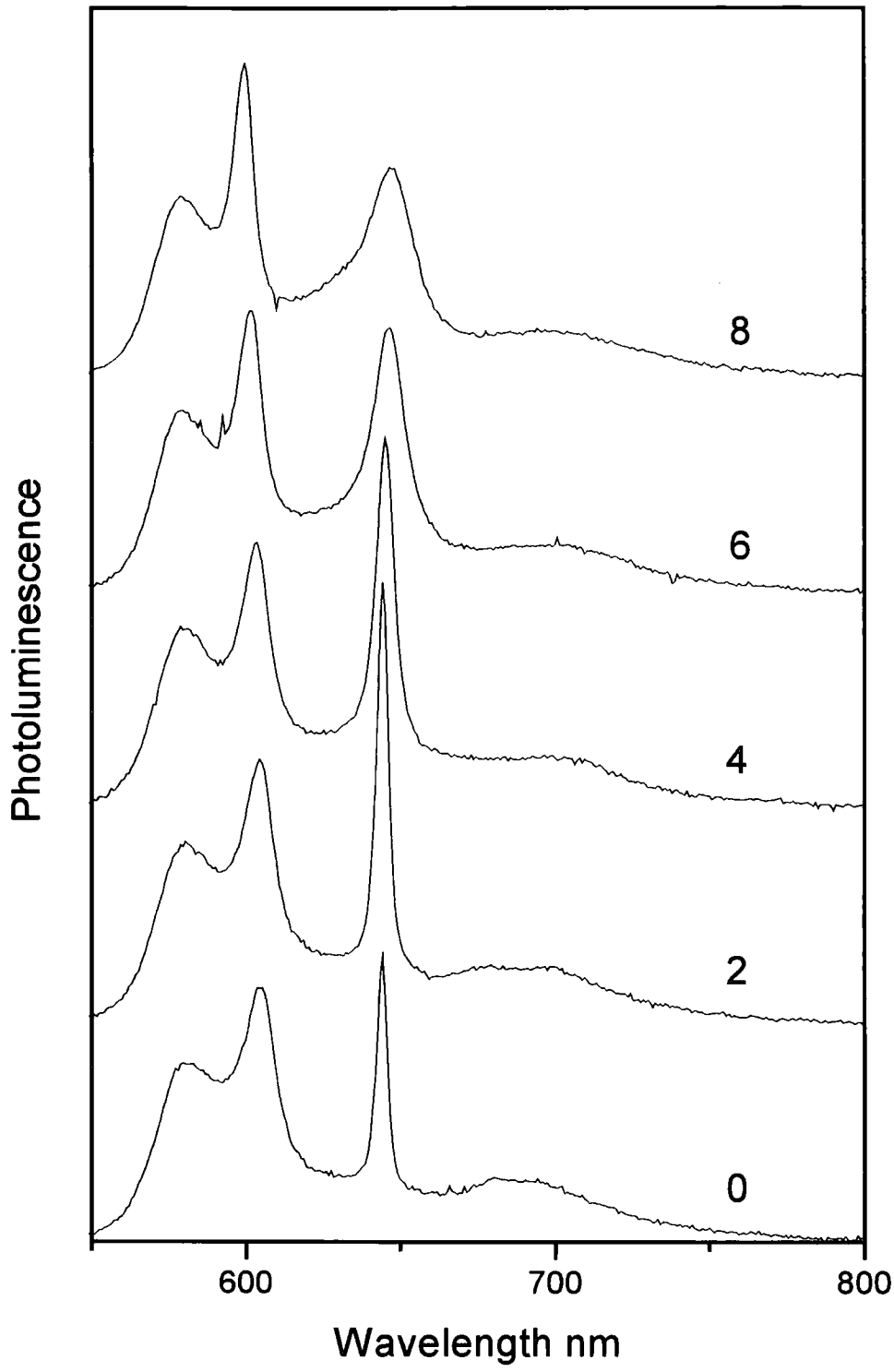

Figure 7.16 *Variation of photoluminescence spectrum of MEH-PPV film 260 nm thick on aluminium grating with amplitude 200 nm. Angle of detection normal for lowest curve, increasing by 2 degrees at a time in the θ direction for each higher curve. The peaks at 604 nm and 644 were both strongly polarised (with electric field vector lying parallel to the grating lines).*

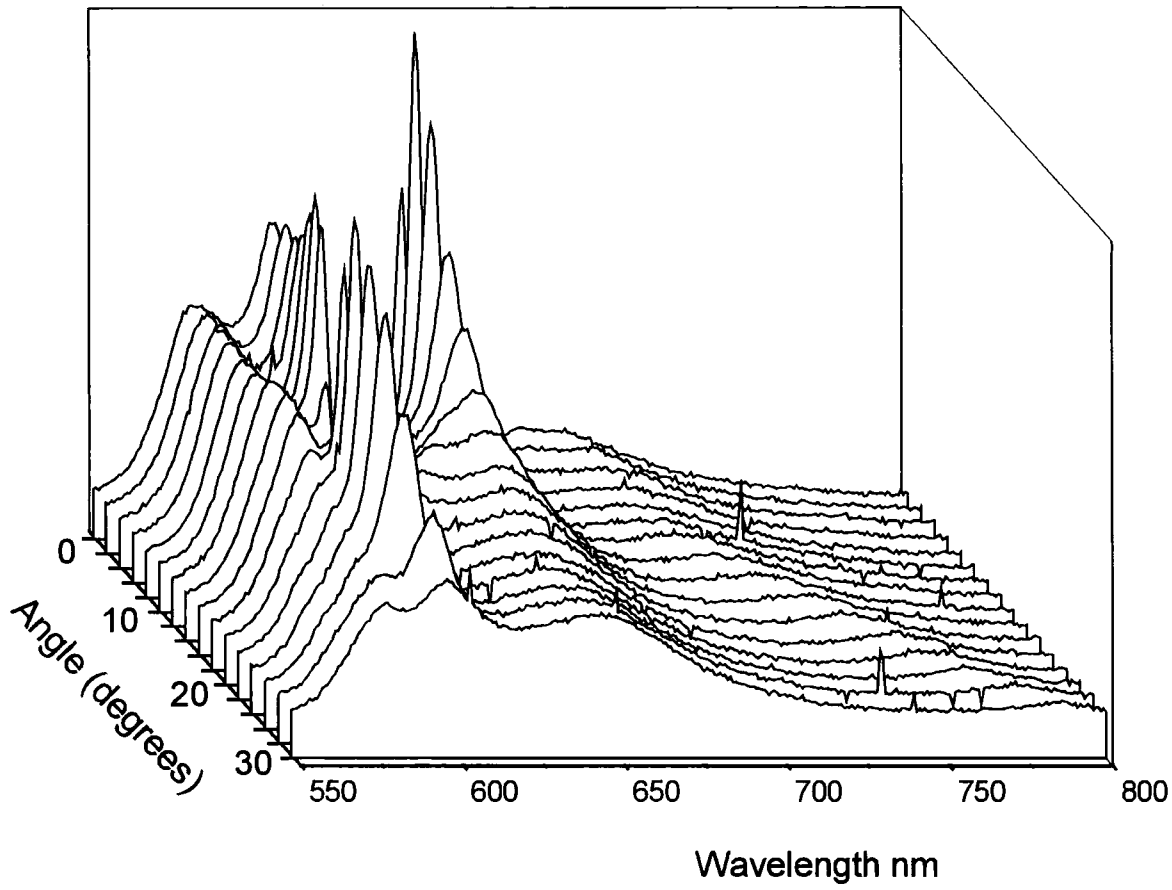

Figure 7.17 *Variation of photoluminescence spectrum of MEH-PPV film 260 nm thick on aluminium grating with amplitude 200 nm. Angle of detection normal for curve at the back, increasing by 2 degrees at a time in the θ direction for each nearer curve, giving a detection angle of (30,0) for the front curve. These graphs demonstrate the complexity of the variations in photoluminescence spectra that can be obtained from high amplitude gratings. The most dramatic features in the graphs are the peak at 644 nm that becomes very high when θ is approximately 2 degrees, and then quickly fades for larger θ, and the peak at 604 nm that becomes high at a θ angle of 10 degrees, almost vanishes when θ is about 16 degrees, and becomes high again when θ is approximately 20 degrees. Both of these features were found to be completely polarised with their electric vector parallel to the gratings lines.*

Figure 7.15 shows the angular dependence of the 220 nm thick MEH-PPV film on the high amplitude grating. Figures 7.16 and 7.17 show angular plots for an MEH-PPV film with thickness 260 nm. One of the most noticeable features of all these plots is the presence of a strongly polarised peak, visible at normal incidence, that dramatically increases in intensity for small angles of θ, and then quickly fades when θ is increased further. It is difficult to be completely sure of the origin of this feature, but a plausible explanation is the presence of a stop band (1D band gap) caused by a harmonic of the corrugated structure.

If a grating structure has a period that is suitable to scatter a waveguide mode into the normal direction, then using the arguments discussed in chapter three, a corrugation with half of this wavelength would be suitable to scatter a waveguide mode directly backwards so that its direction is reversed. The generation of waveguide modes directly within such a corrugated region is actually suppressed by the corrugations, effectively forming a stop band at that wavelength. However wavelengths slightly higher or lower than the 'stopped' wavelength are actually enhanced (as if enclosed by a microcavity).

It is possible that a grating with a high amplitude will have harmonics with frequencies that are integer multiples of the grating's fundamental frequency, since it is unlikely that the corrugations will be perfectly sinusoidal. By this argument, it is possible that a bandgap effect might occur for light scattered at normal angle by the grating. If light generation is suppressed by band gap, then it is expected that light generation will be enhanced at the band edges, causing an increase in photoluminescence at the wavelengths slightly longer or shorter than the bandgap wavelength. This bandgap effect could explain the dramatic increase in size of the polarized peak at 619 nm in figure 7.15, and at 644 nm in figure 7.16 when the detection angle is set a couple of degrees away from normal viewing angle within the xy plane. There is also a feature observable in figure 7.17 that might correspond to a bandgap where the peak at 604 nm is observed to drop dramatically at an angle (θ) of 16 degrees, but with dramatic increase in peak size at this wavelength for angles of 4 degrees greater or less then 16 degrees. The behaviour of this feature would certainly be consistent with a bandgap generated by a grating harmonic. Emission enhancement at band edges is usually observed from polymer films on short period gratings. Short

period gratings are most often used to generate feedback for lasers, but band edge emission increase still occurs below laser threshold[5].

7.3 Corrugated LEDs

If the methods used to enhance photoluminescence from conjugated polymer films could also be used to increase electroluminescence from conjugated polymer LEDs, then it is clear that these techniques would have considerable commercial value. Extending the use of corrugated structures to LEDs is challenging. If the external efficiency of an LED is to be increased using corrugations, then it is vital that the structure does not disrupt the electrical properties of the LED. It might be argued that using a corrugated structure within an LED would cause a non-uniform electric field structure within the device, which could potentially cause the device to fail. The structure that was first used to make a corrugated LED is shown in figure 7.18.

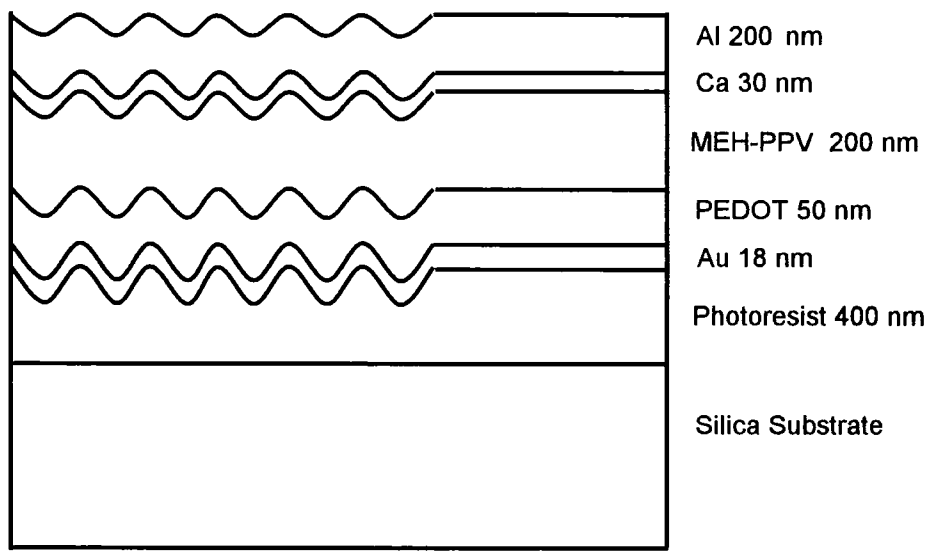

Figure 7.18 *Corrugated LED structure. Corrugated and planar regions on the same substrate were used to compare the performance of corrugated and uncorrugated LEDs. A grating with period 388 nm and amplitude 60 nm was used for this structure.*

7.3.1 LED Design and Manufacture

The substrates used to make corrugated LEDs were coated in photoresist, with grating structures etched into the photoresist using the process described in chapter six. The substrates were only half corrugated, so that for each substrate there would be four corrugated LEDs, and four planar LEDs from which reference spectra could be taken. The corrugation period used was 388 nm, and the corrugation amplitude was 60 nm. Figure 7.19 shows the three dimensional representation of the structure of the LEDs. This design is used so that the pins making electrical contacts with the metal electrodes can be pressed onto the surface of the device without causing any short circuits.

The materials used in the LED structures were chosen because their electrical properties were suitable to allow reasonably efficient injection of electrons and holes into the MEH-PPV layer, whilst still allowing generated light to escape to the surface. The material that is more usually used as anode for conjugated polymer LEDs is ITO, since it combines reasonably high electrical conductivity with reasonably low optical absorption. However, deposition of ITO directly onto a grating surface is a difficult technique that would have required specialised apparatus and considerable cost. The gold anode used for the LEDs in this work was found to be suitable since it could be deposited easily onto the layer of photoresist by evaporation and is a material suitable for injecting holes into the polymer layers. Since the light generated in the polymer layer needs to pass through the gold to escape the LED, it is important that the gold layer is as thin as possible, minimising the absorption from the metal, while still allowing efficient electrical conduction. A thickness of 18 nm was found to be a suitable. A gold strip of this thickness was evaporated onto the substrate to be used as a common anode for all the LEDs on the substrate.

The layers of polymer were deposited next by spinning. The layer on top of the gold was the conducting polymer poly(ethylenedioxythiophene) doped with polystyrene sulphonate (Bayer P EL grade), otherwise denoted PEDOT. The PEDOT layer, spun to a thickness of 50 nm, was intended to improve the injection of holes into the active light emitting layer of MEH-PPV above it. The MEH-PPV was spun using chlorobenzene as a solvent to a thickness of 200 nm, a thickness greater than would normally be used for a planar LED using this material. The thickness of the

MEH-PPV had to be suitable to ensure efficient charge recombination within it, while also allowing the waveguided light to propagate with an effective wavelength that would allow the grating to scatter it out of the film.

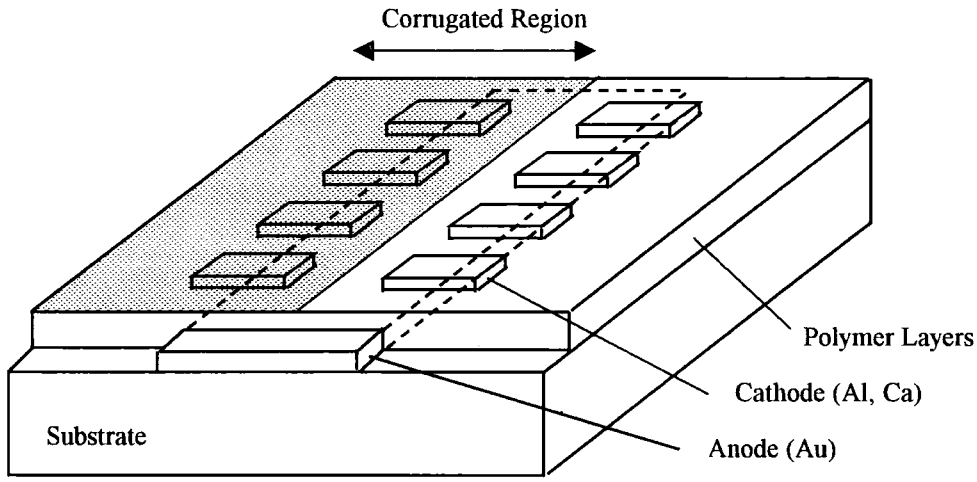

Figure 7.19 *Schematic representation of LED structure.*

The metallic cathodes were evaporated on top of the MEH-PPV, in the pattern shown in figure 7.19. The metal in direct contact with the polymer was calcium evaporated to a thickness of 30 nm, used because its work function is ideal for efficient injection of electrons into conjugated polymers. A layer of aluminium was evaporated on top of the calcium to a thickness of 200 nm. The aluminium served both to protect the reactive calcium layer from oxidation, and also to ensure that all light incident on the cathode would be reflected, and escape through the gold anode.

7.3.2 Increased LED Efficiency

It was found that the corrugated structure did not adversely affect the electrical performance of the LEDs. Figure 7.20a shows typical current voltage characteristics for corrugated and uncorrugated LEDs on the same substrate. It is clear that there is very little change in current density caused by the corrugations.

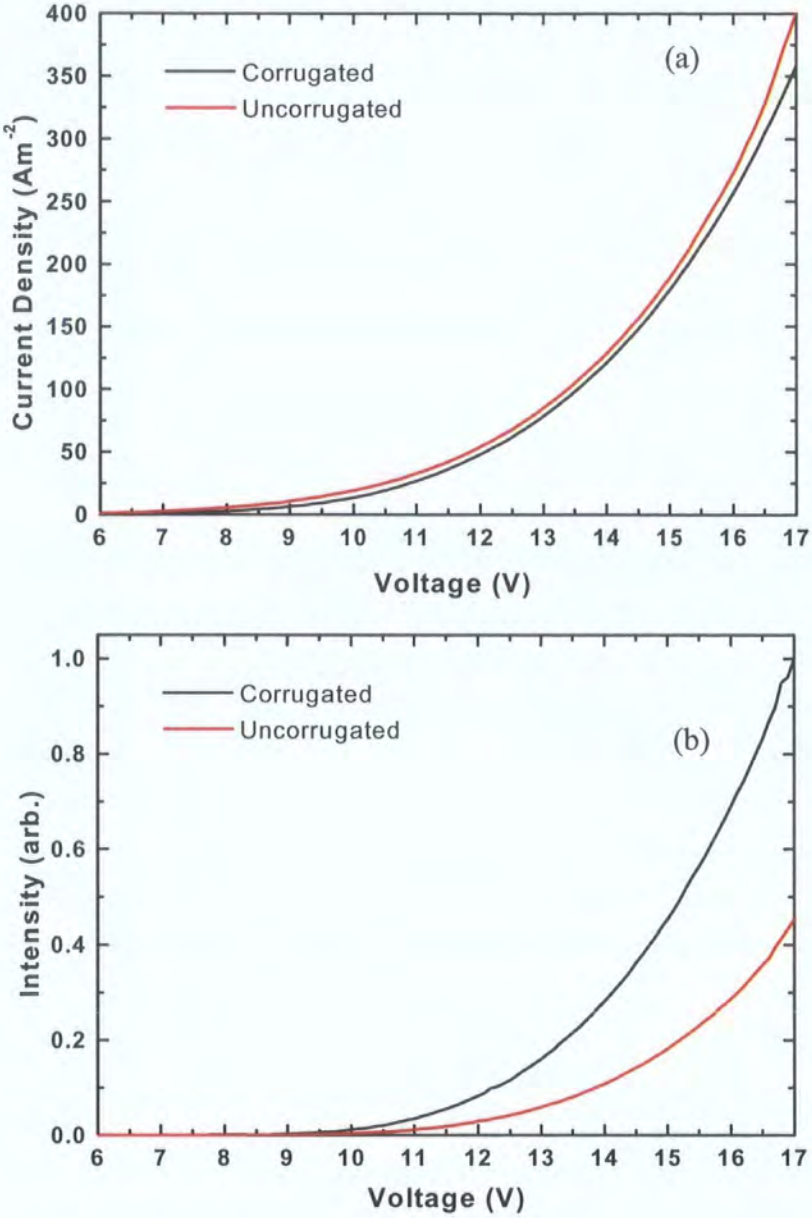

Figure 7.20 *Electrical properties of corrugated LEDs. a) Current-Voltage characteristics. Lower curve is corrugated, upper uncorrugated. b) Light-voltage characteristics. Upper curve is corrugated, lower uncorrugated.*

Figure 7.20b shows the spectrally integrated light output from the corrugated and uncorrugated LEDs as a function of the applied voltage. The light output was measured using a large area photodiode placed close to the polymer so that a full angle of 130° was collected, thus including most of the light emitted from the LEDs. As can be seen from the graph, there is a dramatic increase in light output from the

corrugated LED compared to the uncorrugated LED on the same substrate. The fact the current through the LED was changed very little, suggests that the dramatic increase in light output occurs because more light is able to escape from the corrugated LED, rather than being trapped in waveguide modes and quickly absorbed. Thus the corrugated structure has effectively doubled the efficiency of the LED.

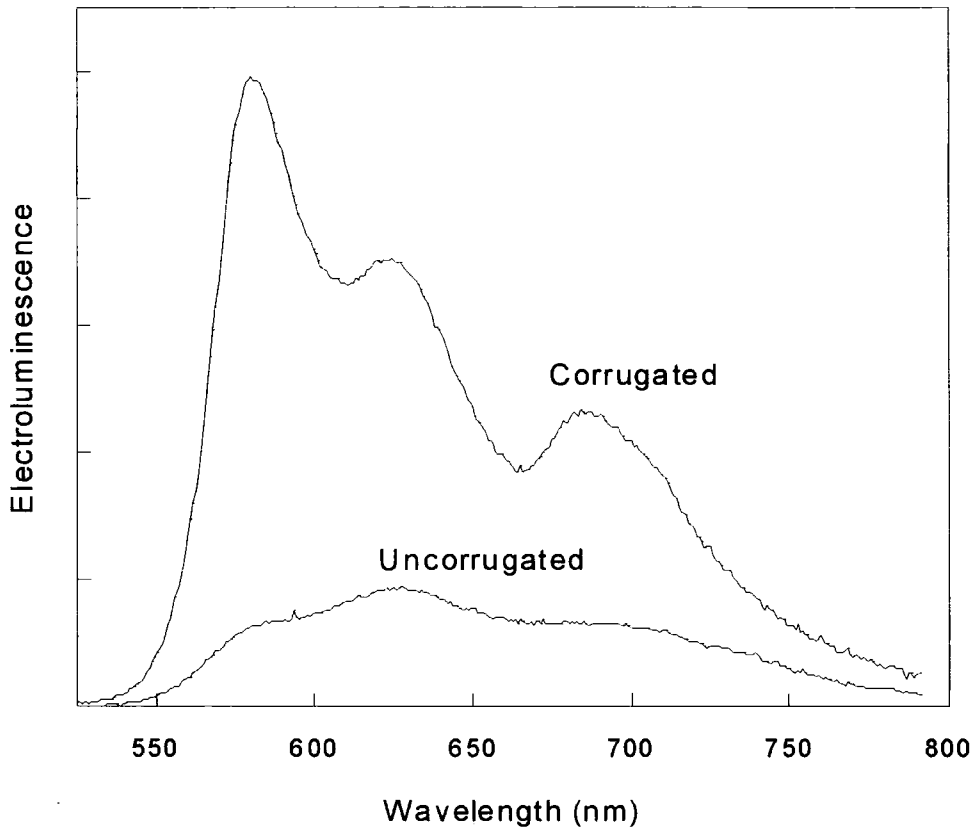

Figure 7.21 *Comparison of emission spectra from corrugated and uncorrugated LEDs on the same substrate. The spectrum was taken for emission at normal angle from the LEDs with a full collection angle of 1.6°, using the CCD spectrometer.*

From figure 7.21 it can be seen that the shape of the emission spectra has been altered considerable by the corrugations. The emission is most dramatically increased in the shorter wavelength end of the spectrum, and peaks at a wavelength of 580 nm. It can also be observed from this graph that the increase in electroluminescence in the forward direction is greater than the factor of two increase in overall emission from the LED. The spectrally integrated emission from the corrugated LED in the forward direction was found to be 3.9 times greater than that for the uncorrugated LED. The

actual efficiencies obtained from this set of LEDs were quite low, with the corrugated LEDs giving 0.007% and the uncorrugated LEDs 0.003%. This is due to the fact that the LEDs were not yet optimised for charge transport. However, the LEDs were a very successful demonstration of the potential use of microstructure to increase light output.

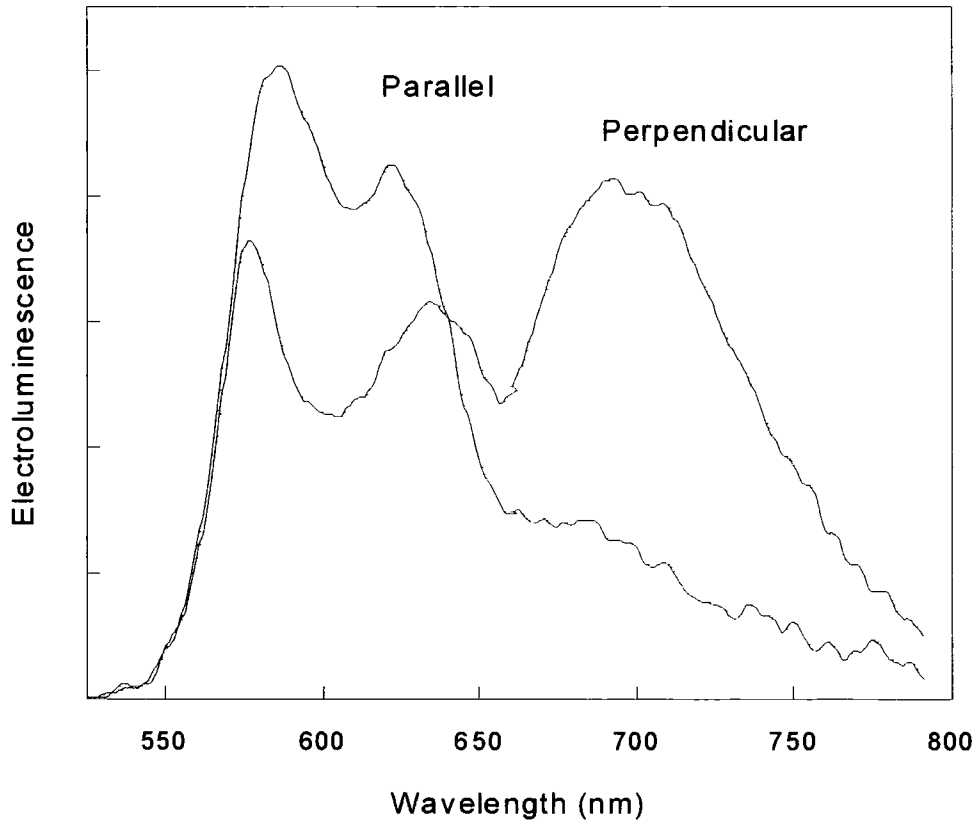

Figure 7.22 *Polarisation of emission normal to LED surface. Emission spectra were taken using a polaroid in front of the detector. Parallel and perpendicular emission spectra were taken with the polaroid rotated to allow through light polarised parallel to perpendicular to the grating lines appropriately.*

In figure 7.22 another important feature of the emission from corrugated LEDs can be seen. Whereas the emission at normal angle from a standard flat LED is unpolarised, the emission from the corrugated LED has a strong polarisation. From the graph it can be seen that for this particular LED, the shorter wavelength emission has a tendency to be polarised parallel to the grating lines, and the longer wavelength emission above 640 nm tends to be polarised perpendicular to the grating lines. It

should be noted that this polarisation dependence of the emission is likely to vary considerably when emission from the LED is examined from different angles.

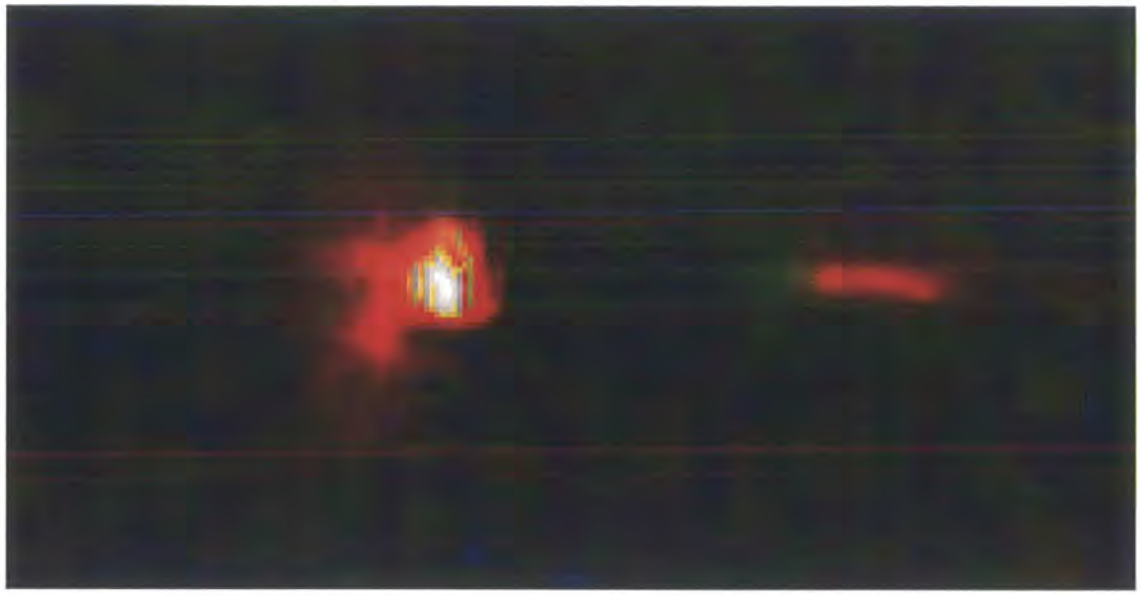

Figure 7.23 *A photograph of a corrugated LED using the conjugated polymer MEH-PPV in operation. The feature on the right hand side of the photograph we attribute to light scattered from a waveguide mode that is propagating through the polymer film and the substrate.*

The second set of LEDs to be made and tested used a similar structure to that shown in figure 7.18, only without the PEDOT layer. It has been demonstrated that gold anodes have a work function suitable for injecting holes[6].

The entire process of LED manufacture was designed to keep the structure free from Oxygen. The gold coated substrates were cleaned in a chlorobenzene solution while in kept in an inert nitrogen atmosphere within a glove box. The polymer layers were spun down without removing the substrate from the glove box. Using a special chamber, the substrates were transferred to the evaporator while still being maintained in a vacuum. The cathode electrodes were then evaporated onto the conjugated polymer layer before it could be degraded by contact with the air.

As before, the height of the corrugations was approximately 60 nm. Once again the corrugations were able to improve the efficiency of the LEDs by a factor of 2.0 ±2. For these LEDs, the averaged overall external efficiency was approximately 0.1% ±0.05, demonstrating that it is possible to fabricate efficient LEDs incorporating

a corrugated structure. A photograph of an LED in operation is shown in figure 7.23. The LED pixel is on the left, and the feature on the right is from light scattered out of a substrate waveguide mode. The scattered light has reflected once from the front of the substrate as shown in figure 7.24, and is then diffracted from the gold using the simple scattering mechanism discussed in section 6.2.4. The colour of this feature changes gradually from green to deep red, giving a visual impression of the range of colours emitted by the MEH-PPV. The spread of the colours is caused by the different scattering conditions for the different wavelengths. Similar features have been observed using alternative methods of scattering substrate modes[7].

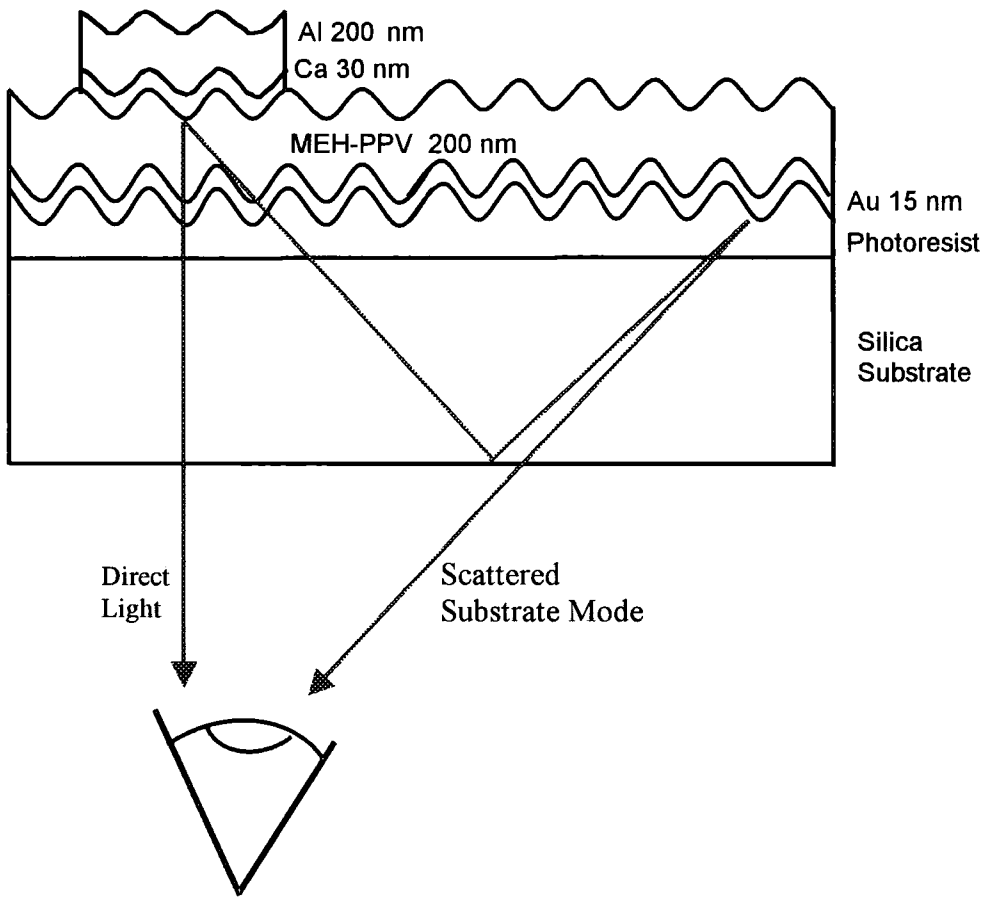

Figure 7.24 *Structure of second set of LEDs, one of which was used to obtain the photograph shown in figure 7.23. The diagram shows the origin of the grating scattering feature on the right hand side of the photograph.*

It is important to note the dramatic increase in efficiency observed from the corrugated LED is attributed primarily to the recovery of light from waveguide modes

that would otherwise be trapped and absorbed only within the conjugated polymer layer. Scattering out guided modes that are propagating through the substrate could also contribute to the increased efficiency, but to a lesser extent. Since the refractive index of the substrate is low compared to the polymer refractive index, there is less light that channelled substrate modes and hence the recoveryof this light is of less importance. There has been previous work done studying methods of recovering light from substrate guided modes in LEDs, using techniques such as roughening[8,9]. However, the work presented here is the first study of the feasibility of corrugating the active layer of a polymer LED to recover light trapped completely in the polymer layer.

7.3.3 Angular Dependence of LED Emission

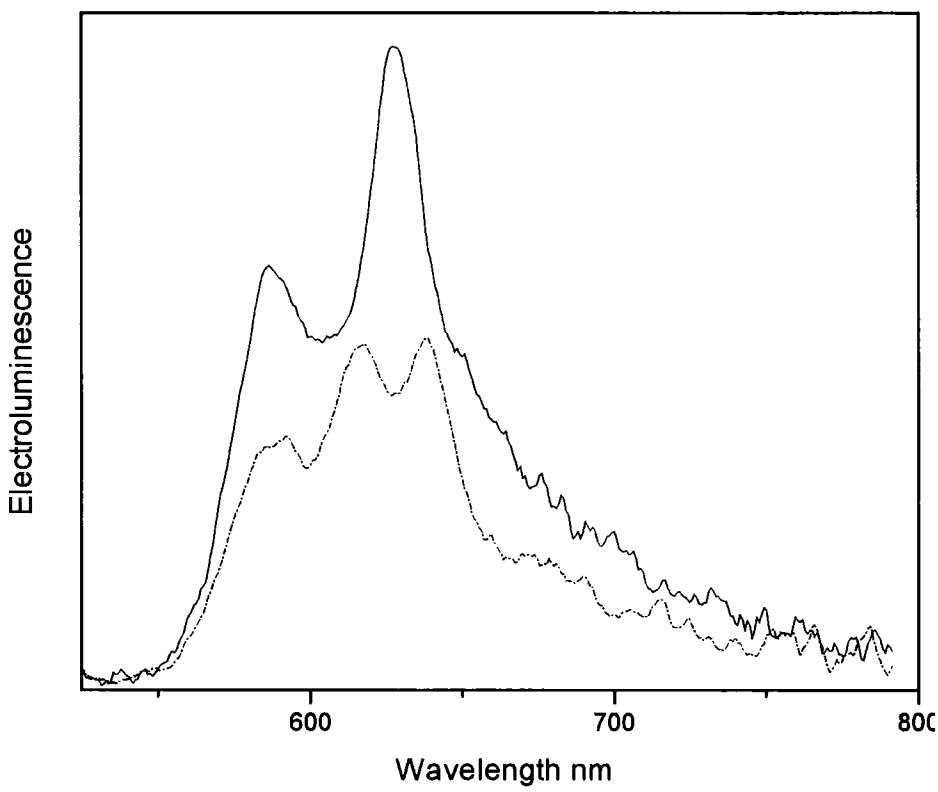

Figure 7.25 *Angular dependence of emission from a corrugated LED, showing emission at normal (θ=0°) angle (continuous line), and θ=5° (dashed line). The peak at 625 nm at normal angle is observed to split into two. The split peaks move further to longer and shorter wavelengths respectively as the observation angle θ is increased.*

The 'peak splitting' effect observed in figure 7.25 from the LED photographed in figure 7.23 is very similar to the angular dependence spectra observed in photoluminescence from conjugated polymers spun onto metal gratings. This suggests that the light scattering mechanism is similar in both photoluminescence and electroluminescence. It is interesting to note that the electroluminescence at normal angle from the LED that included the PEDOT layer (shown in figure 7.21) has its peak at 580 nm and that the second LED without the PEDOT layer (shown in figure 7.25) has its normal angle peak at 625 nm, a noticeably longer wavelength. Since the second LED had no PEDOT layer, the total polymer thickness between the metal layers is reduced. Reducing the thickness of a planar waveguide causes the internal waveguiding angles of modes with fixed colour to become closer to normal, thus for each colour, the effective wavelength within the waveguide becomes shorter. This could explain the observation of the LEDs of lower thickness giving scattered peaks at longer wavelengths.

7.4 Conclusion

This chapter has examined some of the effects of metal gratings on the photoluminescence and electroluminescence of conjugated polymer films. It has been found that the gratings can dramatically alter the emissive properties of these films. There is considerable evidence that the Bragg scattering of waveguide modes provides a major contribution to the altered emission spectra. The complexity of the emission spectra from many of the films suggests that there are other processes affecting the emission. The presence of stop bands associated with the corrugations could explain some of the features observed in the spectra in this chapter.

It has been demonstrated that corrugated LEDs can be made successfully without adverse effects. LEDs with corrugations have been constructed and tested, and found to have in the region of double the efficiency of otherwise identical uncorrugated LEDs. It is clear that the techniques used here could be applied in commercial LEDs, although a technique suitable for mass production of gratings would be required. Since conjugated polymers are quite soft, stamping could provide a cheap and efficient method of grating manufacture. Embossing is used to mass

produce compact discs, and has also been used to create distributed feedback (DFB) lasers[10].

Many materials used to manufacture LEDs have high refractive indices, including some inorganic materials. It is possible that similar methods could be applied to these materials, and perhaps even inorganic LEDs could use corrugated structures to substantially improve their efficiency.

---

[1] Safonov AN, Jory M, Matterson BJ, et al. Synthetic Metals, 116 (1-3): 145-148 (2001)

[2] Matterson BJ, Lupton JM, Safonov AF, et al. Advanced Materials, 13 (2): 123-127 (2001)

[3] Lupton JM, Matterson BJ, Samuel IDW, et al. Applied Physics Letters, 77 (21): 3340-3342 (2000)

[4] I. D. W. Samuel, W. L. Barnes, B. J. Matterson, J. M. Lupton, UK Patent 9910901.9 (1999)

[5] M. D. McGeehee, M. A. Diaz-Garcia, F. Hide, R. Gupta, E. K. Miller, D. Moses, A. J. Heeger, Applied Physics Letters, 72 (13), 1536 (1998)

[6] J. C. Scott, G. G. Malliaras, W. D. Chen, J. C. Breach, J. R. Salem, P. J. Brock, S. B. Sachs, C. E. D. Chidsey, Applied Physics Letters, 74, 1510 (1999)

[7] T. Yamasaki, K. Sumioka, T. Tsutsui, Appl. Phys. Lett. 76, 1243 (2000)

[8] I. Schnitzer, E. Yablonovitch, C. Caneau, T. J. Gmitter, A. Scherer, Applied Physics Letters, 63 (16), 2174 (1993)

[9] R. Windisch, P. Heremans, A. Knobloch, P. Kiessel, G. H. Dohler, B. Dutta, G. Borghs, Applied Physics Letters, 74, 2256 (1999)

[10] M. Berrgren, A. Dodabalapur, R.E. Slusher, A. Timko, O. Natamasu, Applied Physics Letters, 72, 410 (1998)

Chapter 8

Conclusions

The work presented in this thesis has investigated the potential use of photonic microstructure to modify and enhance photoluminescence and electroluminescence from films of conjugated polymer. While much previous work has been done using planar microcavities to modify the emission from conjugated polymers, this work has primarily focussed on using non planar corrugated structures to increase the light output from luminescent polymer films.

One of the main factors limiting the efficiency of LEDs made from conjugated polymers (and indeed LEDs made from many other materials), is that the high refractive index of the materials causes most of the generated light to become trapped in waveguide modes, rather than being emitted in a useful direction. Previous investigations have suggested that the refractive index of conjugated polymers is usual higher than two, and therefore that more than eighty five percent of generated light can be lost to waveguide modes.

Clearly it is important to measure the refractive index of these materials in order to understand the photonic characteristics of conjugated polymer devices and in order to design improved LEDs. The first task performed in this work was to measure the refractive index of the conjugated polymers PPV and MEH-PPV across the range of wavelengths that they exhibit luminescence. These polymers are birefringent, and only available as thin film samples. For this reason the refractive index was measured by analysing the waveguide modes able to propagate within the films. It was found that both of these materials are highly dispersive. The refractive index of MEH-PPV was found to be higher than 1.8 across its emission spectrum, increasing above 2.0 for wavelengths shorter than 590 nm.

The effects of corrugations on the photoluminescence of thin films of MEH-PPV were investigated. Substrates coated in photoresist were exposed to optical interference patterns in order to generate a sinusoidal corrugated grating on the surface. Films of MEH-PPV were deposited onto the corrugated substrates and onto uncorrugated reference substrates by spinning. Photoluminescence was generated by exciting the films with a blue laser, while maintaining the films under vacuum.

It was found that the photoluminescence spectra of the MEH-PPV were strongly modified by the corrugations. Using a grating with a period of 400 nm and peak to trough depth of 100 nm, dramatic extra peaks were observed that were not present in the spectra from the reference films. The size of the peaks was sufficient to suggest that a substantial increase in light output cold be obtained. The wavelengths of the peaks changed gradually with the position of the detector and they were strongly polarised.

The extra peaks present in the spectra from corrugated MEH-PPV films were attributed to light escaping from waveguide modes by scattering. By treating the corrugated samples as a perturbation from the planar case, it was possible to explain the polarisation of the peaks, and the wavelength dependence of the peak position when the detector was moved with respect to the substrate.

Further investigation of luminescence of corrugated MEH-PPV films was carried out using corrugated substrates of different period and depth. It was found that changing the period of the gratings allowed the peak of the emission normal to the sample to be tuned in wavelength. Increasing the depth of the gratings caused the scattered peaks to become larger.

Corrugated substrates were coated with thin layers of metal to form metal gratings. It was found that photoluminescence from MEH-PPV spun onto metal gratings exhibited much more dramatic extra peaks than was observed from non metal gratings. Spectra from low amplitude metal gratings, with a peak to trough depth in the region of 5 nm showed a substantial reduction in light output compared to planar reference samples. However for stronger gratings with a depth of 30 nm and upwards, there was a substantial increase in light output caused by the grating structure. The extra peaks from metal gratings were attributed to the scattering of waveguided light. However, as the gratings were increased in amplitude to a depth of 200 nm or more, it was found that the spectra became substantially more complex.

When the photoluminescence was examined for different angles of emission, it was found that certain peaks would vanish at particular wavelengths, rather than just gradually changing in wavelength as the detector was moved. Modelling the effects of deep gratings on photoluminescence is a complex task, since the grating can no longer be considered as a perturbation from the planar case. It is possible that the behaviour of the vanishing peaks can be attributed to partial band gaps (or stop bands) caused by harmonics of the periodic grating.

LEDs incorporating corrugated structures were created using MEH-PPV as the emissive layer, and using metal electrodes to inject charge. The metal layers were deposited by evaporation and the MEH-PPV by spinning. Planar reference LEDs were created on the same substrate to ensure identical processing. Although it might be thought that the corrugated structure would disrupt the electric field distribution within the LED, it was found that the corrugations had no adverse effects on the electrical properties of the LEDs. Plots of current versus voltage for corrugated and planar reference LEDs were almost identical.

It was found that the total light output from a corrugated LED was more than doubled, compared to a planar LED, while using the same electrical power. This is substantial increase in efficiency, and clearly has considerable commercial potential.

There is considerable potential for further work in this field of research. A method of completely modelling the spontaneous emission processes from within a strongly corrugated multilayer structure would be highly desirable. Although the perturbation from the planar case modelling used in this thesis has been able to provide considerable insight into the effects observed, it is not able to explain all the details of the photoluminescence spectra from the strong gratings.

The diffraction grating substrates used in this work have been approximately sinusoidal in form. More complicated patterns would be very interesting to test under photoluminescence, or in an LED. Superimposing more than one sinusoidal pattern on the grating might be able combine bandgap effects with scattering effects and allow very subtle manipulation of the luminescence. A hexagonal pattern etched into the substrate could be a very efficient design for scattering waveguide modes propagating in any direction across the substrate.

The techniques used to increase the efficiency of LEDs in this thesis could in principle be applied to the design of LEDs using any material that has a high refractive index. Conjugated polymers have high refractive index compared to most organic materials. However, most inorganic materials used to create LEDs also have high refractive indices. It is possible that inorganic devices could also be made more efficient using the techniques developed in this work.

Appendix

This subroutine, written in Fortran, calculates reflection and transmission from an arbitrary stack of thin films with complex refractive index, and was used to generate several of the diagrams in this thesis. The arrays rndx(0:40), kndx(0:40) and thick(40) contain the refractive indices, absorption and thickness of the appropriate layers. The angle of incidence is designated by the variable ang, the wavelength by colour, the polarisation by pol (1=TE, 2=TM), and the reflected and transmitted power by pr and pt appropriately.

```
      subroutine rtbot(tlay,nblay,ang,rndx,kndx,thick,pr,pt,einc,eref,etra,colour,pol,inmax)
      complex(4) ebnd(0:40),hbnd(0:40),i,einc,eref,etra,gj,uj,uj0,ujt
      real(4) ang,k,pi,colour,thick(40),rndx(0:40),kndx(0:40),pr,pt,inmax
      integer(4) nblay,tlay,b,pol
      i=cmplx(0,1)
      pi=3.14159265
      k=2.0*pi/colour
      etra=cmplx(1,0)
      ebnd(1)=etra
      uj0=((rndx(0)**2)-(kndx(0)**2)-(inmax**2)*(sin(ang)**2)-
2*i*rndx(0)*kndx(0))**0.5
       if (pol.eq.2) then
       uj0=((rndx(0)-i*kndx(0))**2)/uj0
       endif
       hbnd(1)=etra*uj0
       if (nblay.ge.1) then
        do 750 b=1,nblay
        gj=k*thick(b)*((rndx(b)**2)-(kndx(b)**2)-(inmax**2)*(sin(ang)**2)-
2*i*rndx(b)*kndx(b))**0.5
         uj=((rndx(b)**2)-(kndx(b)**2)-(inmax**2)*(sin(ang)**2)-
2*i*rndx(b)*kndx(b))**0.5
          if (pol.eq.2) then
          uj=((rndx(b)-i*kndx(b))**2)/uj
          endif
          ebnd(b+1)=ccos(gj)*ebnd(b)+(i/uj)*csin(gj)*hbnd(b)
          hbnd(b+1)=i*uj*csin(gj)*ebnd(b)+ccos(gj)*hbnd(b)
750      continue
       endif
      ujt=((rndx(nblay+1)**2)-(kndx(nblay+1)**2)-(inmax**2)*(sin(ang)**2)-
2*i*rndx(nblay+1)*kndx(nblay+1))**0.5
       if (pol.eq.2) then
       ujt=((rndx(nblay+1)-i*kndx(nblay+1))**2)/ujt
       endif
      einc=0.5*(ebnd(nblay+1)+hbnd(nblay+1)/ujt)
      eref=0.5*(ebnd(nblay+1)-hbnd(nblay+1)/ujt)
      pr=((abs(eref/einc))**2)
      pt=((abs(etra/einc))**2)*uj0/ujt
      return
```

LIST OF PUBLICATIONS

I. D. W. Samuel, W. L. Barnes, B. J. Matterson, J. M. Lupton
Light-emitting diode with improved efficiency
UK PATENT 9910901.9 1999

B. J. Matterson, J. M. Lupton, A. Safonov, M.G. Salt, W.L. Barnes, I.D.W. Samuel
Increased efficiency and controlled light output from a microstructured light-emitting diode
ADVANCED MATERIALS 13 (2): 123-127 JAN 16 (2001)

A. Safonov, M. Jory, B. J. Matterson, J. M. Lupton, M. G. Salt, J. A. E. Wasey, W. L. Barnes, I. D. W. Samuel
Modification of polymer light emission by lateral microstructure
SYNTHETIC METALS 116 (1-3): 145-148 JAN 15 (2001)

J. M. Lupton, B. J. Matterson, I. D. W. Samuel, M. J. Jory, W. L. Barnes
Bragg scattering from periodically microstructured light emitting diodes
APPLIED PHYSICS LETTERS 77 (21): 3340-3342 NOV 20 (2000)

A. Boudrioua, P.A. Hobson, B. Matterson, I. D. W. Samuel, W. L. Barnes
Birefringence and dispersion of the light emitting polymer MEH-PPV
SYNTHETIC METALS 111: 545-547 JUN 1 (2000)

B. J. Matterson, M.G. Salt, W. L. Barnes, I. D. W. Samuel
Effect of lateral microstructure on conjugated polymer luminescence
SYNTHETIC METALS 101 (1-3): 250-251 MAY (1999)